NATIONAL LIBRARY
PUBLIC ARCHIVES BUILDING
OTTAWA 2

CANADA

BIBLIOTHÈQUE NATIONALE
ÉDIFICE DES ARCHIVES PUBLIQUES
OTTAWA 2

NAME OF AUTHOR.....William...Leung...Lee.....

473

TITLE OF THESIS.....Dynamics...Of...A...Theta..
.....Dynamics...Of...A...Theta.....
..Pinch...Discharge...In...A.....
UNIVERSITY..Transverse...Magnetic...Field.....

DEGREE.....Ph.D.....YEAR GRANTED....1966.....

Permission is hereby granted to THE NATIONAL LIBRARY OF CANADA to microfilm this thesis and to lend or sell copies of the film.

The author reserves other publication rights, and neither the thesis nor extensive extracts from it may be printed or otherwise reproduced without the author's written permission.

(Signed)...W. L. Lee.....

PERMANENT ADDRESS:

..1299...W...King...Ed...Ave.
..VANCOUVER...9,...B.C
.....

DATED.....MAY...13.....1966

NL-91

Reproduced with permission of the copyright owner. Further reproduction prohibited without permission.

DYNAMICS OF A THETA PINCH DISCHARGE IN A TRANSVERSE MAGNETIC FIELD

by

WILLIAM LEUNG LEE
B.Sc., University of Washington, 1960
M.Sc., University of Purdue, 1962

A THESIS SUBMITTED IN PARTIAL FULFILMENT OF THE REQUIREMENTS FOR THE DEGREE OF

DOCTOR OF PHILOSOPHY

in the Department

of

PHYSICS

We accept this thesis as conforming to the required standard

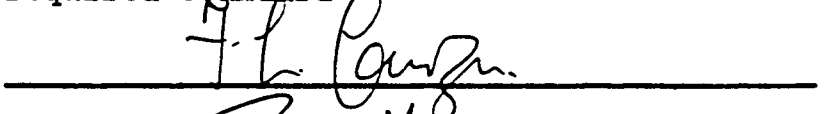

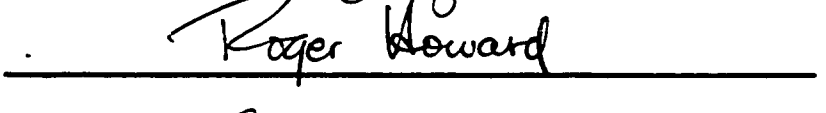

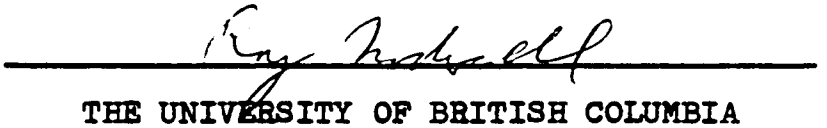

THE UNIVERSITY OF BRITISH COLUMBIA
April, 1966

© William Leung Lee 1966

Reproduced with permission of the copyright owner. Further reproduction prohibited without permission.

ABSTRACT

The suppression of radial hydromagnetic oscillations of a theta pinch plasmoid produced in air has been investigated with magnetic probes and a framing camera. In the presence of essentially static and uniform magnetic bias fields (produced by Helmholtz coils) it was found that the oscillations are suppressed by a flip instability of the plasmoid and the direction of flip is controlled by the transverse magnetic field.

Using the suppression of radial hydromagnetic oscillation as the criterion for flip, it is found experimentally that if $\frac{B_T}{ap^{\frac{1}{2}}}$ is greater than a critical value, then the plasma ring flips. 'B_T' is the strength of the bias field perpendicular to the axis of the theta coil, 'a' the radius of the discharge vessel and 'p' is the gas pressure.

The experimental results are interpreted in terms of a snowplough model for the discharge, in which the plasma current forms two concentric cylinders. The predictions of the theory agree with the experimental observations.

F. L. Ribe

Reproduced with permission of the copyright owner. Further reproduction prohibited without permission.

TABLE OF CONTENTS

Abstract	ii
List Of Illustrations	v
Acknowledgements	ix
CHAPTER I - Introduction	1
CHAPTER II - Experimental Apparatus	7
Section A - Theta Pinch Apparatus	7
Section B - Bias Field Apparatus	14
1. Large Field Bank	14
2. Small Field Bank	17
3. Helmholtz Coil	19
Section C - Diagnostic Equipment	22
1. Magnetic Probes	22
a. Single Axial Probe	24
b. Directional Probe	27
2. High Speed Framing Camera	30
CHAPTER III - Results	33
Section A - Discharge Of Theta Bank With No Bias Field	33
Section B - Theta Pinch With A Bias Field	40
1. Photographic Measurements	44
a. $\phi = 90^{\circ}$	44
b. $\phi \approx 0^{\circ}$	48

Reproduced with permission of the copyright owner. Further reproduction prohibited without permission.

2. Probe Measurements 51
a. $\phi \approx 0^{\circ}$ 51
b. $\phi = 90^{\circ}$ 56
3. Variation In The Discharge Radius 59
4. Directional Probe 61
Section C - Theory 68
1. Radial Equation Of Motion 69
2. Axial Equation Of Motion 74
3. Discussion Of The Assumptions 79
4. Discussion Of The Interpretation Of The Suppression Of Oscillations As The Flip Instability 87
5. Variations Of The Theoretical Model 90
Section D - Suggestions For Further Work 93

CHAPTER IV - Conclusions 95

APPENDIX A - Effect Of Preionization On The Stability Constant 97
B - Change In The Stability Constant With Varying Theta Coil Length 99
C - Summary On The Argon Experiments 102
D - Pictures Of Flip At 100 μHg And 250 μHg, Air 105
E - Characteristic Impedance Of Magnetic Probe 108

REFERENCES 111

Reproduced with permission of the copyright owner. Further reproduction prohibited without permission.

LIST OF ILLUSTRATIONS

FIG. I. 1 - Cross Section Of Theta Pinch 2

2 - Top View Of Plasma Flip 4

FIG. II. 1 - Theta Capacitor Bank 8

2 - Cross Sectional View Of Spark Gap Switch, S_1 9

3 - Ultra Violet Trigger Generator 10

4 - Rogowski Coil Circuit 13

5 - Helmholtz Spark Gap Switch 15

6 - Trigger Pulse Generator 15

7 - Helmholtz Trigger Pin 16

8 - Current Waveform For The Small Magnetic Field Capacitor Bank 18

9 - Small Magnetic Field Capacitor Bank Circuit Diagram 18

10 - Geometric Position Of The Helmholtz Coil 20

11 - Magnetic Field Distribution Along Axis AA' And BB' Of Helmholtz Coils 21

12 - RC Integrater Network 22

13 - Axial Magnetic Probe 24

14 - Method Of Mounting Probe In The Theta Pinch Discharge Vessel 25

15 - Capacitative Coupling Signal From Magnetic Probe 27

Reproduced with permission of the copyright owner. Further reproduction prohibited without permission.

FIG. II.16 - Frequency Response Of Axial Magnetic Probe 28

17 - Directional Probe 29

18 - Frequency Response Of Directional Probe 31

19 - Framing Camera Schematic 32

FIG. III. 1 - Schematic Of Theta Pinch Discharge 34

2 - Theta Current Waveform 36

3 - Formation Of The Plasma Shell 36

4 - Integrated Magnetic Probe Signal 38

5 - End-On Photograph ($B_H = 0$) 39

6 - Top-On Photograph ($B_H = 0$) 39

7 - Bias Field Trigger Circuit For The Magnetic Probe 41

8 - Bias Field Trigger Circuit For The Framing Camera 43

9 - Sketch Of Plasma Photographs 46

10 - Top-On Photograph Of Plasma ($\phi = 90^\circ$) 47

11 - Side-On Photograph ($\phi \propto 0^\circ$) 49

12 - End-On Photograph ($\phi \approx 0^\circ$) 49

13 - End-On Photograph Of Plasma With No Transverse Bias Field ($\phi = 0^\circ$) 50

14 - End-On Of Plasma With A Transverse Bias Field 51

15 - Axial Probe Signals With Changes In 'ϕ' 53

16 - Value Of $B_H \sin\phi_c$ For Different Gas Pressures (Air) 54

Reproduced with permission of the copyright owner. Further reproduction prohibited without permission.

FIG. III.17 - Variation Of The Critical Transverse Field With Pressure ($\phi \approx 0^{o}$) 57

18 - Variation Of The Critical Transverse Field With Variation In Pressure ($\phi=90^{o}$) 59

19 - Variation In Stability Constant With Tube Diameter 60

20 - $V_1 - V_2$ Waveform 63

21 - V_1 Waveform 63

22 - Probe Waveforms At $\theta_c \pm 10^{o}$ 65

23 - The Angular Rotation 'δ' 66

24 - Axial Section Of The Theta Pinch Discharge 75

25 - Specification Of The Angle 'θ' 76

26 - Probe Signals Showing B_o Is Constant For Different Pressures At Flip Conditions 80

27 - End-On Photographs Of The Plasma At Flip Conditions 82

28 - Plasma Field Strength At Flip Conditions 85

29 - Magnetic Field Lines Of Theta Coil 89

APPENDIX A.1 - Effect Of Preionization On The Stability 98

A.2 - Stability Constant Variation With Coil Length 101

A.3 - Value Of $B_H \sin\phi_c$ For Different Gas Pressures (Argon) 103

A.4 - Comparison Of The Stability Constant Of Argon And Air 104

Reproduced with permission of the copyright owner. Further reproduction prohibited without permission.

APPENDIX A.5 - Top-On Photograph Of Plasma At 200μHg Pressure (Air) 106

A.6 - End-On Photograph At 200μHg Pressure (Air) 107

A.7 - Top-On Photograph At 100μHg Pressure (Air) 107

A.8 - Equivalent Circuit Of Magnetic Probe 108

A.9 - Damped Probe Circuit 109

Reproduced with permission of the copyright owner. Further reproduction prohibited without permission.

ACKNOWLEDGMENTS

I wish to thank Dr. F.L. Curzon for his encouragement, helpful criticisms and supervision of the entire project and the Ph.D. Committee, Dr. R.A. Nodwell, Dr. A.J. Barnard and Dr. R. Howard, for their constructive criticisms in the writing of this thesis.

I would like to express my appreciation to Dr. R.J. Churchill for guidance in the construction of the theta pinch apparatus. The help of the technical staff, W. Ratzlaff and J.H. Turner in the field of elctronics, A. Fraser and his staff in the machine shop work, J. Lees in the glass work, are all gratefully acknowledged.

To my colleagues go my sincere thanks for their helpful suggestions, particularly to C.C. Daughney for pointing out the two current rings in the photographs.

Lastly, I wish to thank the Atomic Energy Control Board of Canada for financially supporting the work.

Reproduced with permission of the copyright owner. Further reproduction prohibited without permission.

CHAPTER I

INTRODUCTION

The theta pinch has been extensively investigated because it can generate relatively pure, high temperature plasmas ($T \sim 10^5$ ^{o}K) having high electron densities ($n_e \sim 10^{16}$ cm^{-3}). To generate the plasma, a large current is discharged through a coil surrounding a cylindrical discharge tube. The resultant azimuthal electric field induced in the discharge gas generates an electric current resulting in the formation of a plasma cylinder. For short coils the plasma tends to form a ring discharge. The discharge vessel is sometimes immersed in a constant magnetic field (i.e. bias magnetic field) in order to improve the breakdown characteristics of the discharge gas and to stabilize the plasma.

From the geometry of the electric and the magnetic fields it can be seen that the plasma is compressed radially, that is, a theta pinch occurs. (The "theta" specifies the azimuthal direction of the current flow in the plasma). After the plasma has compressed to a minimum radius, it experiences radial oscillations due to the pressures exerted by the magnetic fields within and external to the plasma (Niblett and Green, 1959).

Reproduced with permission of the copyright owner. Further reproduction prohibited without permission.

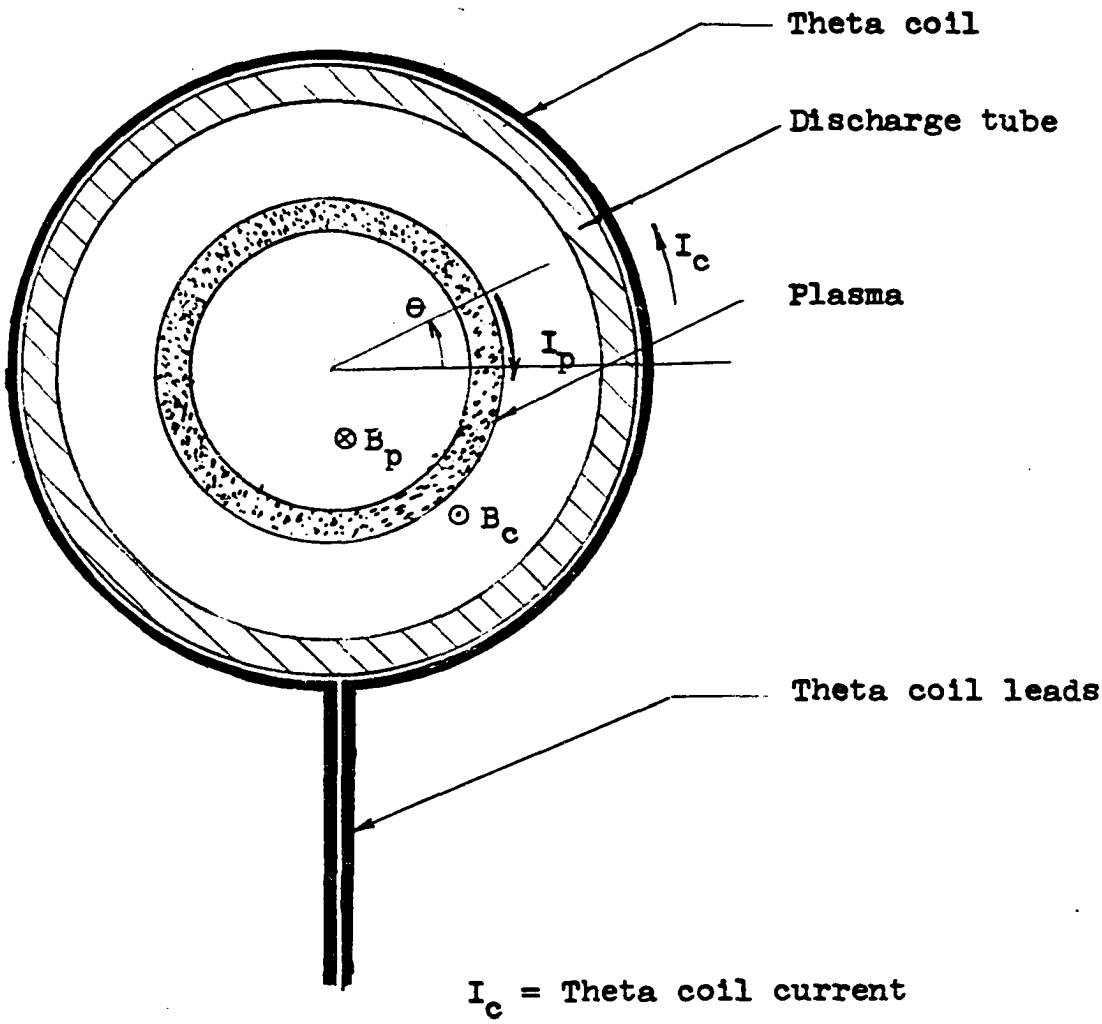

I_c = Theta coil current

I_p = Plasma current

B_c = Theta coil magnetic field

B_p = Plasma magnetic field

Θ = Azimuthal angle

Fig. I.1. Cross Section Of The Theta Pinch

Reproduced with permission of the copyright owner. Further reproduction prohibited without permission.

It has been observed (W. Cilliers et al., 1963) that under certain experimental conditions, after the plasma has pinched, the magnetic field enclosed by it suddenly disappears as may be detected by a small search coil inserted along the axis of the discharge vessel.

When the internal magnetic field vanishes, the radial oscillations of the plasma also disappear. The investigation of this disappearance is of considerable practical interest in thermonuclear research work because it indicates that the plasma confinement is unstable, that is, the plasma has a short lifetime.

In this thesis, it is shown that the disappearance of the oscillations can be attributed to the rotation of the plasma ring about a diameter. The rotation is due to the interaction of the plasma current with a superimposed transverse magnetic field which induces axial motions. The transverse field need not be large and may be produced by an inhomogeneous theta coil field. The combination of the radial and axial motion of the plasma causes the plasma ring to rotate about its diameter. As the plasma rotates, the magnetic field can no longer confine it with the result that the plasma and the enclosed flux are dissipated. This rotation was first observed by Clarke and Wuerker (1962), and they referred to it as the "flip instability". They used an image converter camera to take successive pictures of the rotation. They did not use a bias magnetic field to influence the plasma.

Reproduced with permission of the copyright owner. Further reproduction prohibited without permission.

Bartoli and Green (1964) gave a theoretical model of the flip, treating the plasma as a rigid magnetic dipole in a reverse magnetic field, (see Fig. I.2.).

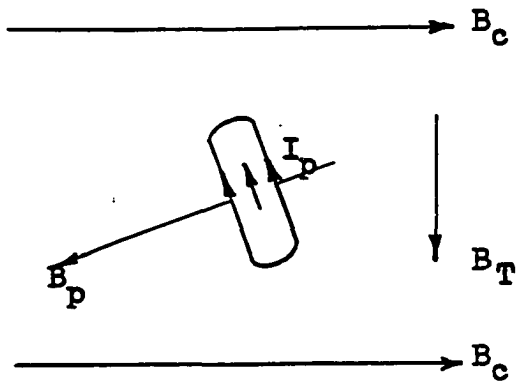

B_c = Theta Coil Magnetic Field

B_p = Plasma Current Magnetic Field

B_T = Transverse Magnetic Field

I_p = Plasma Current

Fig. I.2. Top View Of Plasma Flip

To the author's knowledge, no quantitative experimental studies of the flip instability have been made. This is primarily because the plasma tends to rotate about different diameters in successive discharges making it extremely difficult to measure the rate of rotation of the plasma ring.

Reproduced with permission of the copyright owner. Further reproduction prohibited without permission.

In the present work, the plasma is given a preferential axis of rotation by applying a small transverse magnetic field. An axial motion of the plasma is caused by the interaction of the plasma current with this transverse field and the plasma rotates about an axis perpendicular to the theta and transverse fields. If the axial velocity issmall, the radial velocity can be large enough for radial oscillations to develop. However, as the axial velocity increases, the oscillations will be suppressed because the plasma will escape out through the ends of the coil before radial oscillations can develop.

In this thesis the oscillations are detected by a magnetic probe and the suppression of oscillation is chosen as the criterion for the occurrence of the flip instability. The occurrence of flip is determined as a function of the following parameters: the density of the discharge gas (air), the strength and the direction of the bias magnetic field, and the radius of the discharge tube. It is found that the flip instability occurs whenever $\frac{B_T}{a\rho^{1/2}} > 0.02 \frac{\text{weber}}{m^3(\mu Hg)^{1/2}}$. Where "$B_T$" is the transverse magnetic field, "a" is the radius of the discharge vessel, and "ρ" is the density of the gas.

The axial and radial equations of motion of the plasma are derived and solved approximately and predict that if $\frac{B_T}{a\rho^{1/2}}$ is greater than a given constant, the flip instability will occur, in agreement with the experimental results.

Reproduced with permission of the copyright owner. Further reproduction prohibited without permission.

In the development of the axial equation of motion, a two current model of the plasma is used (T.S. Green, 1962). One current maintains the magnetic flux trapped by the plasma and the second current is induced by the theta coil magnetic field. The two currents flow in opposite azimuthal directions.

The validity of this model is supported by framing camera photographs of the discharge in a transverse magnetic field. In the absence of the transverse field, the magnetic forces acting on the current will be in opposite radial directions and the current sheets are therefore compressed together, rendering them indistinguishable from each other. However, a transverse magnetic field, moves the current rings in opposite axial directions enabling the rings to be distinguishable from each other.

Although the theoretical model is only a crude representation of the actual plasma, the agreement with the experimental results indicate that the model is a reasonable approximation.

A summary of the original contributions of this thesis is given in the abstract.

The apparatus used in this work is discussed in the first part of Chapter II and the diagnostic techniques are discussed in the latter part of Chapter II. The experimental results are presented in Chapter III, together with the theoretical interpretation of the results.

Reproduced with permission of the copyright owner. Further reproduction prohibited without permission.

CHAPTER II

EXPERIMENTAL APPARATUS

This chapter is divided into three sections which contain descriptions of:

Section A - Theta Pinch Apparatus,

Section B - Bias Magnetic Field Apparatus,

Section C - Diagnostic Equipment.

Section A - Theta Pinch Apparatus

A theta pinch is produced by rapidly discharging a large capacitor bank through a copper coil that is wound around a glass tube. The resultant changing magnetic flux produces an azimuthal electric field in the glass tube. If the gas pressure is appropriate, the gas is ionized and forms a plasma cylinder. The plasma current flows in the azimuthal direction and interacts with the axial magnetic field of the theta coil. Considering the direction of the magnetic forces (see Fig. I.1.), it is seen that the plasma shell contracts radially giving a pinch effect.

The plasma loses energy rapidly through radiation, thermal conduction, etc. To produce and maintain a hot plasma it is therefore necessary to provide a large amount of energy in a short time to offset these energy losses. To achieve the necessary high input power, a large capacity, high voltage

Reproduced with permission of the copyright owner. Further reproduction prohibited without permission.

capacitor bank is employed. The input power is optimized by minimizing the inductance in the discharge circuit. The characteristics of the theta pinch apparatus used in this work are:

Charging Potential	10.4 kv	13.3 kv	15.3 kv
Total Capacitance	-	25 μf	-
Total Inductance	-	170 nH	-
Material of Discharge Vessel	-	Pyrex Glass	-
Length of Discharge Vessel	-	69 cm	-
Inner Diameter of Discharge Vessel	3.4 cm	5.1 cm	7.1 cm
Discharge Period	-	13 μsec	-
Peak Magnetic Field	-	2.8 webers/m^2	-

The essential components of the theta capacitor bank are depicted in Fig. II.1.

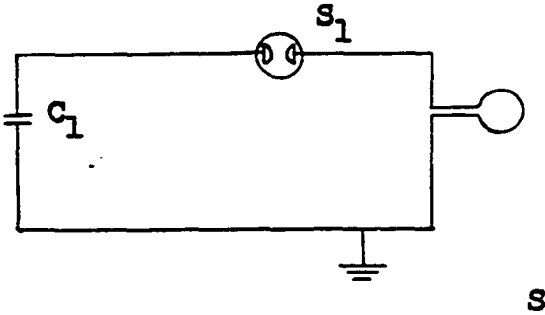

S_1 = Spark Gap Switch

C_1 = Capacitor Bank

Fig. II.1. Theta Capacitor Bank

Reproduced with permission of the copyright owner. Further reproduction prohibited without permission.

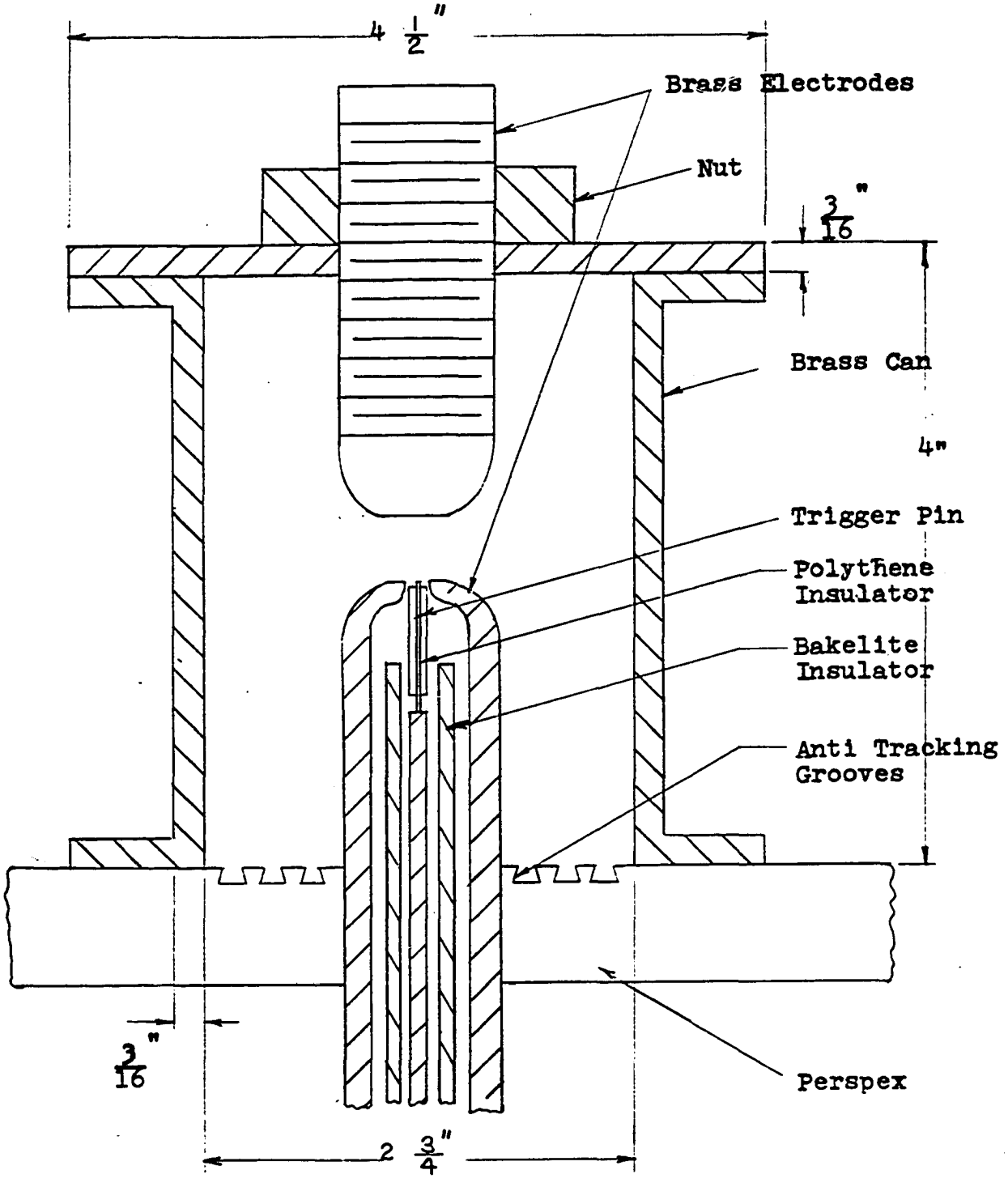

Fig. II.2. Cross Sectional View Of Spark Gap Switch, S_1

Reproduced with permission of the copyright owner. Further reproduction prohibited without permission.

The spark gap switch, S_1, (see Fig. II.2.) is triggered by applying a fast rise time, high voltage pulse to a trigger pin. The capacitor bank, C_1, is then discharged through the spark gap switch, S_1, into the theta coil.

The command signal is provided by a pulse generator (Theophanis, 1960), which produces an 18 kv pulse with a 40 nsec rise time. This generator can be activated manually or by a low voltage pulse. In principle the high voltage pulse produced by the Theophanis unit could be used to trigger the theta coil spark gap. However, this pulse is too weak for reliable operation and also the trigger unit is not isolated from the theta bank current. To avoid these difficulties an ultraviolet (uv) trigger system is used. The uv trigger consists of a capacitor, C_2, a spark gap, S_2, and a resistor, R_2, all connected in series (see Fig. II.3.).

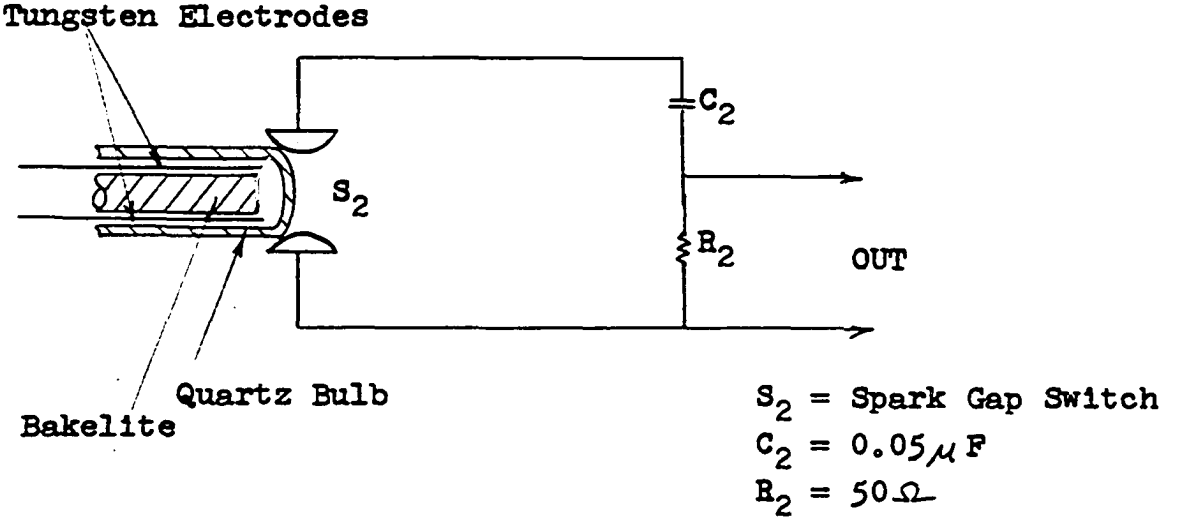

Fig. II.3. Ultra Violet Trigger Generator.

Reproduced with permission of the copyright owner. Further reproduction prohibited without permission.

The pulse from the Theophanis unit is sparked across two tungsten electrodes contained in a quartz bulb mounted near the electrodes of S_2 (see Fig. II.3.). The spark produces photons that pass through the quartz tube and cause a breakdown of the spark gap S_2. The capacitor, C_2, discharges and a voltage pulse is produced across R_2. This pulse is used to trigger the theta spark gap, S_1.

The uv trigger system effectively amplifies the energy available from the Theophanis unit from a fraction of a joule up to 3 joules. Also the operating equipment is electrically isolated from the main discharge circuit by the quartz bulb, thus improving the safety of the equipment and reducing the electrical noise coupled from the high discharge current into the measuring apparatus. The capacitor, C_2, is charged with a potential divider across the theta bank C_1 (see Fig. III.1.). The jitter of the complete triggering circuit is less than $1/2\mu$sec. More details of the triggering circuit can be found in the note by Curzon and Smy (1963).

The theta capacitor bank consists of 5 Cornell Dubilier Model NRG 201 capacitors connected in parallel. Each capacitor has a capacity of 5μF and a maximum operating potential difference of 20 kvdc. A low inductance geometry is obtained by connecting the capacitors together with a parallel plate transmission line consisting of copper sheets 2mm thick. The spark gap (see Fig. II.2.) is located at one end of the bank and is connected in series with the bank and the theta coil (Fig. II.1.).

Reproduced with permission of the copyright owner. Further reproduction prohibited without permission.

The transmission line from the spark gap to the theta coil is a pair of parallel copper plates 2 mm thick, 13 cm wide, and 100 cm long separated by a 3 mm layer of polyethylene and clamped together with wooden clamps. The spark gap electrodes are insulated from each other by a disc of perspex. The disc has been grooved to increase the length of the tracking path between the electrodes, thus decreasing the possibilities of spurious breakdown (Fig. II.2.). The physical dimensions of the theta coils are as follows:

Material of Theta Coil	Copper Gauze		
Coil Diameter	4.1 cm	6.1 cm	7.6 cm
Coil Length	4.6 cm	6.4 cm	7.6 cm

The current, I_c, in the theta coil is monitored with a Rogowski coil consisting of a solenoid made from an 11 cm length of delay cable (RG 65 AU) with the outer ground shield removed. A matching resistance is placed in series with the coil to dampen the resonance response of the coil. (For more details, see Appendix E). The coil is placed in between the high current leads to the theta coil.

The output voltage of the Rogowski coil is proportional to the rate of change of current, dI_c/dt. To obtain the current an RC integrator is used (see Fig. II.4.).

Reproduced with permission of the copyright owner. Further reproduction prohibited without permission.

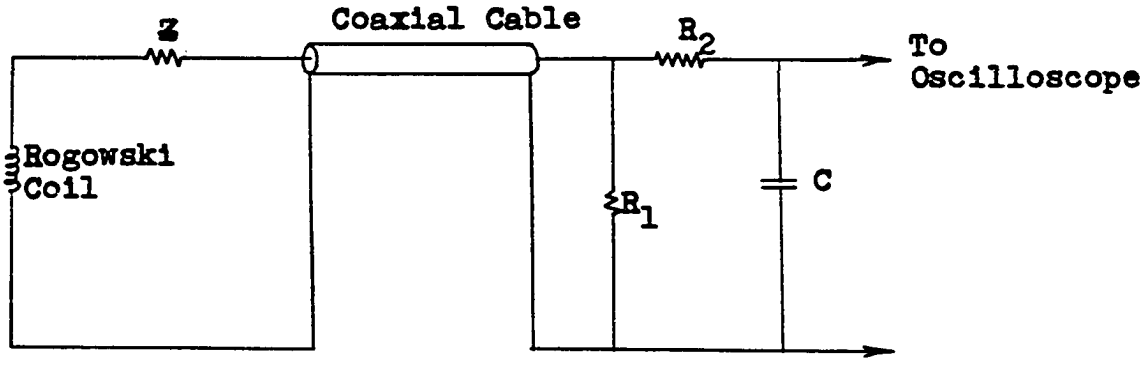

Z = Matching Impedance, 220Ω

R_1= Terminating Resistance, 50Ω

R_2= Integrating Resistance, 100K

C = Integrating Capacitor, 1μF

Fig. II.4. Rogowski Coil Circuit

The vacuum system consists of a Precision Model 150 roughing pump and a Balzer Model 120 diffusion pump. The base pressure of the complete vacuum system is < 1μ Hg measured with a Macleod Gauge. The leak rate of the discharge vessel is ~20μHg per hour.

Reproduced with permission of the copyright owner. Further reproduction prohibited without permission.

Section B - Bias Magnetic Field Apparatus

The source of the bias magnetic field used in the experiment is a pair of Helmholtz coils. The coils are powered by two different capacitor banks. One bank is used to produce a large field (0.6 weber/m^2), and it is connected to the Helmholtz coils through a spark gap switch. At low fields ($\sim$ 0.1 weber/m^2), this spark gap switch cannot be reliably triggered and this necessitates using a second bank which has a solid state triggering device. This extends the operating range of the Helmholtz field to lower values ($\sim$ 0.009 weber/m^2).

Section B.1 - Large Field Bank

The bank consists of 3 Cornell Dubilier (Model NRG 212) capacitors, 220 μF each and rated at 5 kvdc, which are connected in parallel by copper plates 2 mm thick. The capacitors are connected to the Helmholtz coils through a spark gap switch which is located at one end of the bank.

The spark gap switch (see Fig. II.5.) is triggered by a high voltage pulse produced by amplifying the output of a thyratron pulse generator (see Fig. II.6.) with a pulse transformer with amplification of $\sim$ 33. A 660 ohm resistor (1 watt, carbon) is connected in series with the pulse transformer and the trigger pin (see Fig. II.7.). This reduces the electrical noise signals produced by the trigger spark. The characteristics of the bank are given on Page 17.

Reproduced with permission of the copyright owner. Further reproduction prohibited without permission.

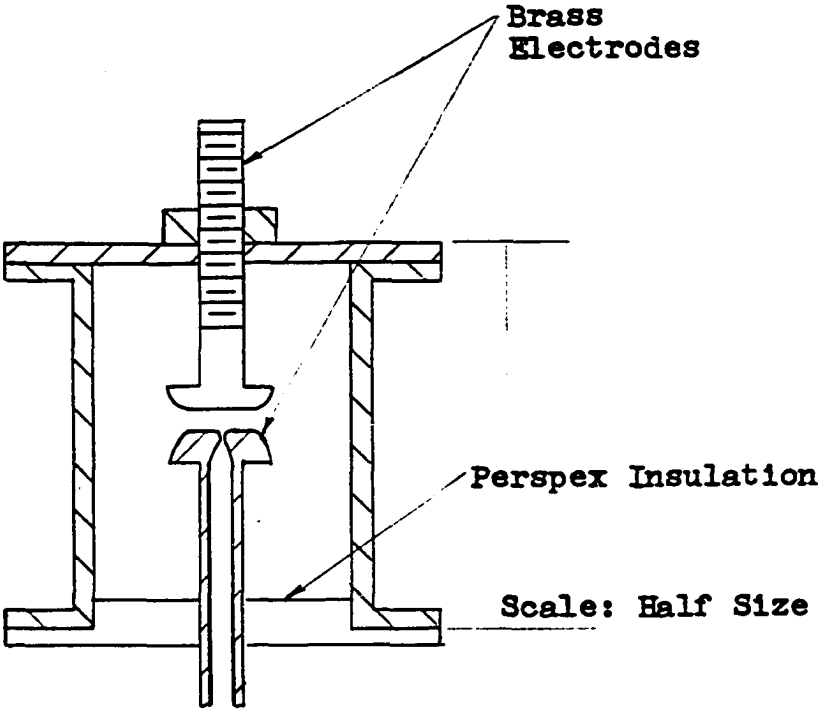

Fig. II.5. Helmholtz Spark Gap Switch

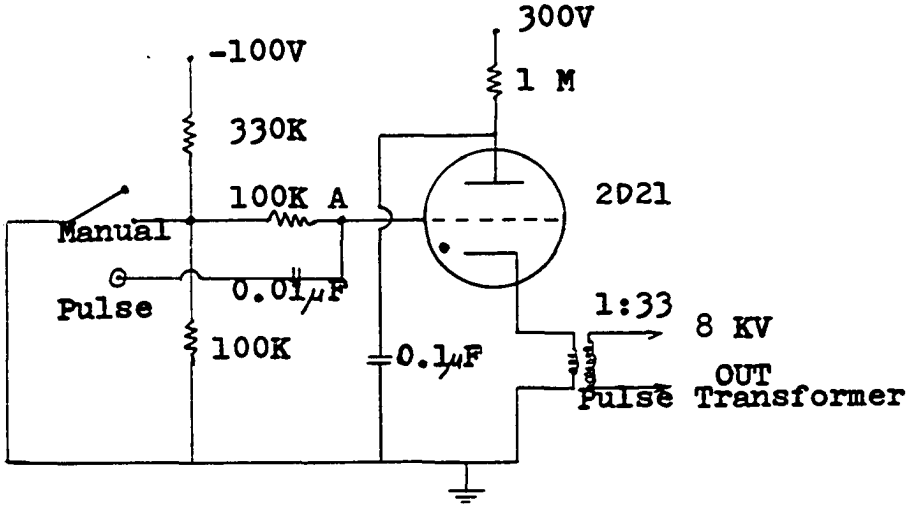

Fig. II.6. Trigger Pulse Generator
(Fires When 'A' is Shorted to Ground)

Reproduced with permission of the copyright owner. Further reproduction prohibited without permission.

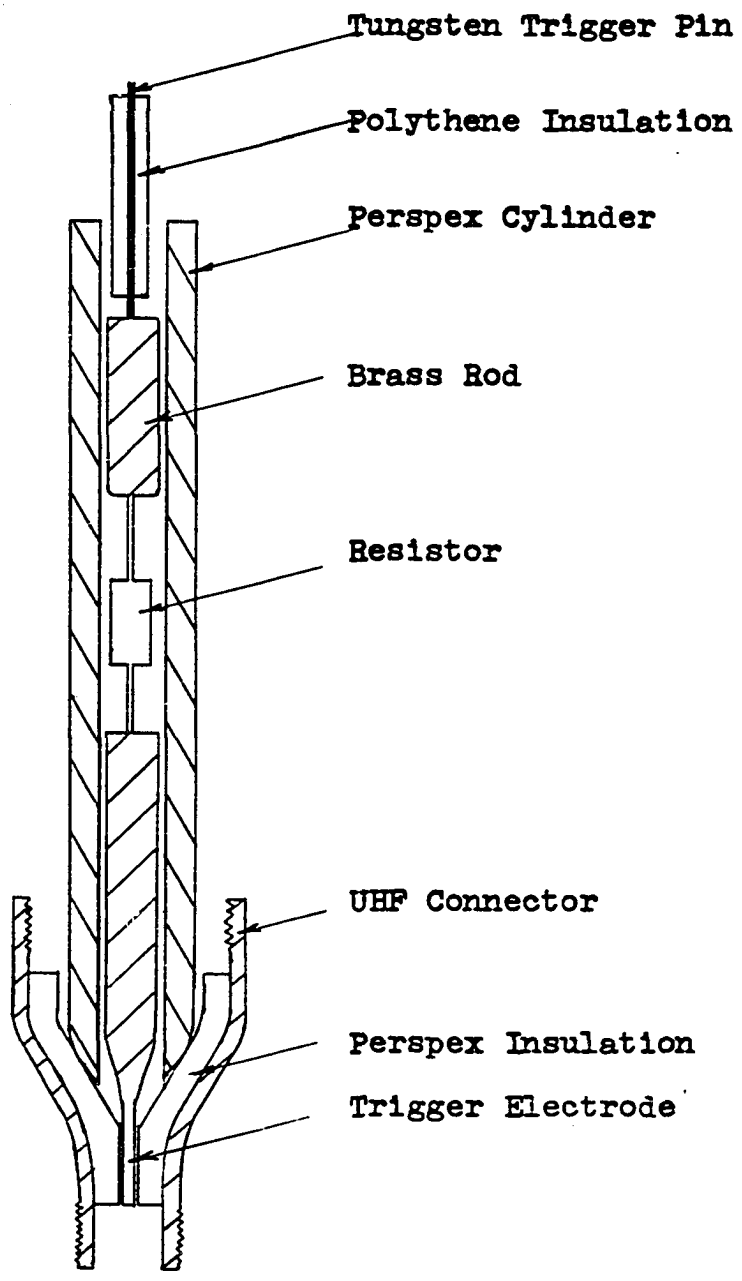

Fig. II.7. Helmholtz Bank Trigger Pin

Reproduced with permission of the copyright owner. Further reproduction prohibited without permission.

Capacitance	660 μ F
Charging Potential	500 v - 3000 v
Total Inductance (with coil)	69 μH
Discharge Period	1.35 msec
Peak Magnetic Field	0.6 weber/m^2

Helmholtz Capacitor Bank

The electrodes of the spark gap switch tend to burn away quickly because of the long time constant of the circuit. It is necessary to readjust the polythene insulation (see Fig. II. 7.) on the trigger pin every $\sim$40 shots, otherwise the spark gap does not have reliable timing characteristics.

Section B.2 - Small Field Bank

The low field bank consists of ten (DCM 539-2657-01) capacitors rated at 10,000 μ F each, at 75vdc. This bank is connected to the Helmholtz coils through a silicon controlled rectifier (C80 Type 2N2542), which serves as a trigger switch. The maximum current produced by this bank is $\sim$400 amps and the time required for the coil current to reach its maximum value is $\sim$2 msec. A trace of the discharge wave form is given in Fig. II.8.

Reproduced with permission of the copyright owner. Further reproduction prohibited without permission.

Time Scale: 1msec/cm Vertical Scale: 160amp/cm

Fig. II.8. Current Waveform For The Small Magnetic Field Capacitor Bank

A circuit diagram is given in Fig. II.9.

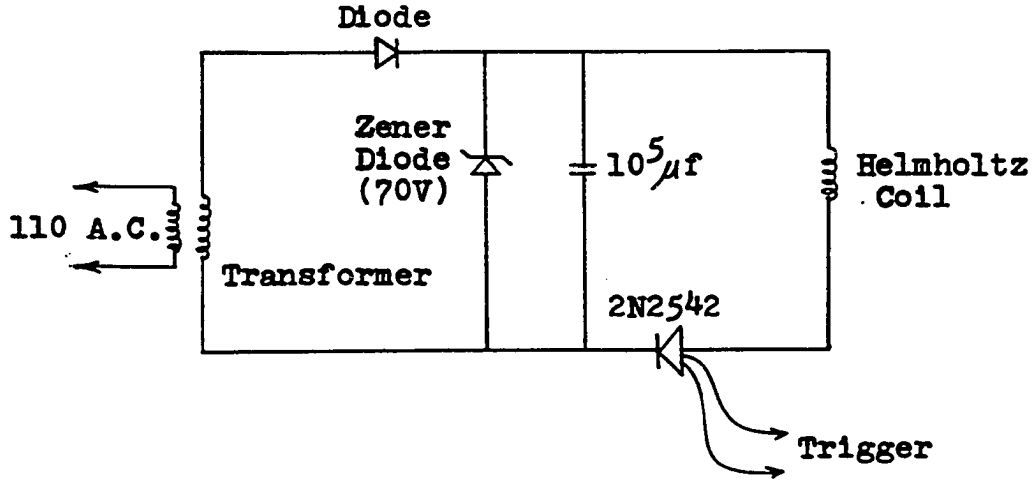

Fig. II.9. Small Magnetic Field Capacitor Bank Circuit Diagram

Reproduced with permission of the copyright owner. Further reproduction prohibited without permission.

Section B.3 - Helmholtz Coil

The Helmholtz coil is constructed as a pair of coils, each having 19 turns of No. 2 AWG copper wire. The inner and outer diameters of coil are 25 cm and 28 cm respectively. The coil frames are made of bakelite and wood, and brass rods are used to hold the frames together. The angle between the axis of the Helmholtz coil and the axis of the theta coil is measured with a large protractor of 25 cm radius (see Fig. II.10.).

The field distributions along the axes AA' and BB' (Fig. II.10.) were measured by a solid state ' Bell 240 Incremental Gaussmeter ' and the results are given in Fig. II. 11. To ensure proper measurements, the gaussmeter probe is rotated about its axis to locate the position of maximum signal before the measurements are taken.

Reproduced with permission of the copyright owner. Further reproduction prohibited without permission.

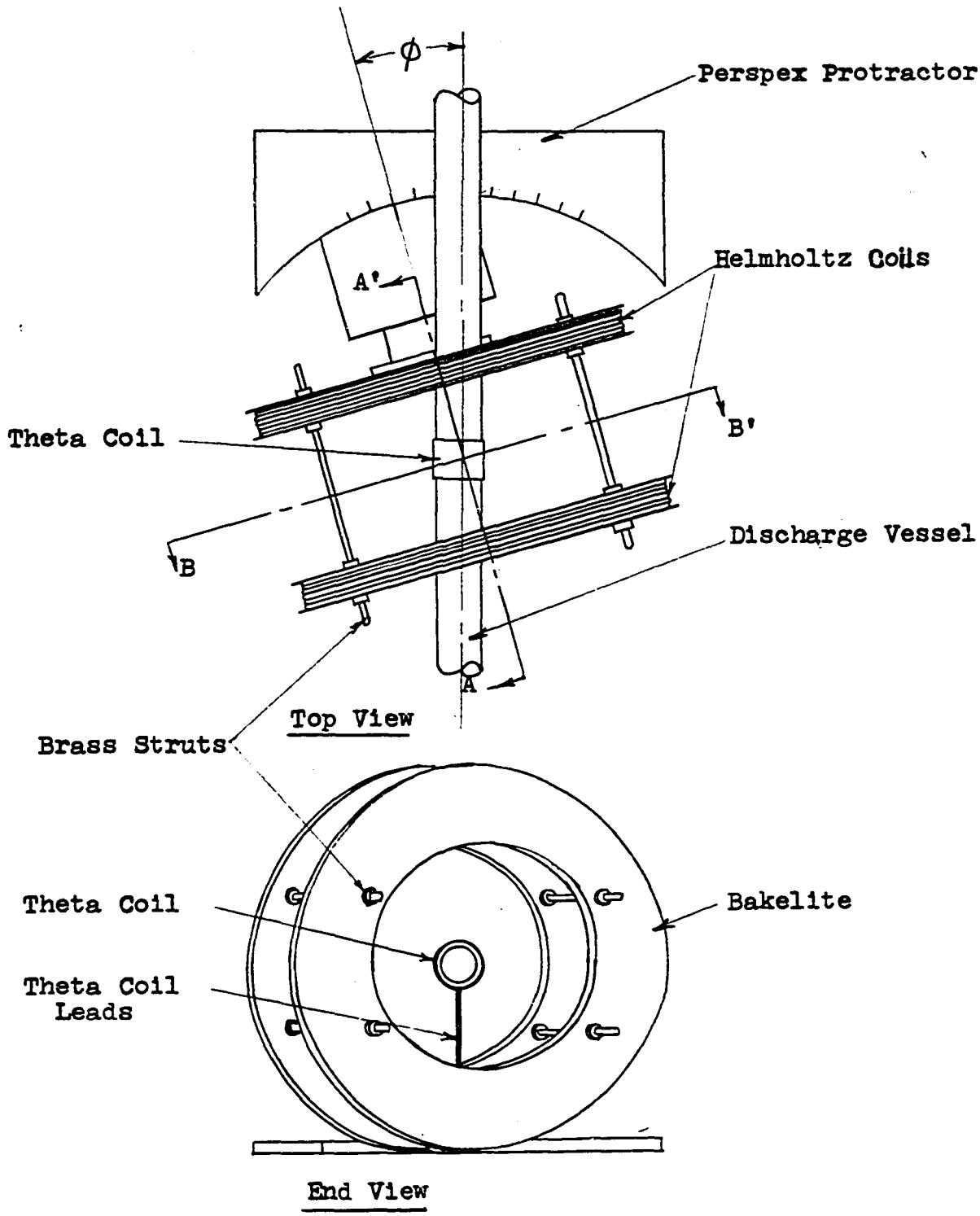

Fig. II.10. Geometric Position Of The Helmholtz Coil

Reproduced with permission of the copyright owner. Further reproduction prohibited without permission.

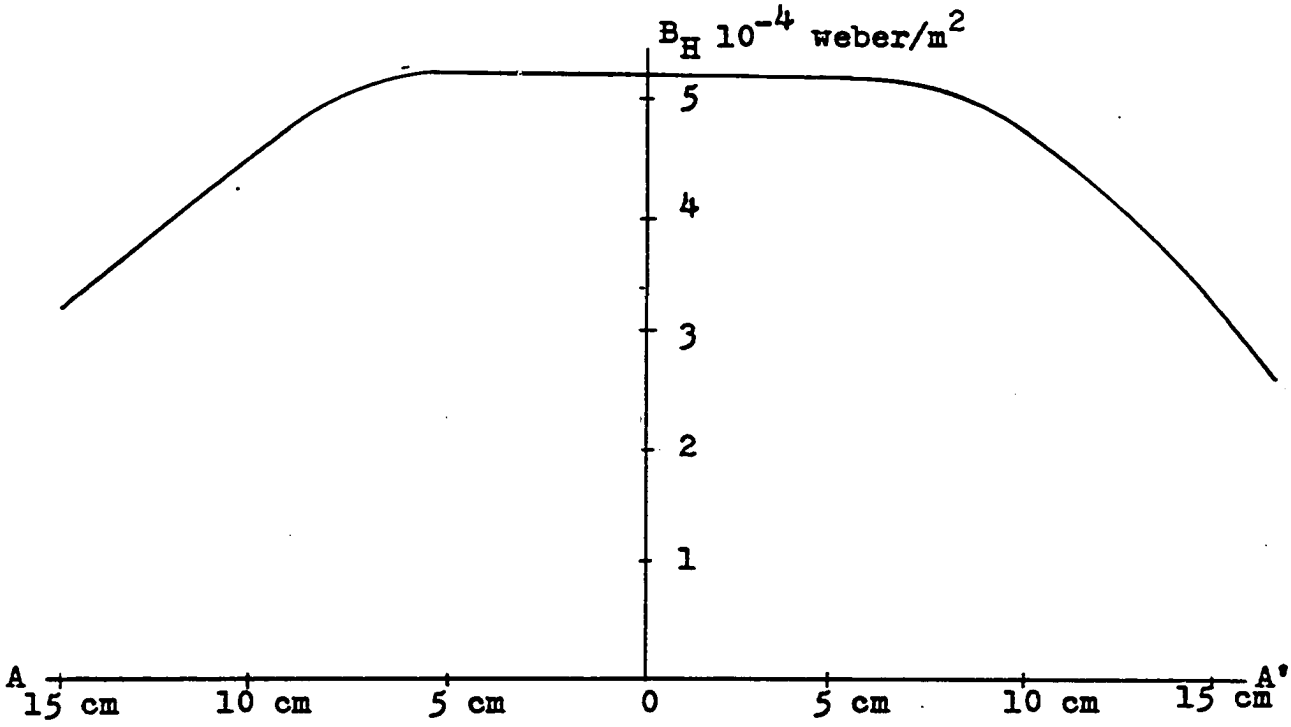

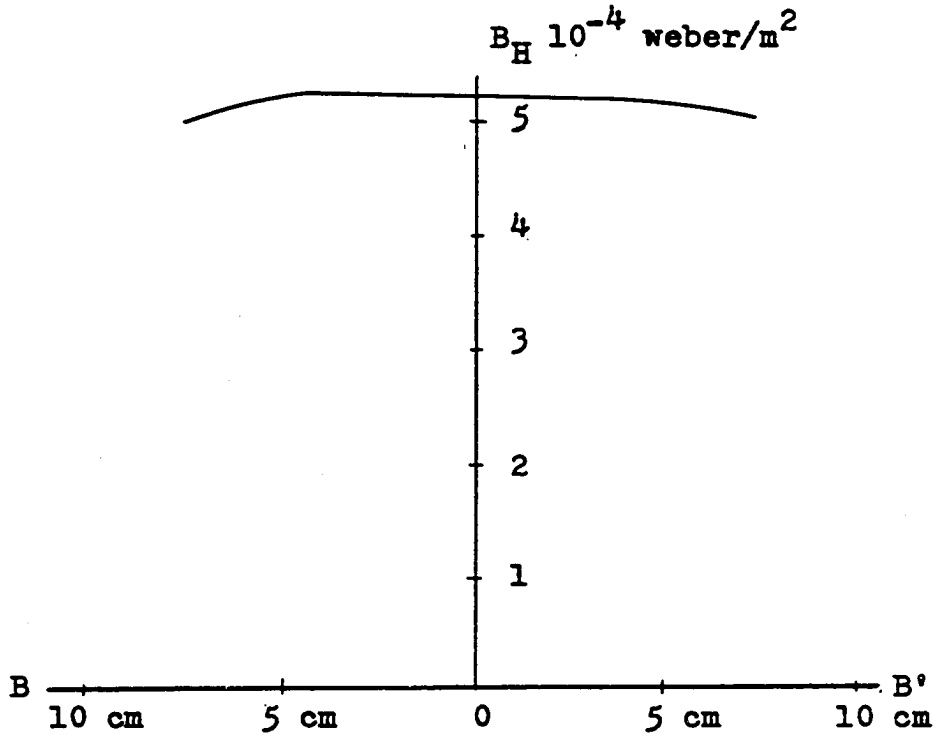

Fig. II.11. Magnetic Field Distribution Along Axis AA' and BB' Of Helmholtz Coils (Coil Current: 2.5 amp/coil)

Reproduced with permission of the copyright owner. Further reproduction prohibited without permission.

Section C - Diagnostic Equipment

Two main diagnostic techniques are used in this experiment. In the first, magnetic probes are employed to measure the magnetic fields associated with the plasma. In the second, a framing camera is employed to measure the shape of the luminous plasma.

Section C.1. - Magnetic Probes

A magnetic probe is essentially a small search coil, (the small size ($\sim$ 1 mm) means that measurements of the magnetic fields can be made with good spatial resolution). An emf, V, is produced between the ends of the coil by a change in the magnetic flux through the coil. Thus a coil placed in a time dependent magnetic field which remains fixed in direction will generate a signal proportional to the rate of change of that magnetic field. If this signal is integrated with an RC circuit (see Fig.II.12.) the resultant signal will be proportional to the total change of the magnetic field B.

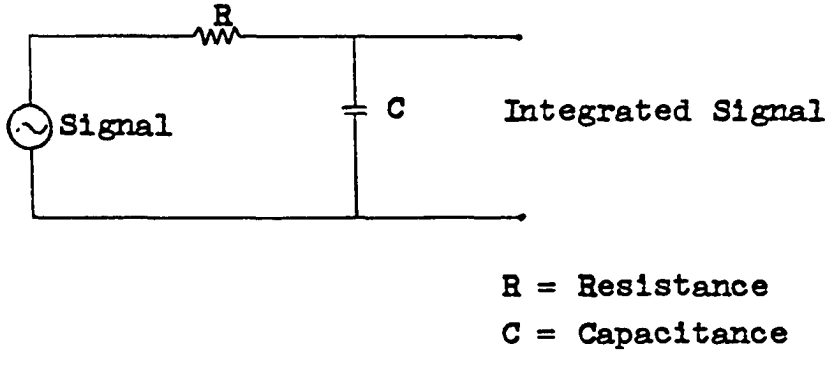

Fig. II.12. RC Integrating Network

Reproduced with permission of the copyright owner. Further reproduction prohibited without permission.

When a signal is integrated, it is also attenuated. The size of the output signal and the distortion both vary inversely with the time constant, RC, of the integrating circuit. Therefore, the time constant must be small enough to produce a measureable signal, but sufficiently large to cause negligible distortion in the integrated waveform. In this experiment, RC is chosen to be ten times the characteristic time of the measured event, (i.e. RC = 10 μ sec for magnetic probes).

In the theory of the probe presented above, the inductance and the stray capacitance of the coil itself have been ignored. These produce a resonant response in the probe signal. Therefore the gain of the circuit will depend on the frequency of the signal measured. This is an undesireable effect which can be removed by damping the resonant response of the probe with a series resistance (Segre and Allen, 1960). This resistance is referred to below as the matching impedance and its value is equal to $\sqrt{\frac{L}{2C}}$ where L is the self inductance of the probe and C is the stray capacitance (see Appendix E).

The frequency response of the "damped" probe has been measured by mounting it inside a solenoid that is connected to a signal generator. The voltage across the leads of the solenoid is measured with an oscilloscope and from this, the rate of change in magnetic field can be calculated. The output signal from the magnetic probe is recorded on the oscilloscope with the circuitry normally employed in the plasma investigation.

Reproduced with permission of the copyright owner. Further reproduction prohibited without permission.

The plasma current is monitored by two types of magnetic probes. The first is a single axial probe to detect the radial hydromagnetic oscillations in the plasma (Niblett and Green, 1959); for further details see Chapter III. The second, is a directional probe to measure the rotation of the plasma ring about its diameter. Each probe is described below in more detail.

Section C.1a - Single Axial Probe

The single axial probe consists of 35 turns of thin copper wire, No. 44 (AWG) wound on a glass rod ~ 1 mm in diameter. Much care is used in winding the coil uniformly and the coil is held together by epoxy glue. The leads are tightly twisted together so that the net magnetic flux enclosed by the coil leads ($\int_{\text{AREA ENCLOSED BY LEADS}} \underline{B} \cdot d\underline{A}$) is negligible in comparison to the magnetic flux enclosed by the coil (see Fig. II.13.).

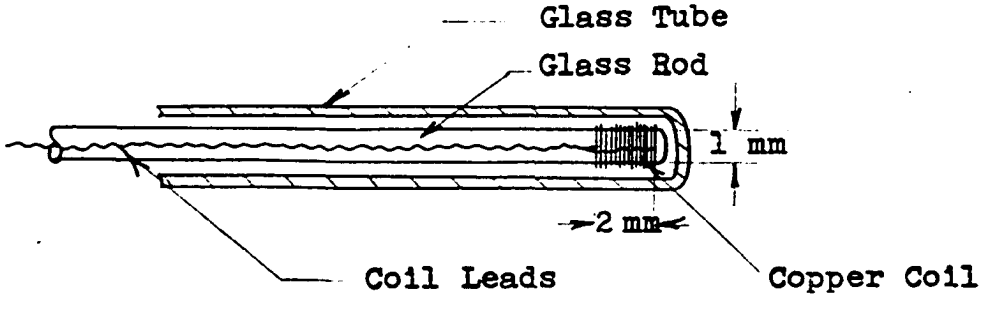

Fig. II.13. Axial Magnetic Probe

Reproduced with permission of the copyright owner. Further reproduction prohibited without permission.

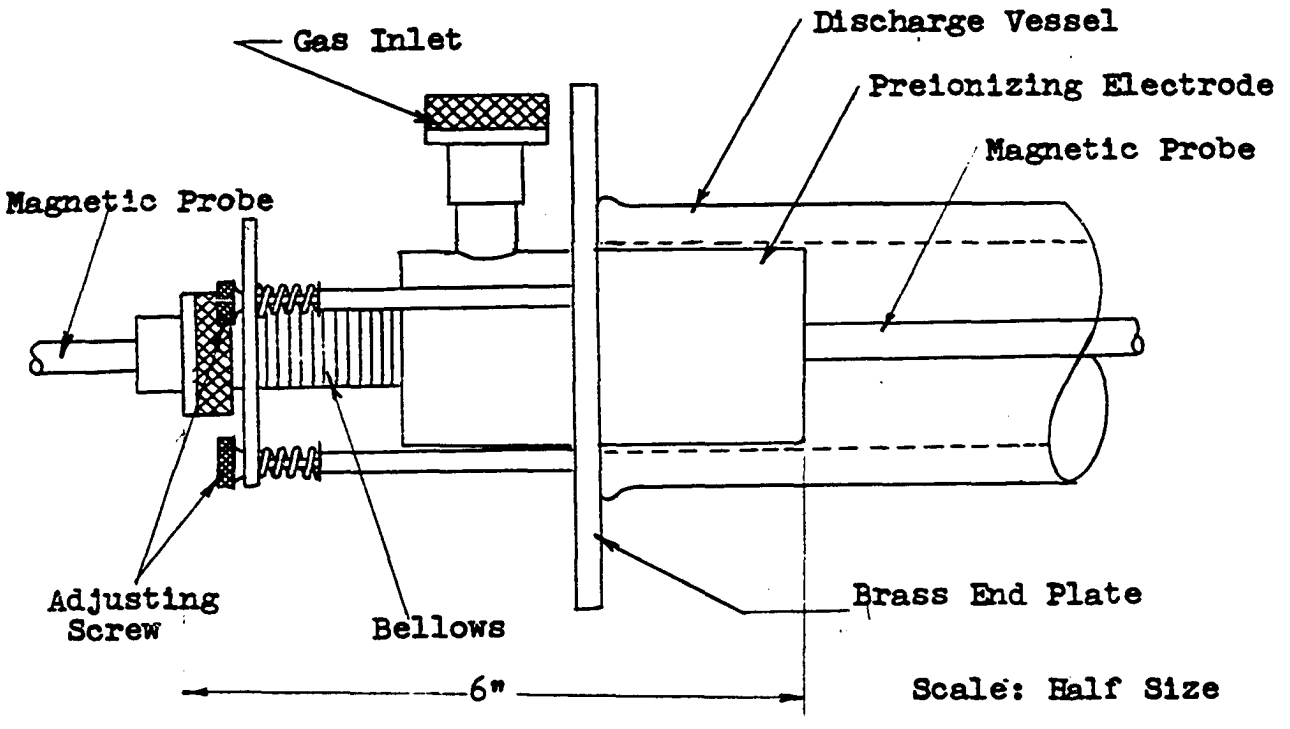

Fig. II.14. Method Of Mounting Probe In The Theta Pinch Discharge Vessel

The probe rod is joined to another glass rod of larger diameter for rigidity. The whole probe system is then inserted into a glass tube 75 cm long and 5 mm dia. to protect the probe from the plasma. The glass tube is supported by a flexible joint at one end of the discharge tube as shown in Fig. II.14, and is positioned in the center of the theta coil by a set of adjusting screws on the electrode.

The probe leads are connected to the oscilloscope by RG 58 coaxial cable which is terminated in its characteristic impedance so as to reduce reflections of the signal in the cable.

Reproduced with permission of the copyright owner. Further reproduction prohibited without permission.

The matching impedance of the probe is calculated (see Appendix E) to be 43Ω. The terminating resistance for the cable is 50Ω and this resistor therefore also serves to match the impedance of the probe.

The signals are displayed on a Tektronix 551 double beam oscilloscope with a Type G differential preamplifier, and are recorded by a Polaroid Land camera. The probe signal is proportional to $\frac{d}{dt}(I_c + I_p)$ where I_c is the coil and I_p is the plasma current per length. To obtain $\frac{dI}{dt}$, a suitably attenuated signal from the Rogowski coil (i.e. $\frac{dI}{dt}$, see Page 13) is subtracted from the magnetic probe signal. This procedure will be referred to below as the 'double probe technique', (Green, 1962). A potential divider is placed across the output leads of the Rogowski coil and is adjusted to obtain the suitably attenuated signal. Thus, if the theta bank is discharged with no resultant plasma formation, then there should be no net signal produced.

To obtain the plasma current I_p, the probe and the Rogowski coil signals are integrated by an RC circuit (see Fig. II.4.). The characteristic time of the plasma current oscillation is $\sim 1\mu$sec, thus the integrating time constant, RC, chosen is 10μsec.

It is found that the capacitative coupling between the plasma and the magnetic probe leads to no recordable signal. This is determined by replacing the normal probe by a straight wire and comparing the signal obtained with the normal probe signal (see Fig. II.15.).

Reproduced with permission of the copyright owner. Further reproduction prohibited without permission.

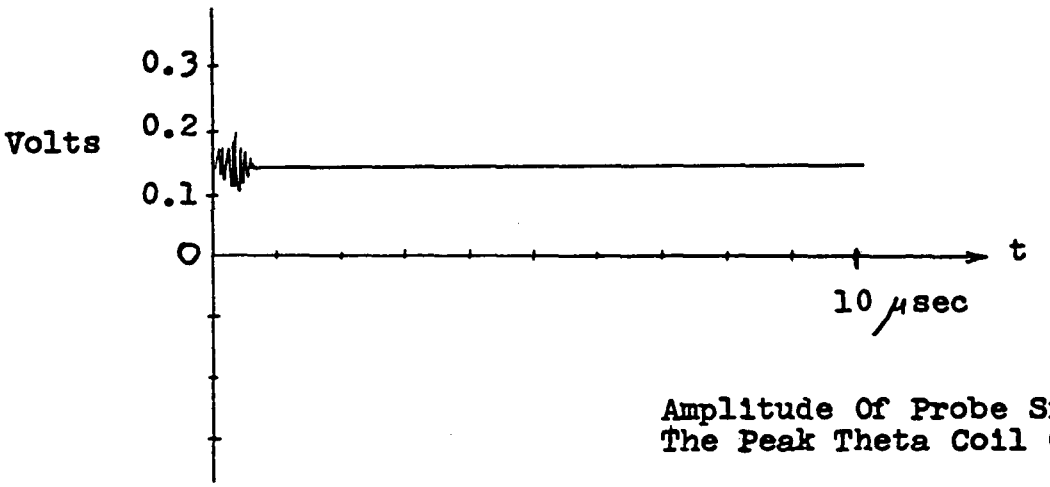

Fig. II.15. Capacitative Coupling Signal From Magnetic Probe

The frequency response of the axial probe is given in Fig. II.16.

Section C.1b - Directional Probe

In general if the magnetic field varies in direction, 3 probes are needed to measure the field completely. However, if the plane of rotation is known, then only two probes are needed. For the experiments described below, a 'V' shaped probe has been used for this purpose. Using the geometric relations and the signals from the two probes, the direction and strength of the magnetic field in the plane of the probe can be calculated.

The directional probe consists of two coils (20 turns) of No. 44 AWG copper wire wound on a 'V' shaped glass rod $\sim$ 1 mm in diameter and $\sim$ 2 mm in length (see Fig. II.17.).

Reproduced with permission of the copyright owner. Further reproduction prohibited without permission.

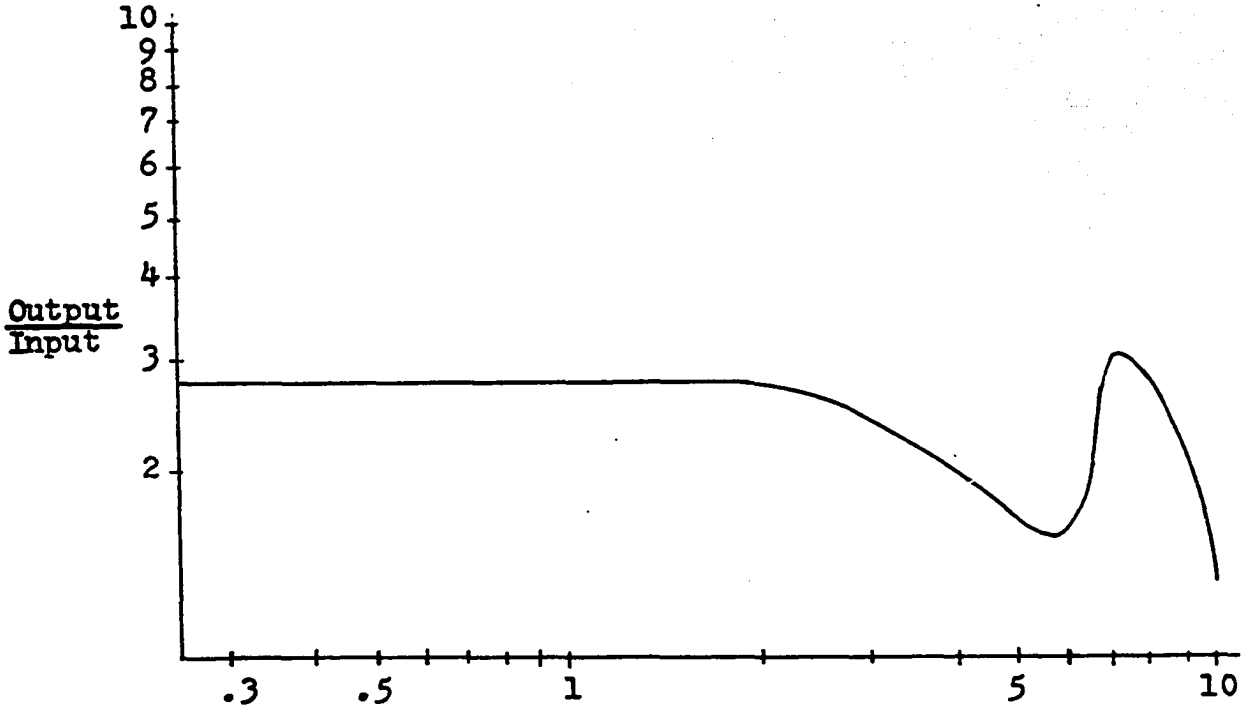

Fig. II.16. Frequency Response Of Axial Magnetic Probe (Integrated Output)

Reproduced with permission of the copyright owner. Further reproduction prohibited without permission.

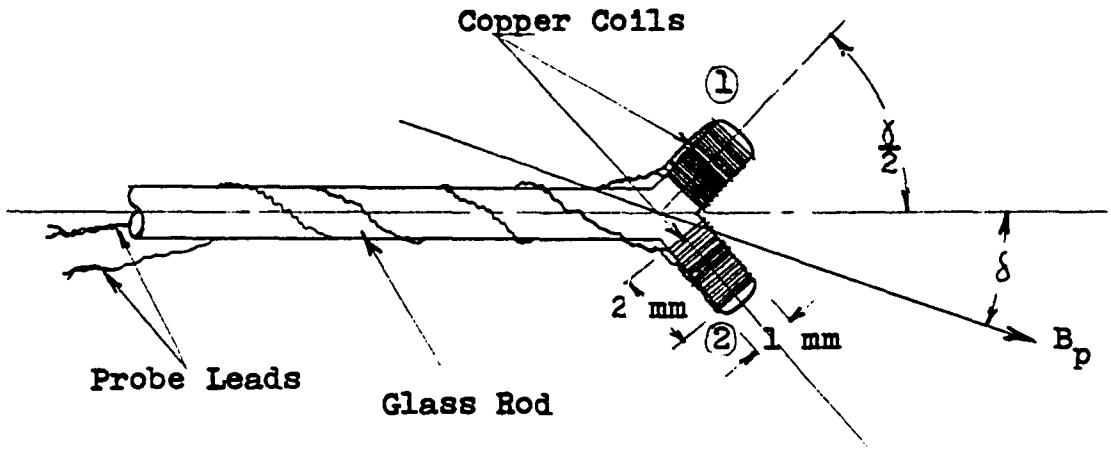

B_p = Plasma Magnetic Field

Fig. II.17. Directional Probe

For convenience the response of both probes should be identical for a given flux change through each probe because the probe signals are quantitatively compared with one another. To satisfy this requirement, both probes are constructed with identical geometry and the output signals are finely balanced by use of a potential divider on one of the probes. The stem of the directional probe is identical to the stem of the single axial probe.

By integrating the signals from the two probes and using the double probe technique (Page 26), the net signals will then correspond to the plasma magnetic field, B_p.

To calculate the direction of the magnetic field from the output signals of the 'V' shaped probes, it is necessary that the magnetic field be approximately uniform over the volume occupied by the two probes and be coplanar with probes 1 and 2 (see Fig. II.17.). Then the signals received from probe 1 (V_1) and

Reproduced with permission of the copyright owner. Further reproduction prohibited without permission.

probe 2 (V_2) are $V_1 = V_0\cos(\frac{\gamma}{2} + \delta)$

(1) $= V_0(\cos\frac{\gamma}{2}\cos\delta - \sin\frac{\gamma}{2}\sin\delta)$

and $V_2 = V_0\cos(\frac{\gamma}{2} - \delta)$

(2) $= V_0(\cos\frac{\gamma}{2}\cos\delta + \sin\frac{\gamma}{2}\sin\delta)$,

where γ is the angle between the axes of the two probes and δ is the angle between B_p and the theta coil axis (see Fig. II.17.). By combining these two signals and letting $\gamma = 90^\circ$, then

$$\frac{V_1}{V_2} = \frac{\cos 45^\circ\cos\delta - \sin 45^\circ\sin\delta}{\cos 45^\circ\cos\delta + \sin 45^\circ\sin\delta}$$

(3) $$= \frac{\cos\delta - \sin\delta}{\cos\delta + \sin\delta}$$

Therefore, knowing the values of V_1 and V_2 as a function of time, the angle δ can also be determined as a function of time. The frequency response of each probe is given in Fig. II.18. (For the experimental procedure, see Chapter III, Section B.4).

Section C.2 - High Speed Framing Camera

The Barr and Stroud Model CP5 high speed rotating mirror framing camera can photograph 60 frames at a maximum rate of 8×10^6 frames/sec.

It consists essentially of an objective lens, L_1 (see Fig. II.19.) and a magnifier lens, L_2, which focuses the image on the surface of the rotating mirror. A lens quadrant, L_3, focuses the mirror surface on the curved film track.

The polished stainless steel mirror runs in flexible mounted white metal bearings. It is driven at a maximum rate of 330,000 r.p.m. by an air turbine operated at 40 psig.

Reproduced with permission of the copyright owner. Further reproduction prohibited without permission.

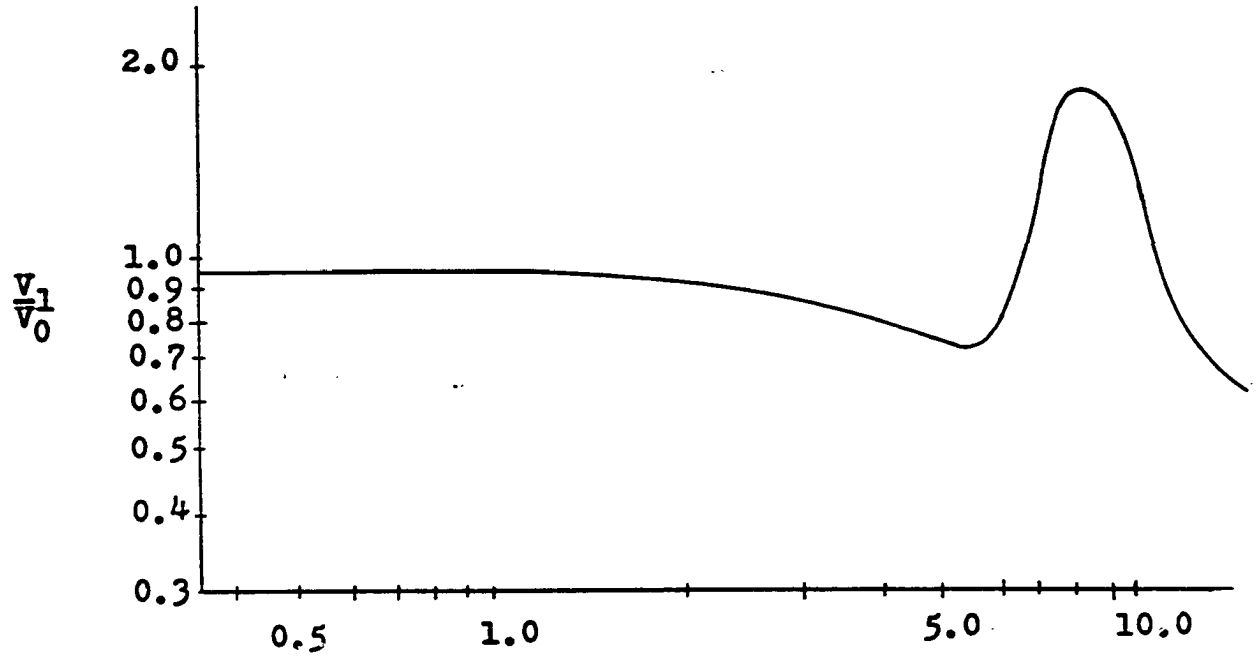

(a) Probe 1

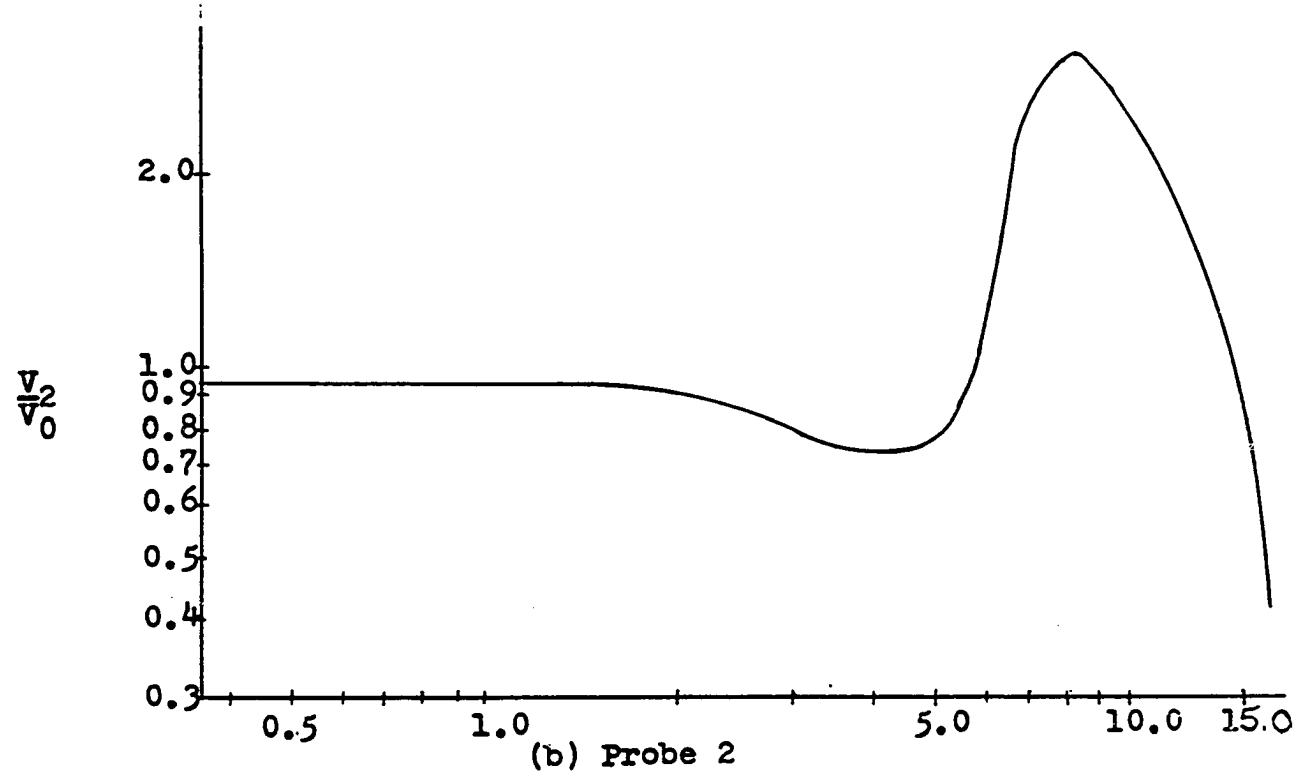

(b) Probe 2

Fig. II.18. Frequency Response Of Directional Probe

Reproduced with permission of the copyright owner. Further reproduction prohibited without permission.

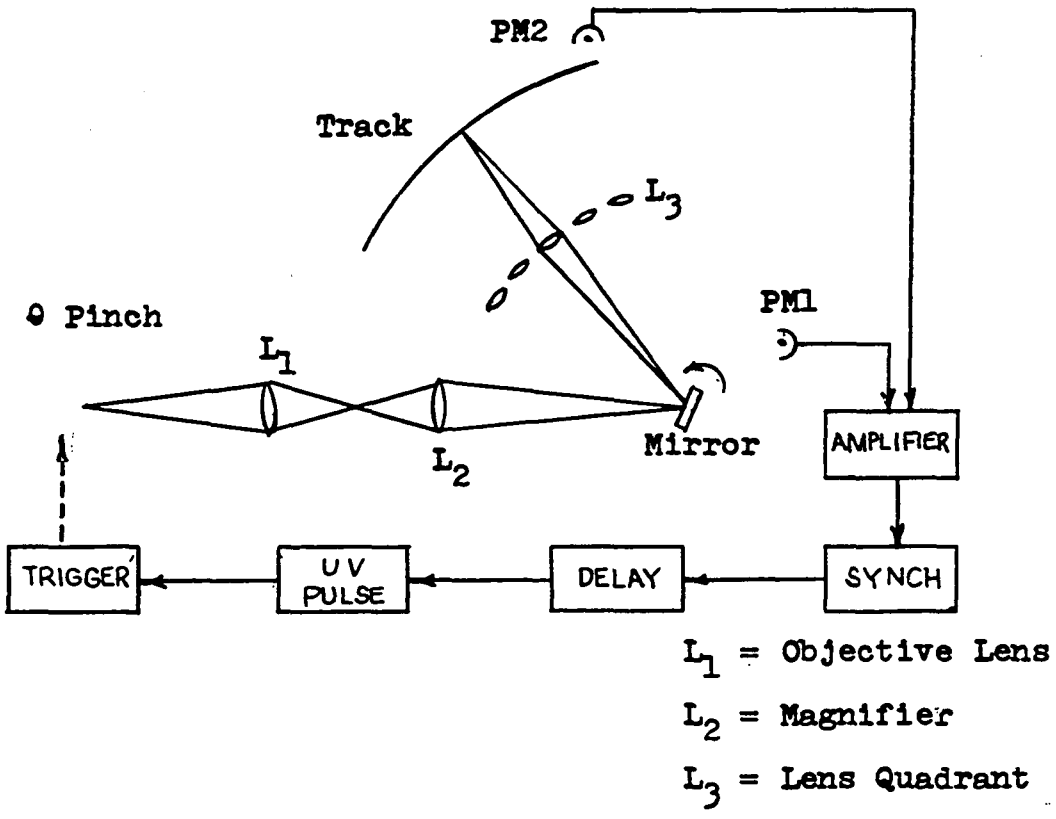

Fig. II.19. Framing Camera Schematic

The event to be photographed must be synchronized with the position of the rotating mirror, since recording can only take place during 15° of each half revolution of the mirror. A pulse to initiate the theta pinch discharge is provided by one of the two photomultipliers, PM 1 or PM 2. Light from a 6 volt lamp is reflected from a part of the mirror surface and directed by a prism to the photomultiplier, so it gives pulses synchronized with the mirror position. The mirror speed is monitored by a frequency meter which receives a signal from a search coil adjacent to a magnetized collar on the mirror shaft.

Reproduced with permission of the copyright owner. Further reproduction prohibited without permission.

CHAPTER III

RESULTS

In this chapter, the experimental measurements of the dynamic behaviour of the plasma with and without a bias magnetic field are presented and discussed. The characteristics of the magnetic probe signals and the framing camera pictures describing the plasma with no bias field are studied. Then by comparing these characteristics with those for a discharge in a bias field, the effect of the bias field on the plasma can be obtained. A theoretical model is then constructed to assist in the interpretation of the results. The predictions of this model are compared with the experimental results and the limitations of the model are discussed.

Section A - Discharge Of Theta Bank With No Bias Field

Experimental Procedure

The discharge tube is evacuated to $< 1 \mu$ Hg pressure and then filled with air to the required pressure as measured by a Macleod Gauge ($\pm$ 5%). The discharge tube is then isolated from the pumping system by a valve and the theta bank is charged to the required potential. Subsequently the Theophanous pulse generator is triggered (manually for the magnetic probe experiments, or by photomultiplier pulses for the framing camera experiments), thus closing the theta spark gap switch (see Page 8).

Reproduced with permission of the copyright owner. Further reproduction prohibited without permission.

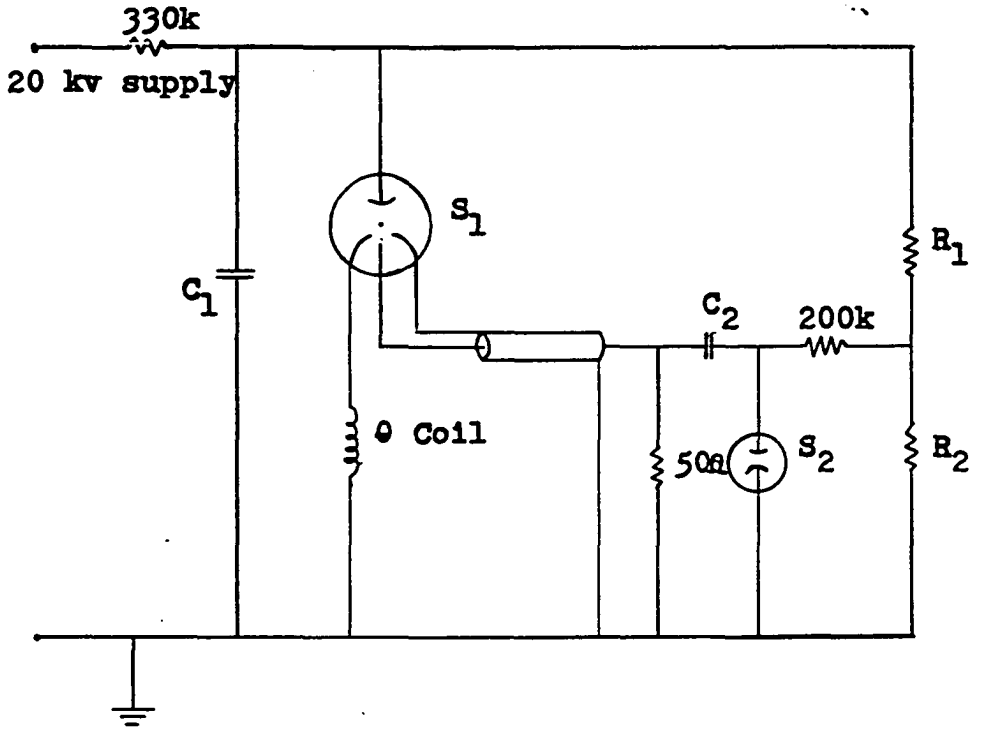

R_1, R_2 = Potential Divider

$C_1 = 25\mu F$

$C_2 = 0.05\mu F$

S_1 = Theta Bank Spark Gap

S_2 = Ultra Violet Trigger

Fig. III.1. Schematic Of Theta Pinch Discharge

Reproduced with permission of the copyright owner. Further reproduction prohibited without permission.

and discharging the capacitor bank. Using the integrated Maxwell's equation, the strength of the azimuthal electric field induced in the discharge tube varies in the following manner:

(1) $$E = \frac{\mu}{2} r \frac{dI}{dt} c ,$$

where r = radius from the axis

I_c = theta coil current per unit length

For coil currents I_c which vary sinusoidally with time, $\frac{dI}{dt}c$ (and therefore E) is maximum when the current goes through zero. Hence, with appropriate conditions, a plasma cylinder will be formed when the theta coil current I_c, goes through zero. If the plasma forms before the theta current reverses, (see Fig. III.2. Position B) the plasma current is compressed to the walls of the discharge vessel by the magnetic forces. Hence, before radial contraction begins, the plasma shell has a definite mass (see Fig. III.3.).

When no bias magnetic field is used, the gas initially breaks down at the end of the first half cycle of the coil current (see Fig. III.2. Position B). As soon as the magnetic field external to the plasma becomes larger than the magnetic field within it, the plasma shell contracts radially and then executes radial oscillations about an equilibrium position (see Fig. III.2. Position D). Further details of these oscillations (which have been discussed by Niblett and Green, 1959) are given in the next section (Page 68).

Reproduced with permission of the copyright owner. Further reproduction prohibited without permission.

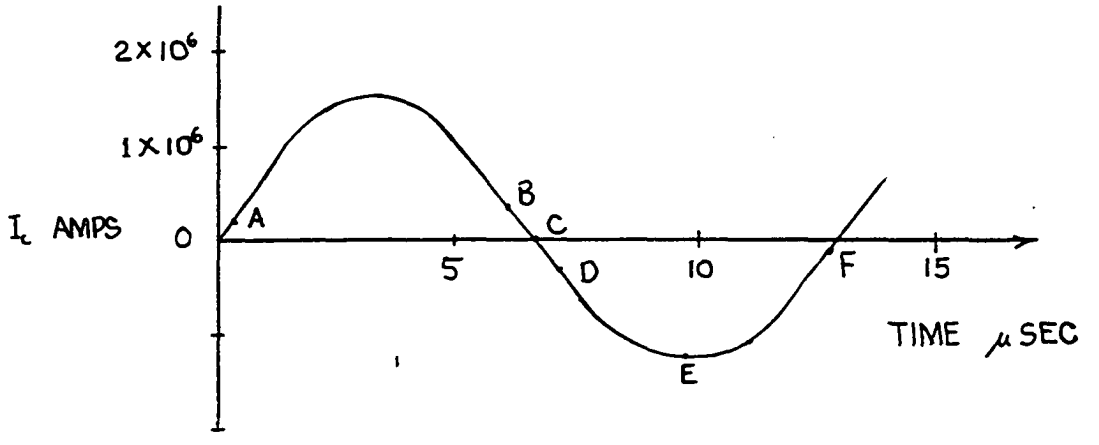

Fig. III.2. Theta Current Waveform

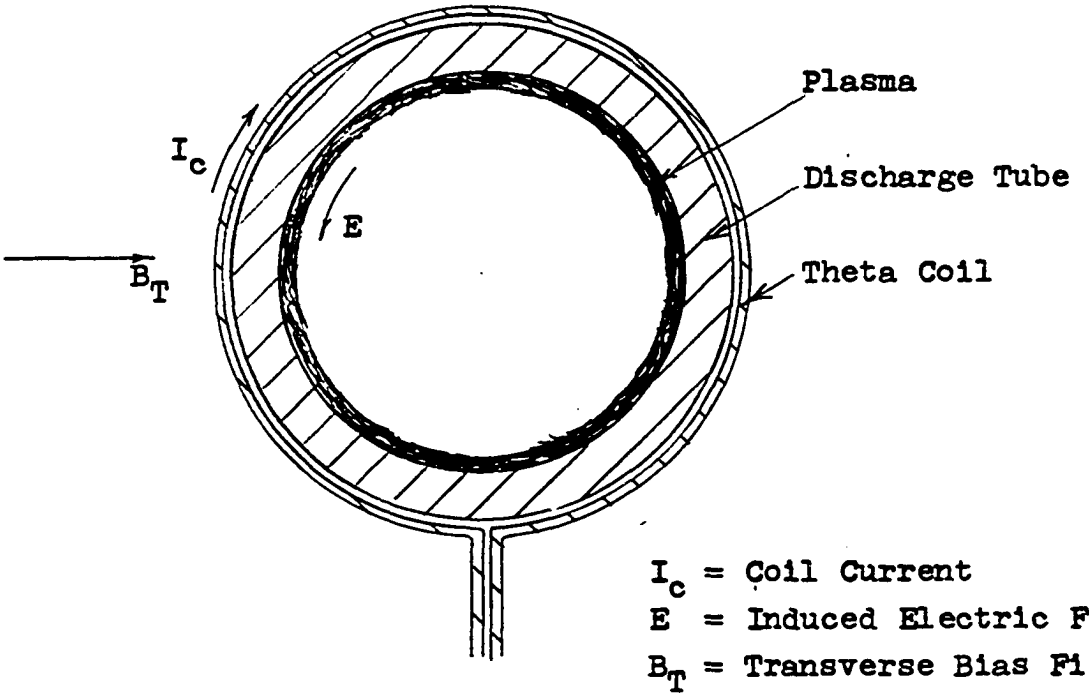

Fig. III.3. Formation of The Plasma Shell

Reproduced with permission of the copyright owner. Further reproduction prohibited without permission.

As the theta current approaches its maximum value (Fig. III. 2. Position E) the electric field goes to zero and the plasma dissipates. When the theta coil current again approaches zero (Fig. III.2. Position F) the breakdown cycle is reiterated. This phenomenon recurs at each half cycle of the coil current until the peak induced electric field is too small to cause a breakdown in the gas.

A magnetic probe placed on the axis in the theta coil records the rate of change in the magnetic field strength within the coil cross section. The integrated signal (see Page 38) corresponds to the change in the magnetic field. In the absence of a plasma, the probe records the change in the theta coil magnetic field. However, when the electric currents flow in the plasma, these produce magnetic fields which are superposed on the theta coil fields. From the flux conservation theorem, that is, $\int_{\text{PLASMA CROSS SECTION}} \underline{B}.d\underline{A}$ = constant, the total magnetic flux enclosed in a plasma ring is constant with respect to the radial motion. Consequently, when the radius of the plasma ring contracts, the strength of the enclosed magnetic field increases. Similarly, when the plasma expands radially, the enclosed magnetic field strength decreases. Thus, when plasma executes radial oscillations, the corresponding oscillations in the magnetic field are recorded on the magnetic probe waveform. A typical integrated probe signal is given in Fig. III.4.

Reproduced with permission of the copyright owner. Further reproduction prohibited without permission.

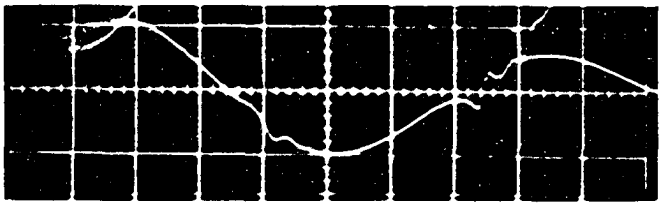

Time - 2 μsec/cm Pres.- 50 μHg, Gas-Air (upper waveform)

Fig. III.4. Integrated Magnetic Probe Signal

The corresponding framing camera pictures of the discharge show that, at breakdown, a plasma sheet is formed at the walls of the discharge tube. This then collapses radially to the equilibrium position about which it executes radial oscillations. The radial oscillations are not clearly seen because the time resolution of the camera is approximately 1/2 the period of radial oscillation. Thus, the oscillatory radial motions are smeared out.

Framing camera pictures have been taken from the ends of the coil (see Fig. III.5.) and from the top of the coil (Fig. III. 6.). There is no evidence of axial motion.

Reproduced with permission of the copyright owner. Further reproduction prohibited without permission.

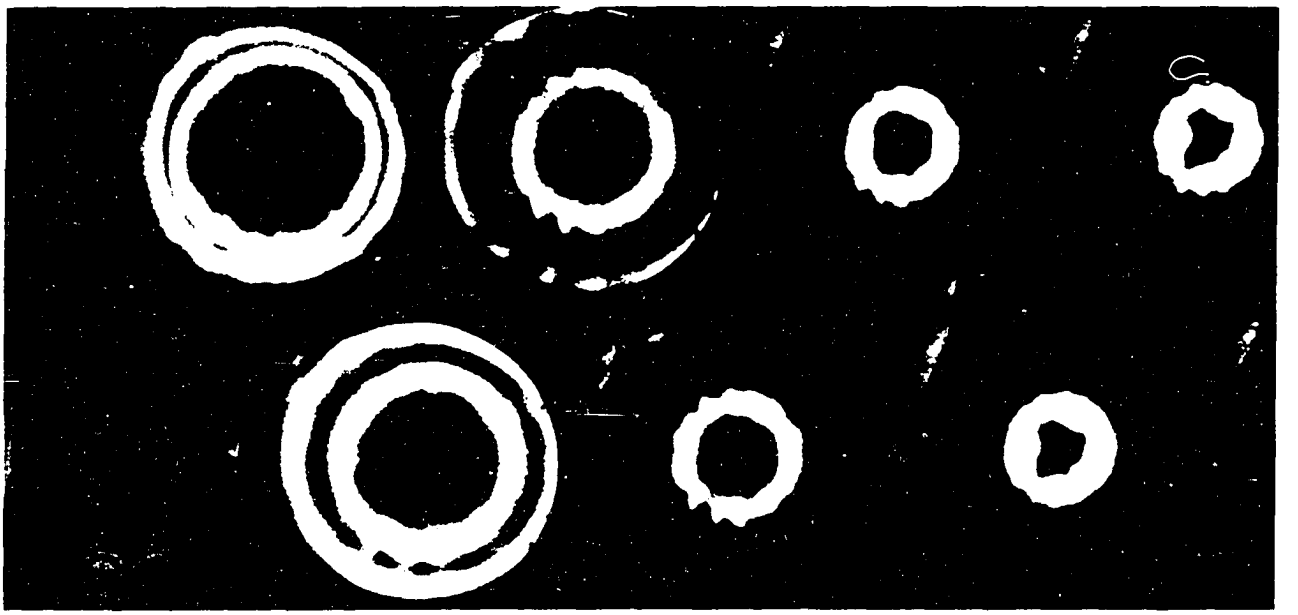

Time Increases Left to Right, Frame Positions are Staggered,
Pres: 50 μ Hg Air, Exposure Time $\sim$ 0.35 μsec.

Fig. III.5. End-On Photograph (B_H=0)

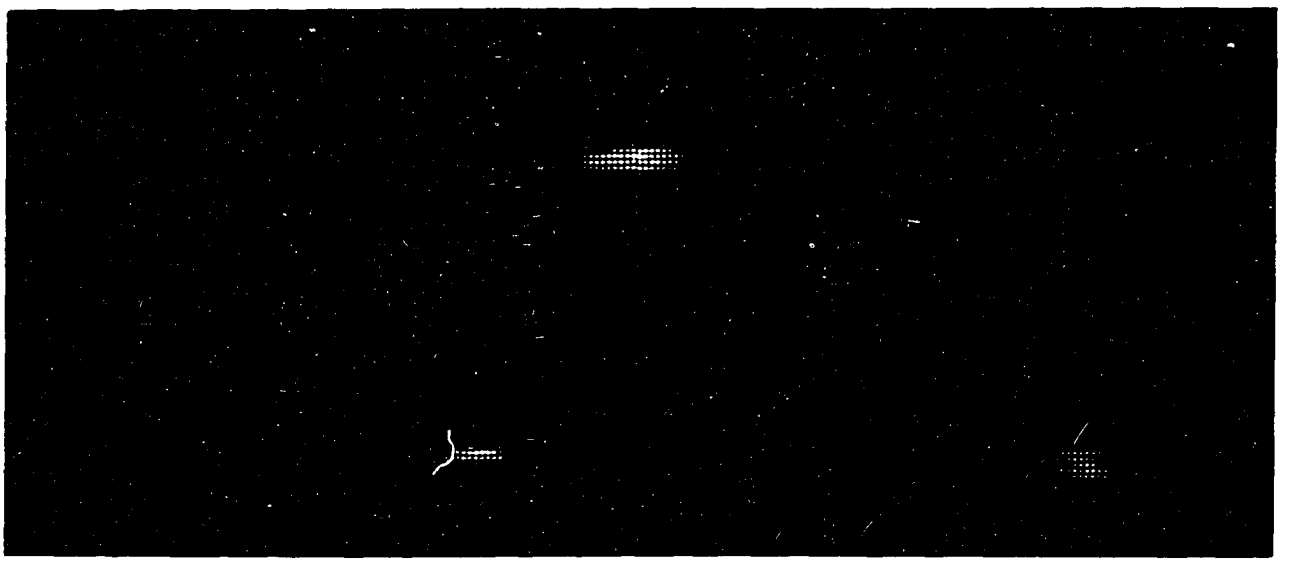

Pres: 75 μ Hg

Fig. III.6. Top-On Photograph (B_H=0)

Reproduced with permission of the copyright owner. Further reproduction prohibited without permission.

Since the coil dimensions and charging potential of the theta bank are not changed in the experiments described between pages 39 and 68, they are stated below and are referred to wherever the information is required, i.e. in figures.

Standard Discharge Conditions

Theta coil diameter	6.1 cm
Theta coil length	6.4 cm
Charging potential of the theta bank	13.3 kv
Capacity of theta bank	25 μf
Peak current in the theta bank	165 kamp
Period of the theta coil current	13.0 μsec

Section B - Theta Pinch With A Bias Field

In the presence of a transverse magnetic field (see Fig. III.3.), axial Lorentz forces exist and these tend to drive the plasma out through the ends of the coil. The combination of the axial and radial motions causes the plasma to appear to rotate (i.e. flip) about a diameter specified by the direction $\underline{B}_H \times \underline{B}_{coil}$ where $\underline{B}_H$ is the bias field and $\underline{B}_{coil}$ is the theta coil field. If the axial velocity is low, radial oscillations can develop. However, as the axial velocity increases the plasma escapes out through the ends of the coil before the oscillations can develop, i.e. oscillations are suppressed.

The bias field B_H is produced by discharging a capacitor bank through the Helmholtz coils. Although the bias magnetic field oscillates (period is $\sim$ 1.3 msec.), the period is long

Reproduced with permission of the copyright owner. Further reproduction prohibited without permission.

compared to the life time of the discharge plasma ($\sim$2-3 μsec.). Hence for the duration of the discharge, the bias magnetic fields are approximately constant. In practice, the experiments are performed by firing the discharge when B_H is at its maximum value. To achieve the proper triggering of the theta and Helmholtz banks, two different methods are employed. The method used in the magnetic probe experiments is relatively simple and is discussed first. This will be followed with the method employed in the framing camera experiments.

Magnetic Probe System

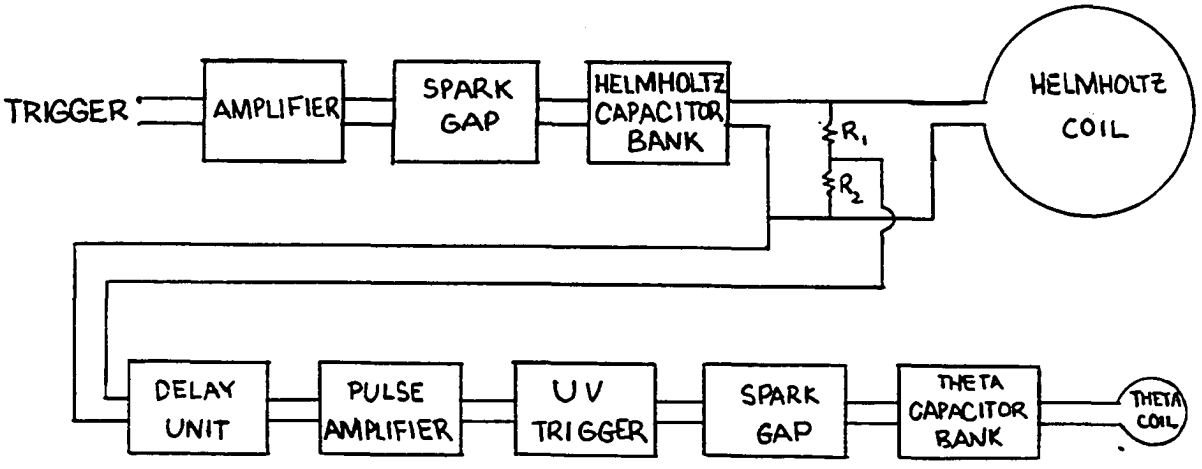

R_1, R_2 = Potential Divider

Fig. III.7. Bias Field Trigger Circuit For The Magnetic Probe

Reproduced with permission of the copyright owner. Further reproduction prohibited without permission.

For the magnetic probe measurements, the Helmholtz bank is triggered manually and a potential divider across the leads of the Helmholtz coil generates a signal which activates the delay unit (Fig. III.7.). Then at a specified delay time, i.e. when the Helmholtz field is maximum, the delay unit emits a pulse which triggers the theta bank.

Framing Camera System

In the framing camera experiments the method for triggering is more complicated because the theta bank must be discharged when the rotating mirror is at a given position (see Page 32) and the Helmholtz field is maximum. This is accomplished in the following way, (see Fig. III.8.). When the framing camera rotor is running at the required speed, the output pulse from one of the photomultipliers triggers the Helmholtz bank. The same pulse also triggers a delay unit which is adjusted to give an output pulse when the Helmholtz field, B_H, is at its maximum value. The delayed pulse is fed into a gate circuit together with the photomultiplier pulses from the framing camera. Hence the first photomultiplier pulse arriving after B_H has reached its peak value, triggers the theta pinch discharge. Consequently, the framing camera records photographs of a theta pinch discharge which has been produced in an essentially constant bias field, B_H. In order to fire the theta bank at peak values of B_H, the mirror speed is selected so that the time interval between the photomultiplier pulses t_m is an integral multiple of (where

Reproduced with permission of the copyright owner. Further reproduction prohibited without permission.

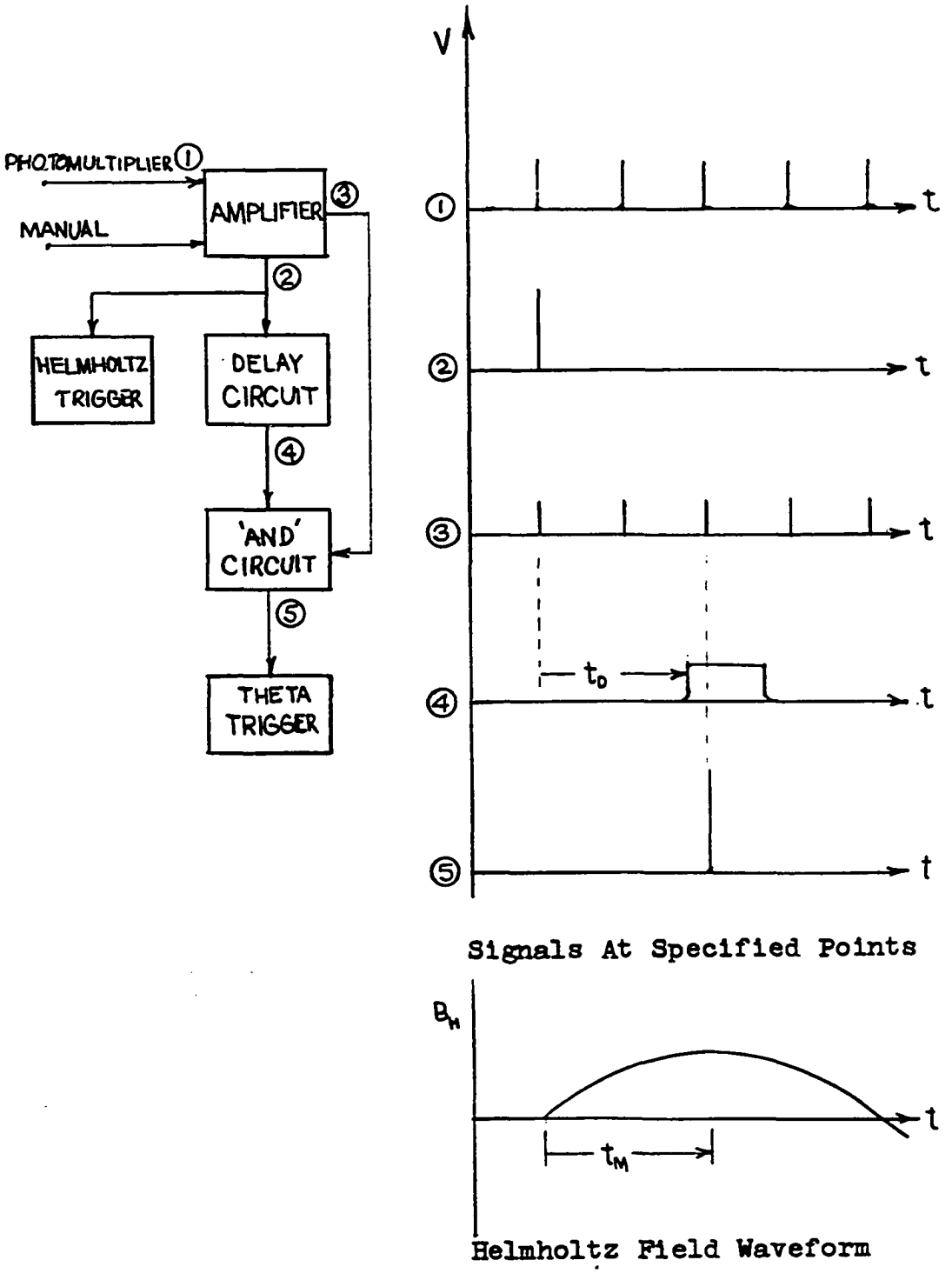

Fig. III.8. Bias Field Trigger Circuit Used For The Framing Camera

Reproduced with permission of the copyright owner. Further reproduction prohibited without permission.

t_M is the time required for the bias field to reach its maximum value.

Bias Magnetic Field Strength

The strength of the Helmholtz field at the time of the discharge can be calculated by superposing a signal corresponding to the time of the discharge of the theta bank, on the Helmholtz voltage waveform. By calculating the current in the Helmholtz coils at this time, assuming a simple LC discharge, the corresponding magnetic field at this time can be calculated. The Helmholtz voltage waveform is monitored by a potential divider across the Helmholtz coil; the signal corresponding to the discharge of the theta bank is given by the Rogowski coil signal.

The experimental results in this section are divided into the photographic results and the probe measurement results. Since the photographic investigation is mainly for qualitative purposes, we discuss this first, treating the two cases, $\phi = 90^\circ$ and $\phi \approx 0^\circ$ separately, where 'ϕ' is the angle between the axes of the discharge vessel and the Helmholtz coil.

Section B.1 - Photographic Measurements

a) $\phi = 90^\circ$

At breakdown, the plasma current begins to flow in a ring whose axis is approximately parallel to the theta coil axis. (see Fig. III.9.). The current ring then separates into two current rings which rotate about an axis parallel to $\underline{B}_c \times \underline{B}_H$

Reproduced with permission of the copyright owner. Further reproduction prohibited without permission.

and in opposite directions. The outer ring then collapses radially whereas the inner current ring appears to have a negligible radial displacement during this time. (see Positions 1 - 3, Fig. III.9a.) After the outer ring has collapsed to an elliptical shape from the end on photographs (Position 3, Fig. III.9b.), the inner ring begins to collapse radially. The outer ring is identified by the fact that it absorbs the light radiated by the inner ring

The two current rings rotate in opposite directions indicating that the current flows in opposite directions in the two rings. In this case one ring should collapse radially whereas the other should be pressed into the wall of the discharge vessel, ($\underline{J} \times \underline{B}$ forces are in opposite directions). This is observed to be true. We suggest that the two rings correspond to the current layers proposed by Niblett and Green, (1959). The outer one is induced by the theta coil field (B_c) whereas the inner one is induced by the conservation of the flux trapped in the plasma ring. In this model the two currents flow in opposite azimuthal directions. Therefore, the transverse field will 'tear' the ring axially producing the two rings which appear in Fig. III.9 . From the Niblett and Green model, we expect that the outer ring will collapse to the axis before the inner one does. This is confirmed by our observations. The reason that the inner ring collapses eventually is that the B_c field induces more current in this ring causing a net inward force on it.

Reproduced with permission of the copyright owner. Further reproduction prohibited without permission.

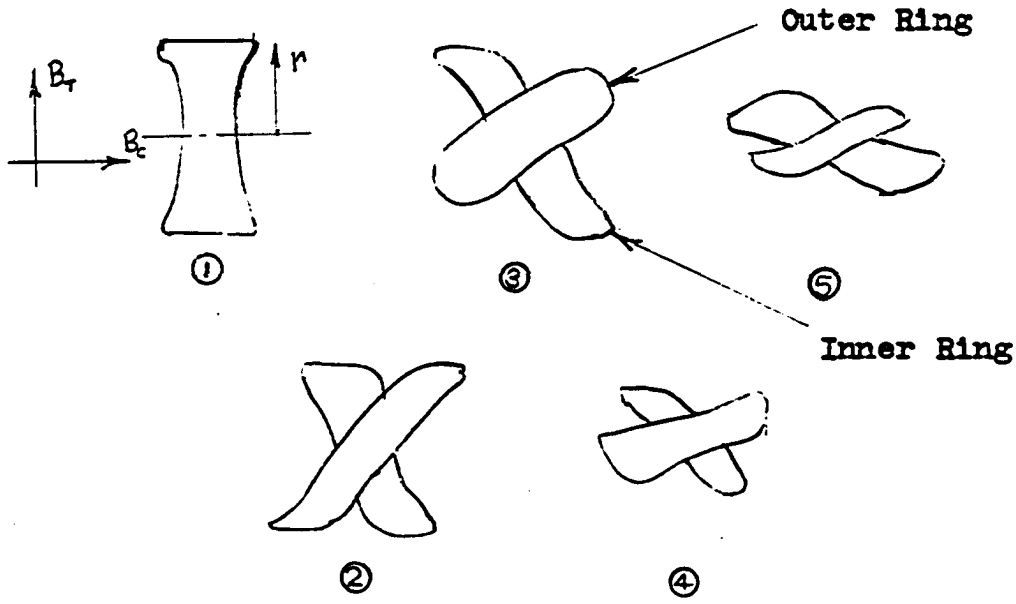

Time Increases Left to Right, Frame Positions Are Staggered, Time between each Frame ~ 0.35 μ sec.

a. Top On View Of Plasma

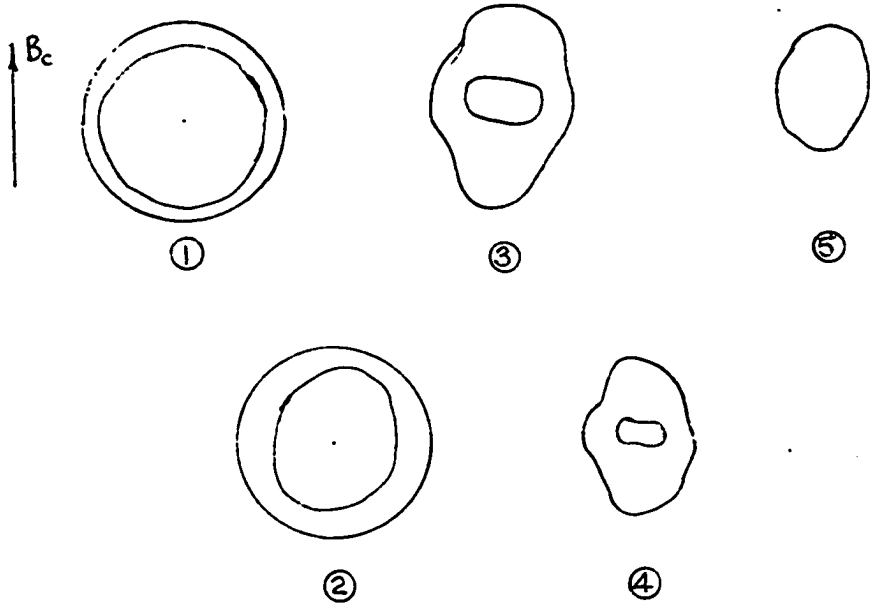

b. End On View Of Plasma

Fig. III.9. Sketch Of Plasma Photographs

Reproduced with permission of the copyright owner. Further reproduction prohibited without permission.

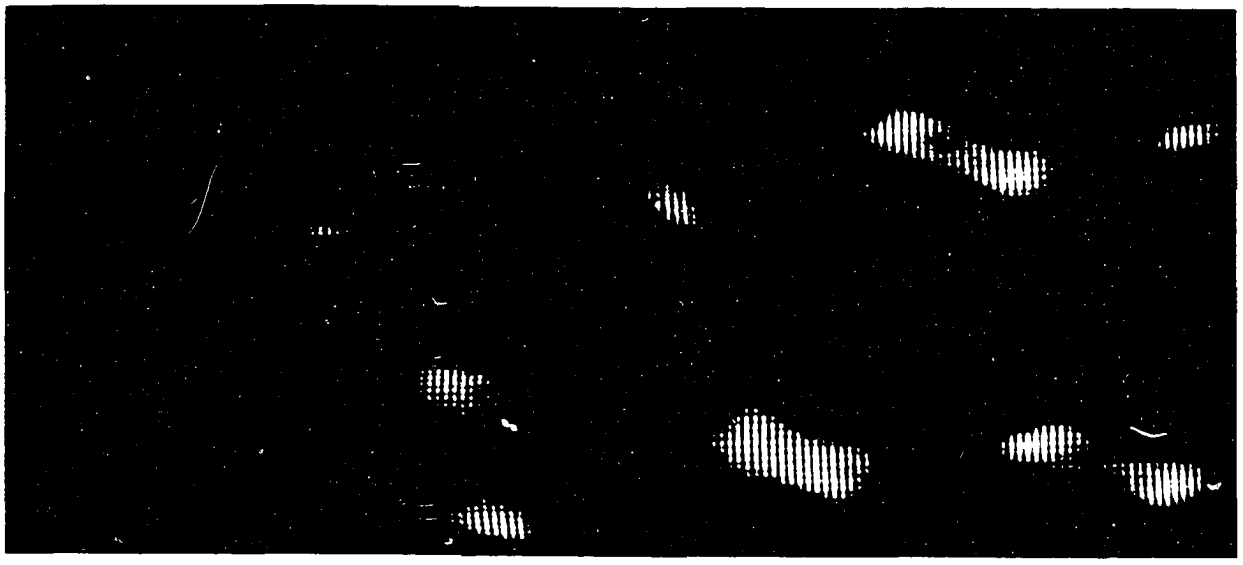

B_T = -0.020 weber/m^2, Gas:Air, Pres = 50μ Hg, ϕ = 90°

a.

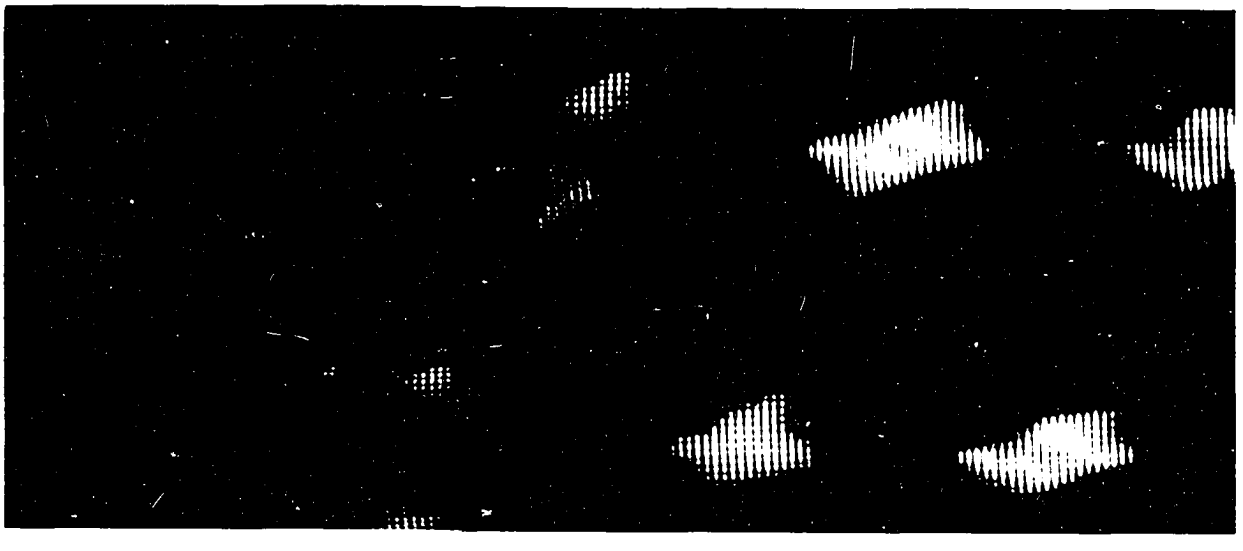

B_T = +0.016 weber/m^2, Pres = 50μ Hg, ϕ = 90°

b.

Fig. III.10. Top On Photograph Of Plasma

Reproduced with permission of the copyright owner. Further reproduction prohibited without permission.

b) $\phi \approx 0^{o}$

In this case the direction and the strength of the bias field radically affects the breakdown of the gas. Breakdown occurs when the total axial magnetic field is approximately zero. This is verified by using the magnetic probe measurements to calculate the magnetic field of the theta coil, $\underline{B}_{coil}$, at the time of the gas breakdown. It is found that when the bias field, $\underline{B}_{H}$, is parallel to the initial direction of $\underline{B}_{coil}$, (i.e. parallel bias field), the plasma is comparatively unstable to the flip instability (i.e. the plasma escapes from the coil). If the bias field $\underline{B}_{H}$, is anti-parallel to the initial direction of $\underline{B}_{coil}$, (i.e. anti-parallel bias field), the plasma is comparatively stable against the flip instability.

The gas breaks down at the end of the first half cycle of the theta coil current, I_{c}, when parallel bias field is used. However, if an anti-parallel bias field of sufficient strength is employed, the gas breaks down at the beginning of the first half cycle of I_{c}. Therefore, the breakdown of the gas can be enhanced or suppressed by using an anti-parallel or parallel bias field respectively.

The plasma dynamics appear to be qualitatively similar to those observed when $\phi = 90^{o}$ (see Fig. III.11.).

Reproduced with permission of the copyright owner. Further reproduction prohibited without permission.

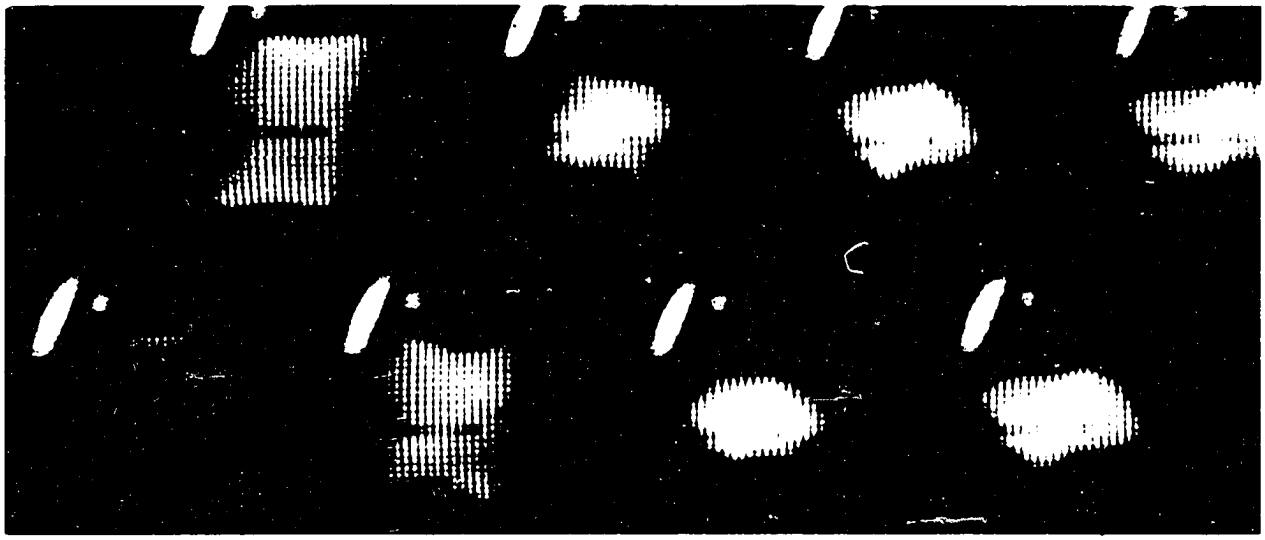

($\phi \approx 0^{\circ}$), B_T = 0.024 weber/m^2 Pres. = 50 μ Hg - Air

Fig. III.11 Top On Photograph

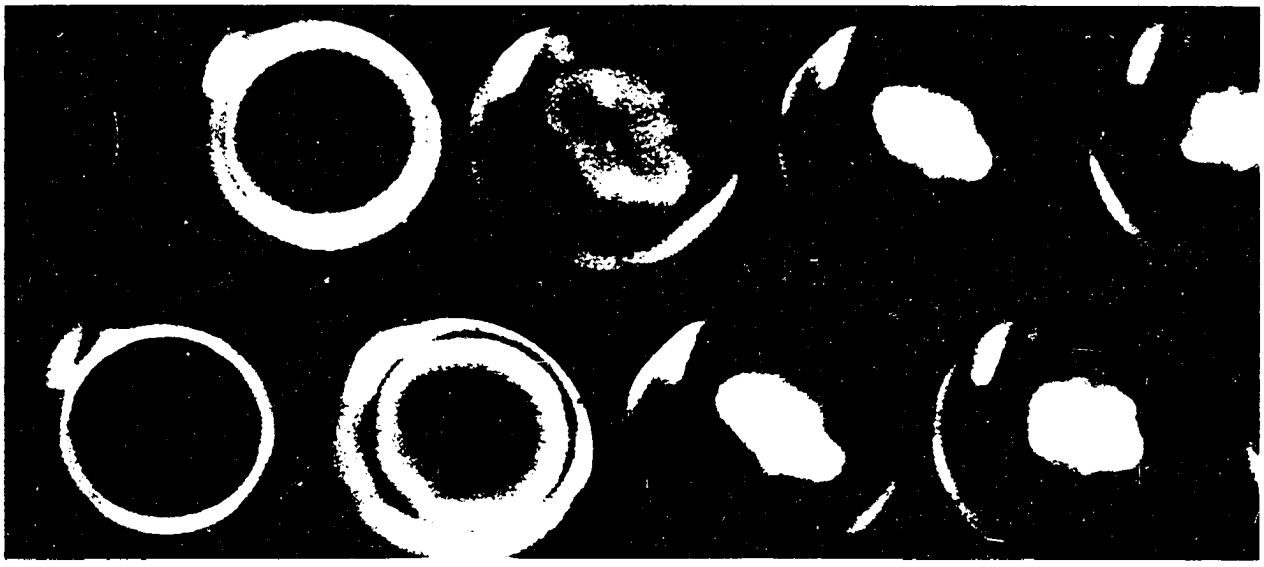

($\phi \approx 0^{\circ}$), B_T = 0.068 weber/m^2 Pres. = 50 μHg - Air

Fig. III.12. End On Photograph

Reproduced with permission of the copyright owner. Further reproduction prohibited without permission.

The rate at which the plasma ring flips, depends critically on the alignment of the theta coil and bias field. When $\phi = 0^{\circ}$, no flip is observed for the experimental conditions reported above, (see Fig. III.12.). However, a misalignment of $\phi \sim 2^{\circ}$ will 'flip' the plasma ring. The most distinct effect of the bias field is observed for the first breakdown of the discharge gas. Sometimes, the plasma ring disintegrates in less than $5 \times 10^{-7}\mu$ sec. (see Fig. III.14.)

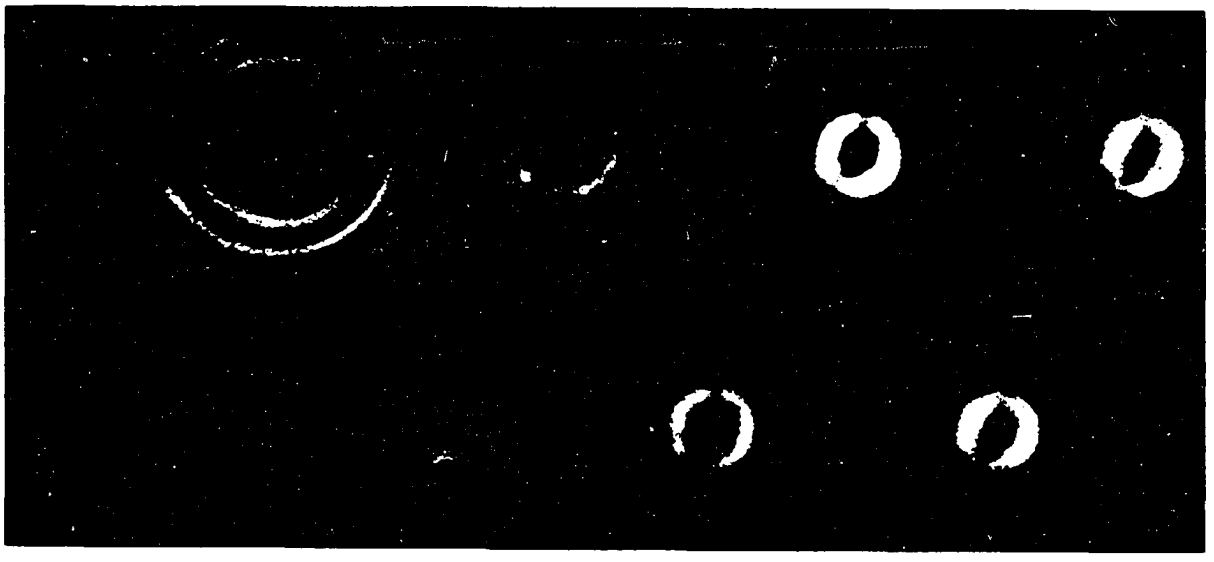

$\phi = 0^{\circ}$ Pres: 50μ Hg - Air

Fig. III.13. End On Photograph of Plasma With No Transverse Bias Field

Reproduced with permission of the copyright owner. Further reproduction prohibited without permission.

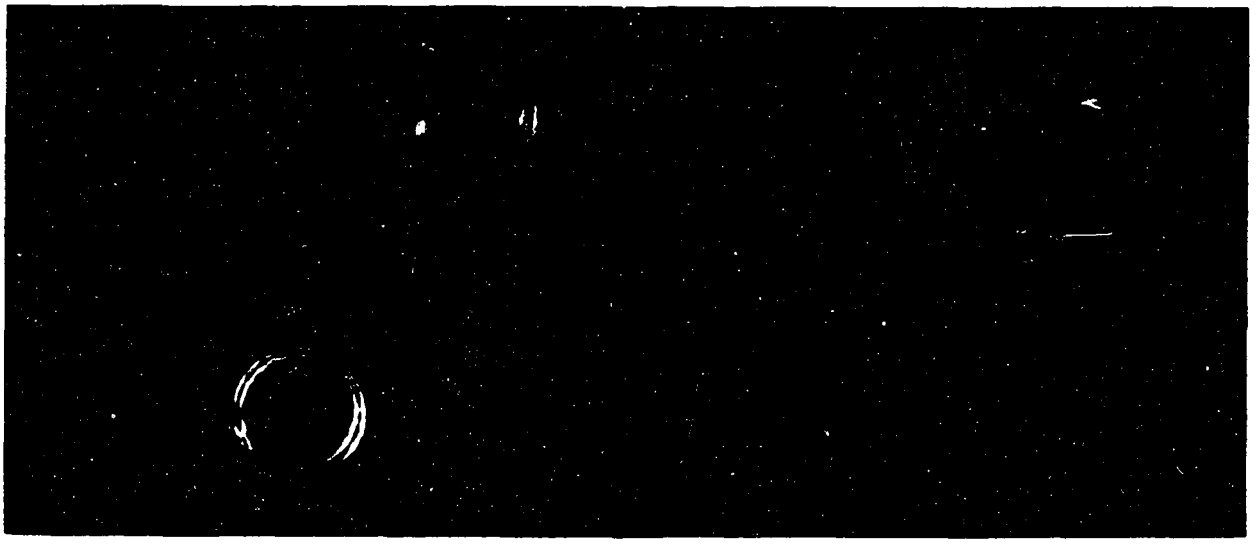

B_T = 0.04 weber/m^2 Pres.=100 μHg, Gas-Air

Fig. III.14. End On Photograph Of Plasma With Transverse Bias Field

Section B.2a. - Probe Measurements ($\phi \approx 0^\circ$)

The initial breakdown at the end of the first half cycle of the theta current is chosen for the probe investigation. Under these conditions the influence of the bias field on the plasma dynamics is most pronounced and the discharge gas is purer. Breakdown of the discharge gas is achieved in the presence of a bias field, B_H, parallel to the initial direction of the magnetic field, B_c, produced by the theta coil.

From the double probe system, (see Page 26), hydromagnetic oscillations of the plasma are observed and as ϕ is increased, these oscillations are suppressed. The corresponding framing camera pictures show that when the oscillations are suppressed,

Reproduced with permission of the copyright owner. Further reproduction prohibited without permission.

a plasma ring forms and disappears in $\sim 1\,\mu$sec, indicating that the plasma has disintegrated.

The flip of the plasma is not readily observed photographically under this condition (see Fig. III.13.), because the plasma moves too rapidly. The flip is clearly observed in framing camera photographs when there are a larger number of oscillations recorded by the probe. However, the suppression of oscillations was chosen as a criterion for flip because it is a readily distinguishable characteristic in the probe waveforms, (see Fig. III.15.).

The gas pressure in the discharge vessel and the strength of the bias field at the time of the theta bank discharge are first set at selected values. After each discharge the angle ϕ is varied in one degree intervals over the range $\pm 18^{\circ}$ and the corresponding magnetic probe waveforms are recorded. In the angular region where flip occurs, ϕ is varied by $1/2^{\circ}$ intervals to ascertain more accurately the actual value of ϕ at which flip occurs, ϕ_c, and referred to as the critical value. Keeping the pressure constant, the Helmholtz field is varied and the value of $\phi_c(B_H)$ is determined for various values of the bias field strength, B_H. The bias field strength was varied from o.1 webers/m^2 to 0.6 webers/m^2 in 0.05 webers/m^2 intervals.

The value of $B_H \sin \phi_c(B_H)$ as a function of the field strength, B_H, is determined and found to be a constant for a given pressure (Fig. III.16.). The above procedure is repeated

Reproduced with permission of the copyright owner. Further reproduction prohibited without permission.

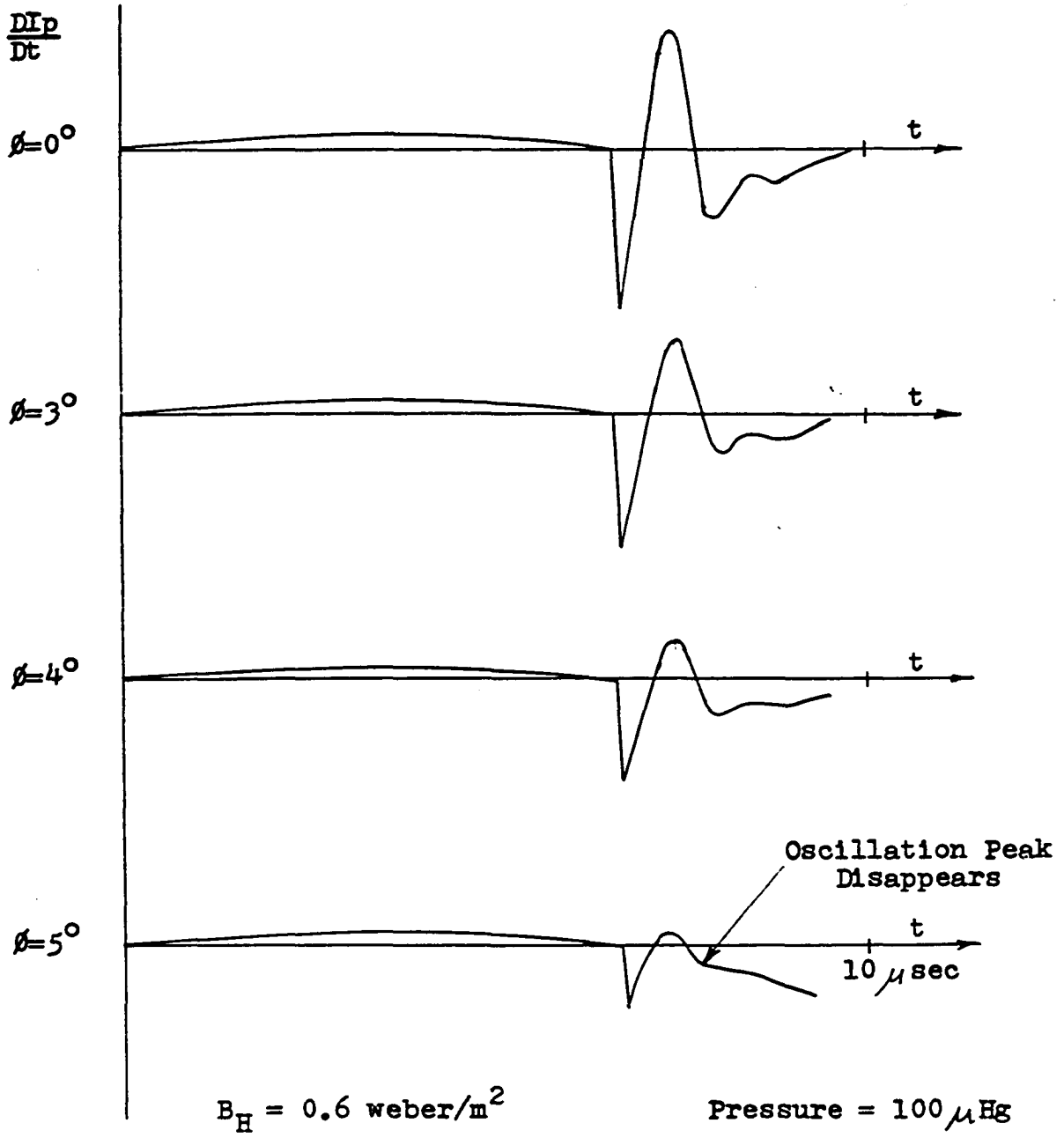

Axial probe signals for changes in 'ø'. Coil dimensions and discharge conditions are specified on Page 40.

Fig. III.15.

Reproduced with permission of the copyright owner. Further reproduction prohibited without permission.

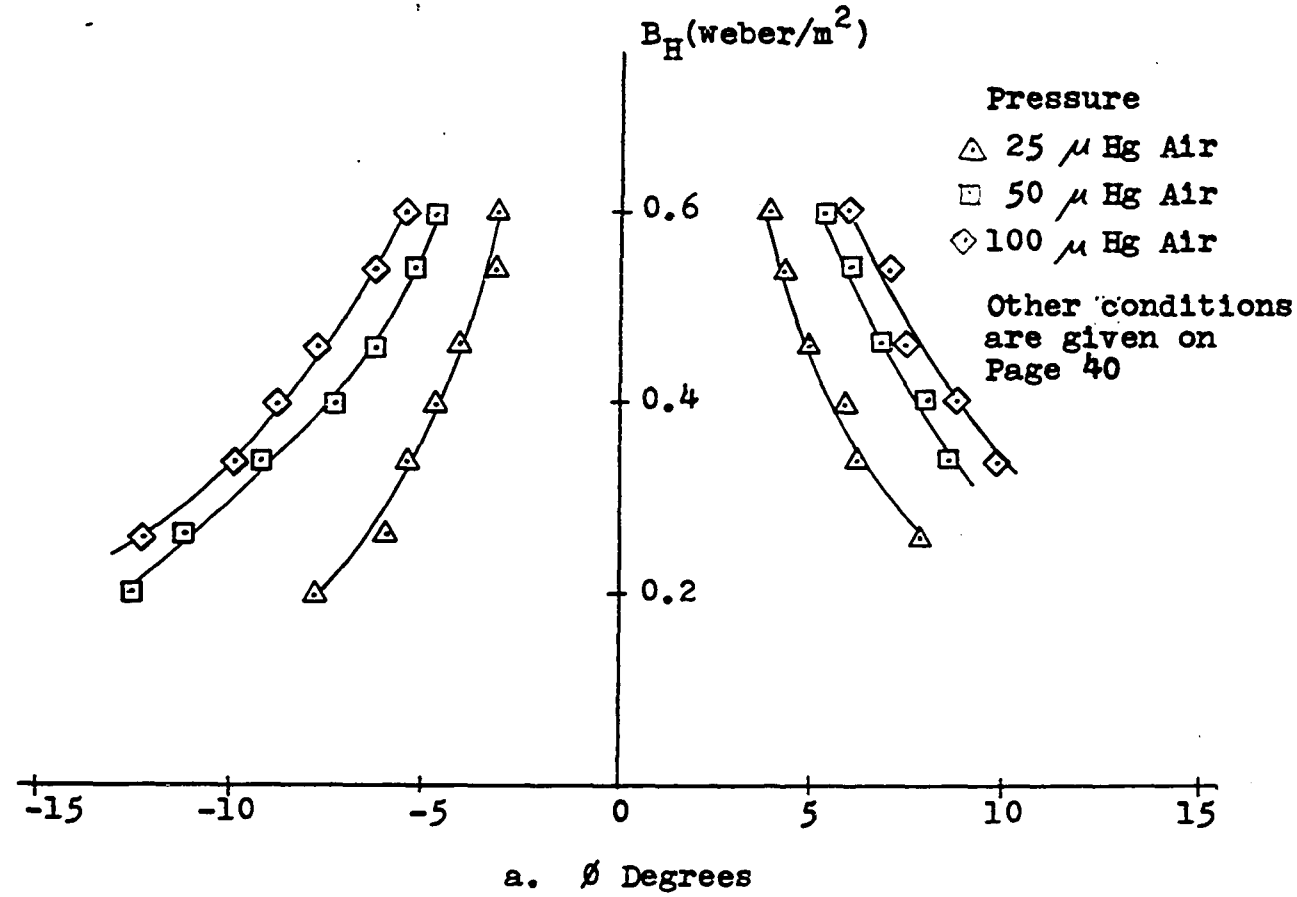

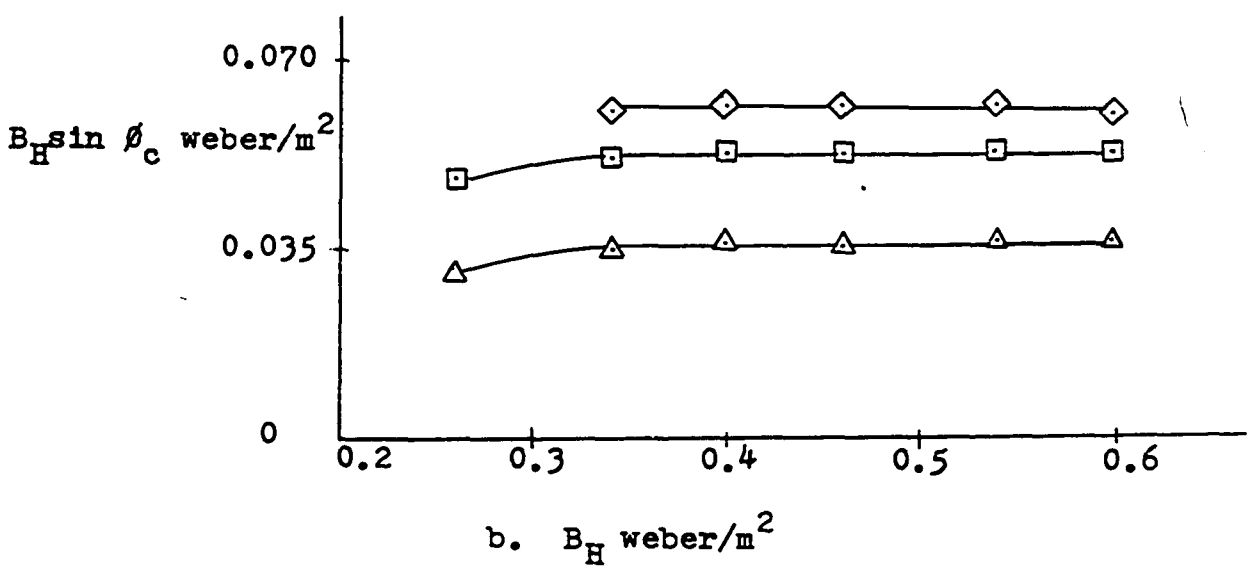

Fig. III.16. Value of $B_H \sin \phi_c$ For Different Gas Pressures

Reproduced with permission of the copyright owner. Further reproduction prohibited without permission.

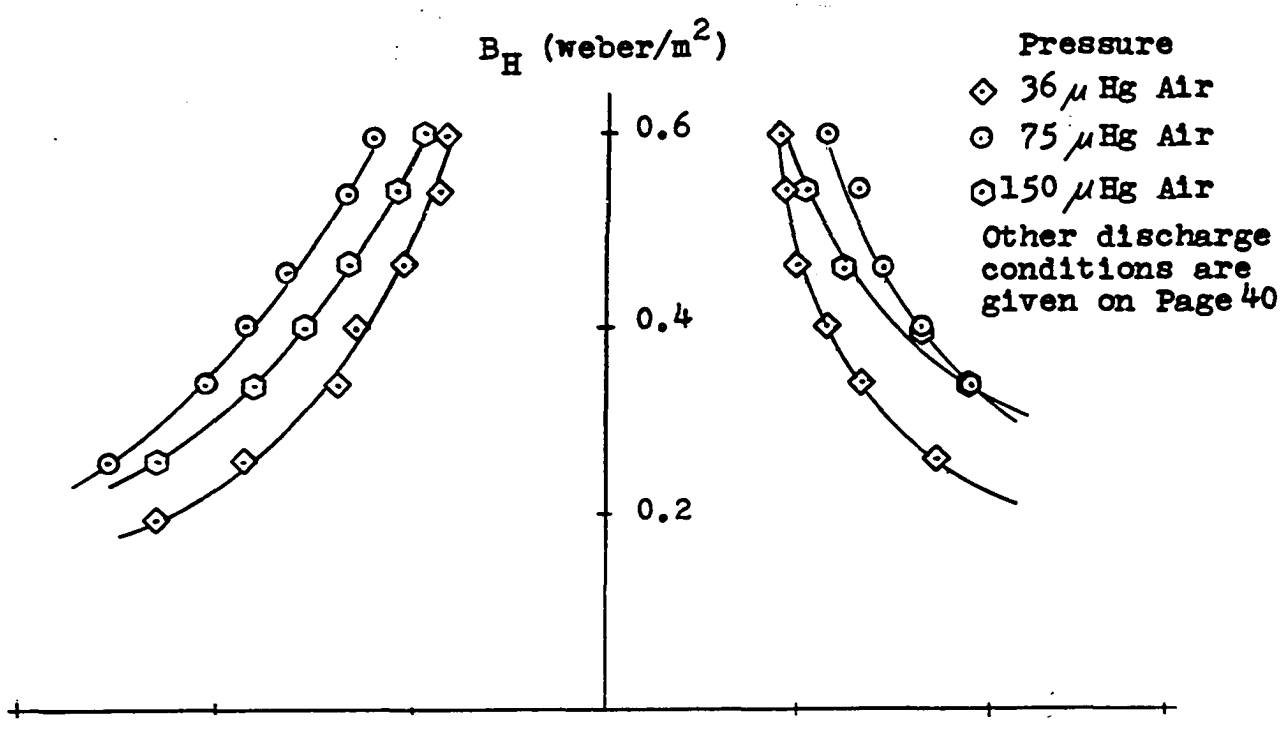

c. ø Degrees

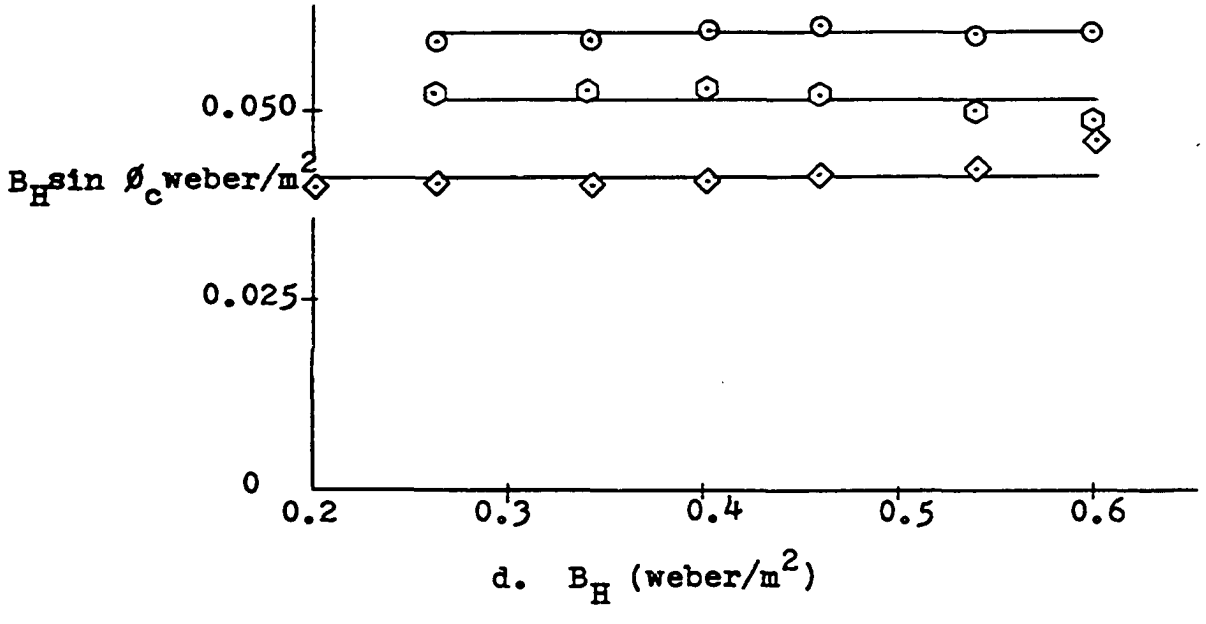

Fig. III.16. Value of $B_H \sin \phi_c$ For Different Gas Pressures

Reproduced with permission of the copyright owner. Further reproduction prohibited without permission.

for the following gas pressures; 16 μHg, 25 μHg, 35 μHg, 50 μHg, 75 μHg, 100 μHg, 125 μHg, 150 μHg, 200 μHg, and 250 μHg. It is found that for pressures between 16 μHg and 75 μHg, the value of $B_H \sin \phi_c$ varies as (pressure)$^{1/2}$, (see Fig. III.17.), however, above 75 μHg, the relation is no longer valid.

Thus for a given coil, $\frac{B_H \sin \phi_c}{p^{\frac{1}{2}}}$ = constant, which will be referred to as the stability constant.

The experimental results that the value of $B_H \sin \phi_c$ is a constant for a flip at a given pressure confirms the hypothesis that the component of the bias field transverse to the discharge axis is the important parameter in the flip instability. For this reason additional experiments have been performed in which only a transverse field was used, (i.e. $\phi = 90^\circ$).

Section B.2b - $\phi = 90^\circ$

In these experiments the bias field has only a transverse component. Following the procedure adopted above, the value of B_H when flip occurs is denoted as the critical value, $(B_H)_c$. To obtain $(B_H)_c$ at a given pressure, the bias field strength is varied from 0.004 webers/m^2 to 0.024 webers/m^2 in increments of 0.002 webers/m^2 after each theta bank discharge. The corresponding magnetic probe waveforms are recorded and in the region of flip the magnetic field increment is changed to 0.0005 webers/m^2. The above procedure is repeated for the following gas pressures; 16 μHg, 25 μHg, 35 μHg, 50 μHg, 65 μHg, 75 μHg,

Reproduced with permission of the copyright owner. Further reproduction prohibited without permission.

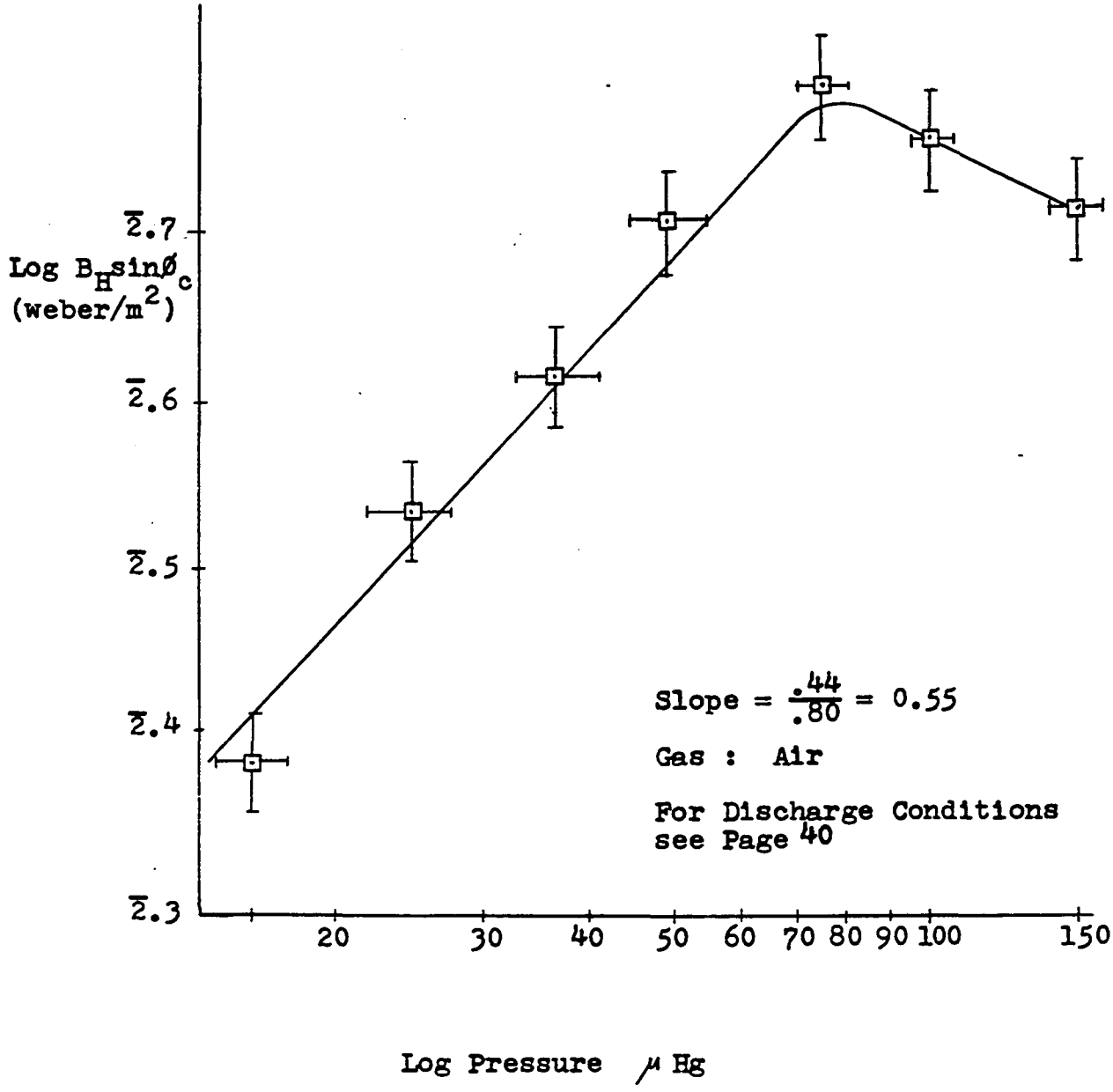

Fig. III.17. Variation Of The Critical Transverse Field With Pressure ($\phi \approx 0^{o}$)

Reproduced with permission of the copyright owner. Further reproduction prohibited without permission.

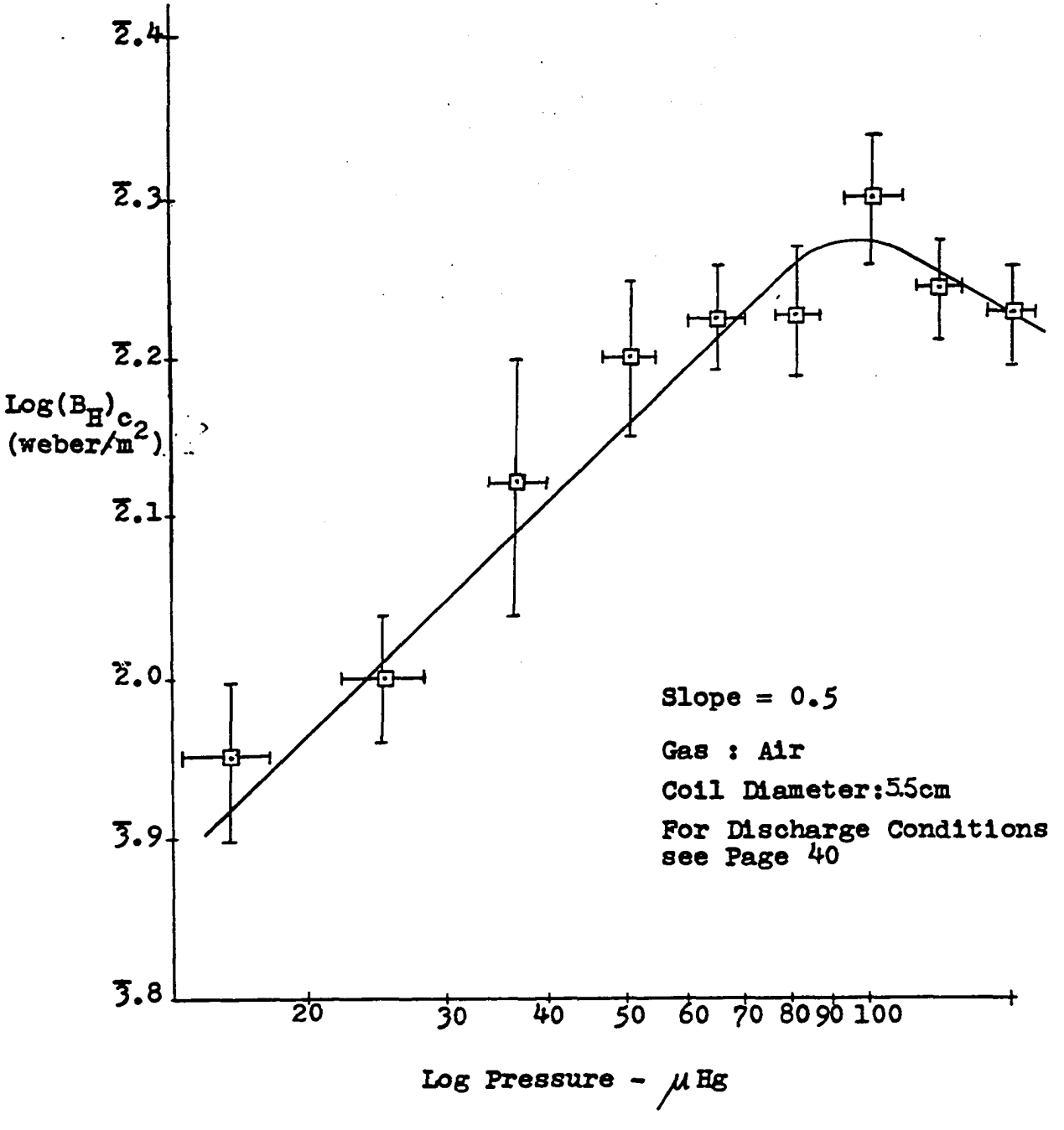

Fig. III.18. Variation Of The Critical Transverse Field With Variation In Pressure ($\phi = 90^{o}$)

Reproduced with permission of the copyright owner. Further reproduction prohibited without permission.

80 μHg, 100 μ Hg, and 150 μHg. It is found that the critical value of B_H varied as (pressure)$^{1/2}$ within experimental error for pressures between 16 μ Hg, to 75 μHg, however this relationship is not valid for pressures greater than 75 μHg (see Fig. III.18).

Section B.3 - Variation In The Discharge Radius

The effect on the stability constant $\frac{B_H \sin\phi_c}{p^{\frac{1}{2}}}$ in the linear pressure region (16 μHg to 75 μHg) due to a variation of the diameter of the discharge tube has also been studied. The internal diameters of the tubes employed were 3.4 cm., 5.1 cm., and 7.1 cm. Theta coils of constant aspect ratio were used and the charging potential of the theta bank were varied to keep the peak magnetic energy density approximately constant.

The procedure described in the previous Section B.2a is used to determine the value of $B_H \sin\phi_c$ at various pressures for each of the three tubes. An approximately parallel bias field was used for these experiments so as to have reproducible breakdown conditions. A summary of the experimental conditions is given below.

Reproduced with permission of the copyright owner. Further reproduction prohibited without permission.

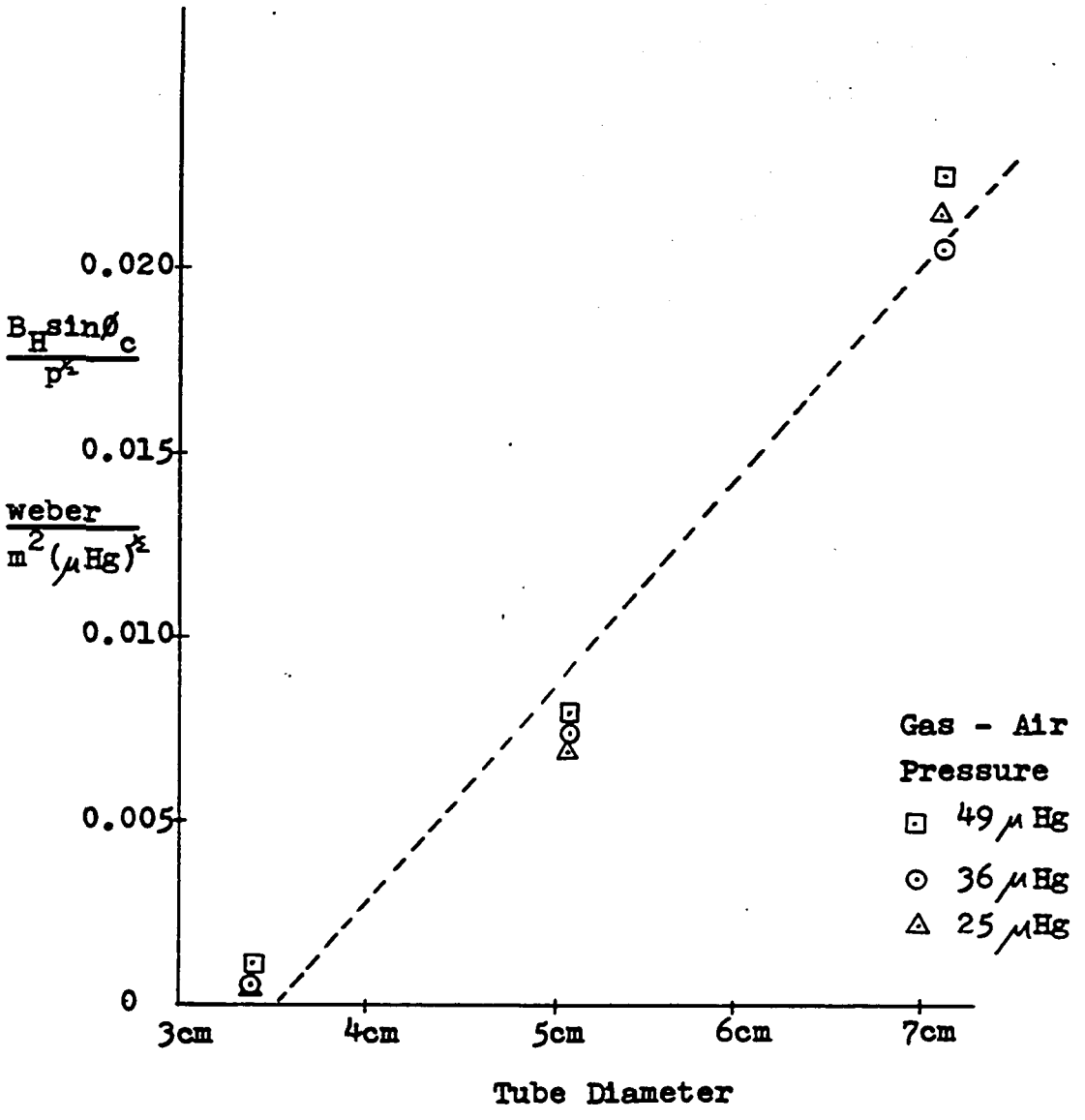

Fig. III.19. Variation In Stability Constant With Tube Diameter (Other Experimental Conditions Appear on Page 40)

Reproduced with permission of the copyright owner. Further reproduction prohibited without permission.

Experimental Conditions For Varying Discharge Radius

Inner Tube Diameter	Coil Diameter	Coil Length	Bank Voltage
7.1 cm	7.6 cm	7.6 cm	15.3 ± .5 kv
5.1 cm	6.1 cm	6.4 cm	13.3 ± .5 kv
3.4 cm	4.1 cm	4.6 cm	10.4 ± .5 kv

The dependence of the stability constant, $\frac{B_H \sin\phi_c}{p^+}$, on the diameter of the discharge is shown in Fig. III.19. It was found experimentally that the plasma showed less tendency to flip as the diameter of the theta tube was increased; further, the stability constant varies roughly linearly with the tube diameter. However, there appears a minimum coil length, below which there are no magnetic oscillations under the present experimental conditions.

Section B.4 - Directional Probe

The directional probes (see Chapter II, Section C.1b.), are devised to measure the angular rotation of the plasma ring. A Tektronix 551 double beam oscilloscope with two differential (Type G) preamplifiers is employed. On the upper beam, V_u, the voltages from the two probes (Fig. III.20.) are subtracted. Therefore,

Reproduced with permission of the copyright owner. Further reproduction prohibited without permission.

(2) $V_u = V_1 - V_2$,

where $V_1 = \frac{V_o}{\sqrt{2}}(\cos\delta - \sin\delta)$,

$V_2 = \frac{V_o}{\sqrt{2}}(\cos\delta + \sin\delta)$,

δ = angle between the axis of the plasma ring and the theta coil axis (see Fig. II.17.).

V_o corresponds to the strength of the plasma field, B_p, (Fig. II.17.)

(3) Therefore, $V_u = -\sqrt{2}\, V_o \sin\delta$.

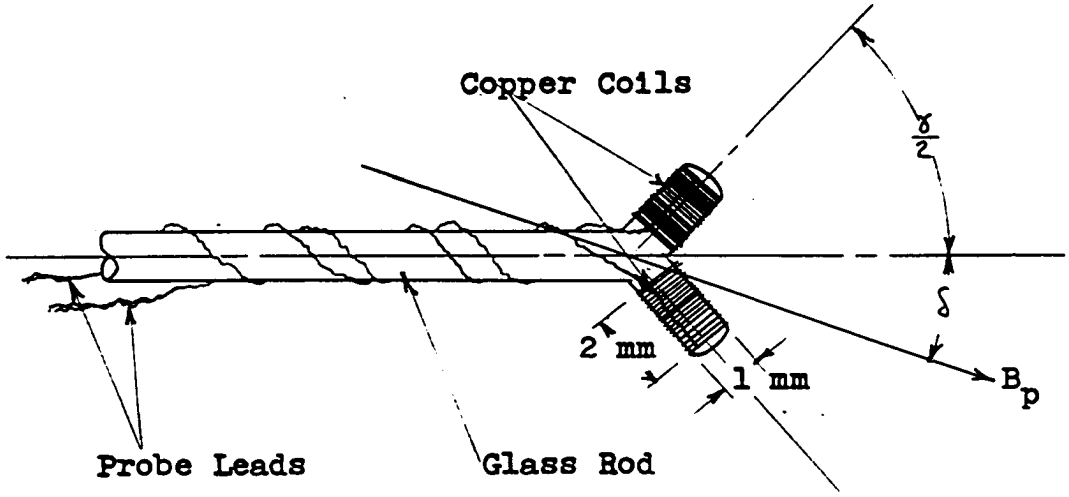

B_p = Plasma Magnetic Field

Fig. II.17. Directional Probe

Reproduced with permission of the copyright owner. Further reproduction prohibited without permission.

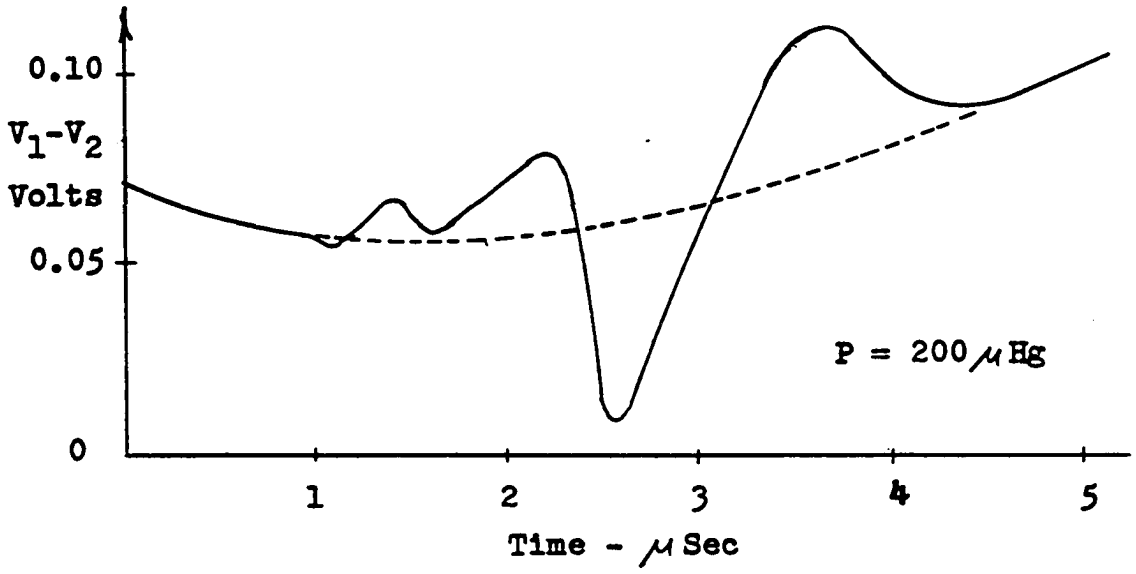

Fig. III.20. $V_1 - V_2$ Waveform

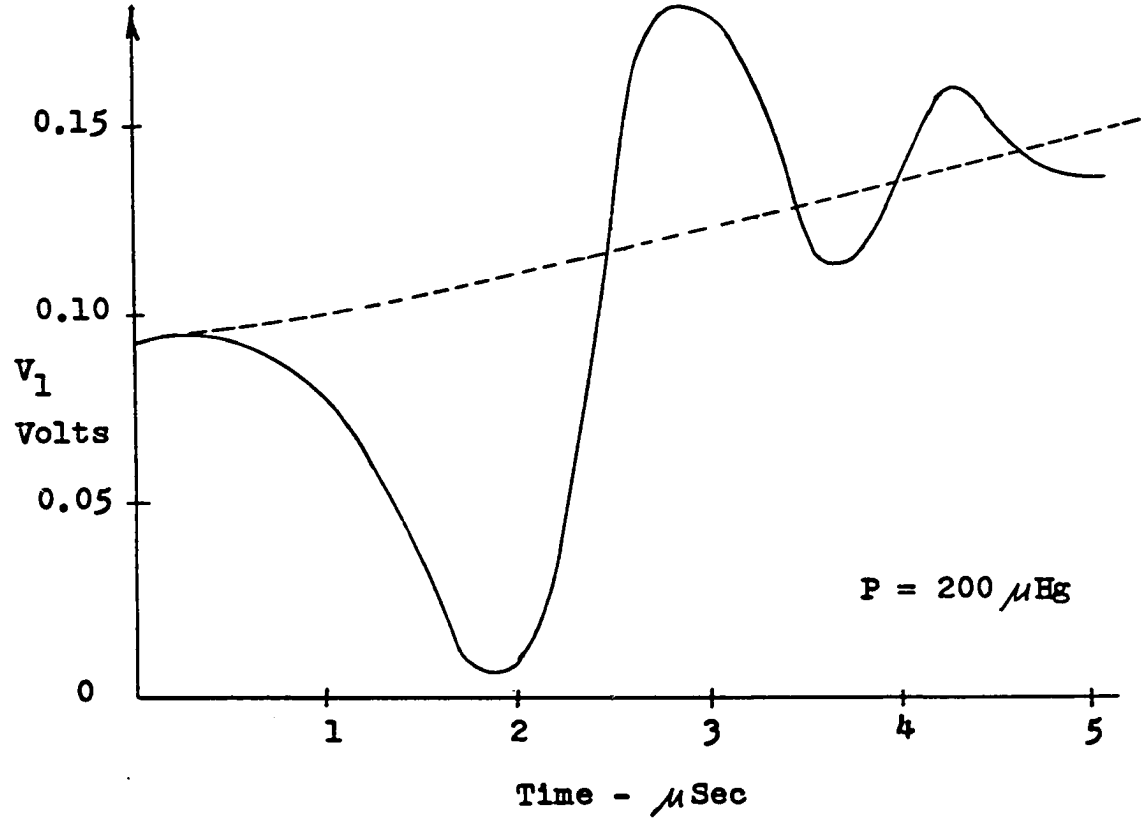

Fig. III.21. V_1 Waveform

Reproduced with permission of the copyright owner. Further reproduction prohibited without permission.

Probe 1 measures the component of the total magnetic field along the axis of probe 1. On the lower beam, V_L, the theta coil component of the magnetic field is subtracted from the output of probe 1, i.e. double probe technique (see Page 26). Thus, V_L measures the component of the plasma field, B_p, along the axis of probe 1,

(4) i.e. $V_L = \frac{V_o}{\sqrt{2}} (\cos\delta - \sin\delta)$. (see Fig. III.21)

By combining equations (3) and (4) the expression for 'δ' is obtained in terms of the measured signals, V_u and V_L,

(5) i.e. $\delta = \arctan \frac{V_u}{V_u - 2V_L}$

Equation (5) is only applicable when the axis of rotation of the plasma ring is perpendicular to the plane of the 'V' probe. In order to locate this plane experimentally, the probe is rotated about its stem (see Fig. II.17.) until a position is found for which $V_1 \approx V_2$, at all times for successive discharges. In practice this position, $\Phi_c = 90^\circ$, was determined to within $\pm 10^\circ$. For this configuration, the plane of the 'V' is clearly perpendicular to the plane containing B_p and the discharge axis. A further rotation of 90° about the stem, therefore, brings the plane of the 'V' into the direction required for equation (5) to be valid.

Reproduced with permission of the copyright owner. Further reproduction prohibited without permission.

Using the two probe signals and equation (5), i.e. $\delta = \arctan \frac{V_u}{V_u - 2V_l}$, the angular rotation of the plasma is calculated. The results agree qualitatively with the framing camera photographs, (see Fig. III.23).

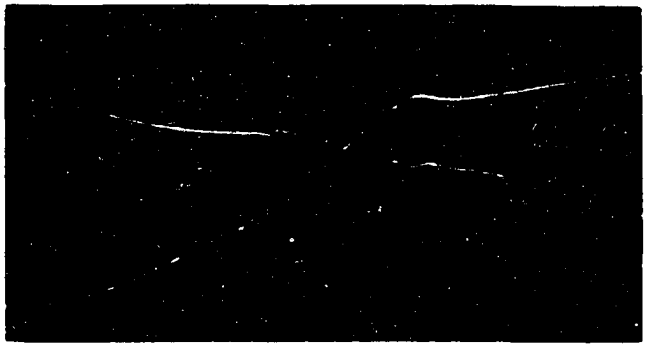

Lower Trace V_1 , Upper Trace $V_2 - V_1$

Probe Waveforms At $\theta_c + 10^\circ$ Pres.- 50 μHg

Gas - Air

Lower Trace V_1 , Upper Trace $V_2 - V_1$

Probe Waveforms At $\theta_c - 10^\circ$ Pres.- 50 μHg

Gas - Air

Fig. III.22.

Reproduced with permission of the copyright owner. Further reproduction prohibited without permission.

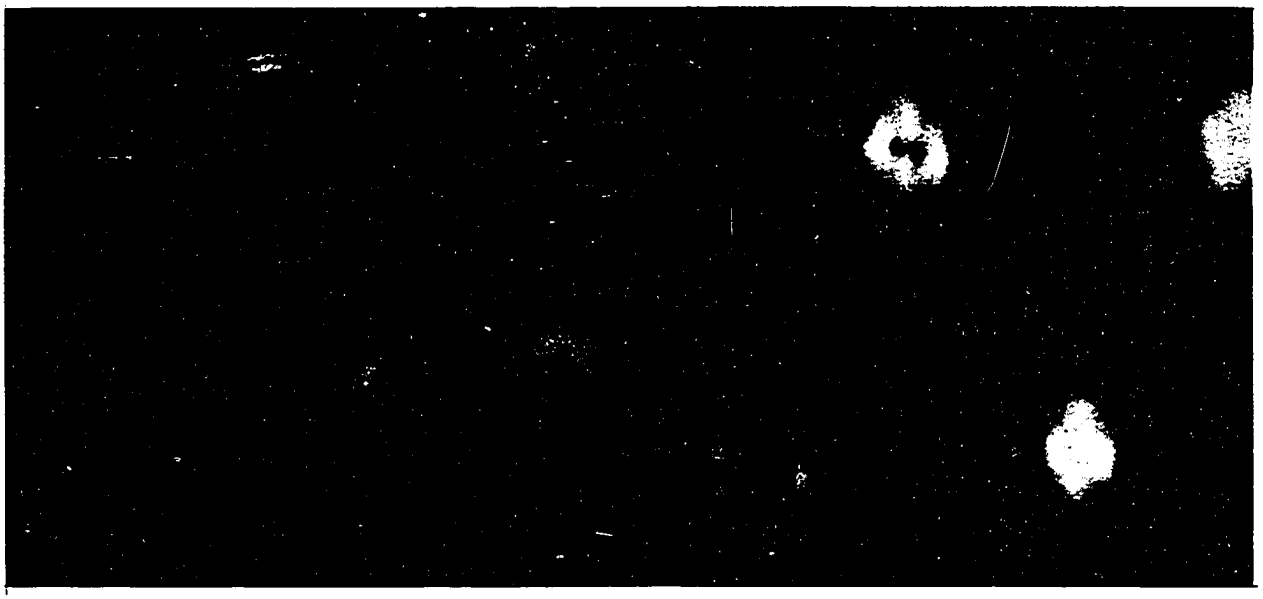

Time between Frames = 0.3 μ sec. End On; 200 μHg
B_T = 0.024 weber/m^2

a.

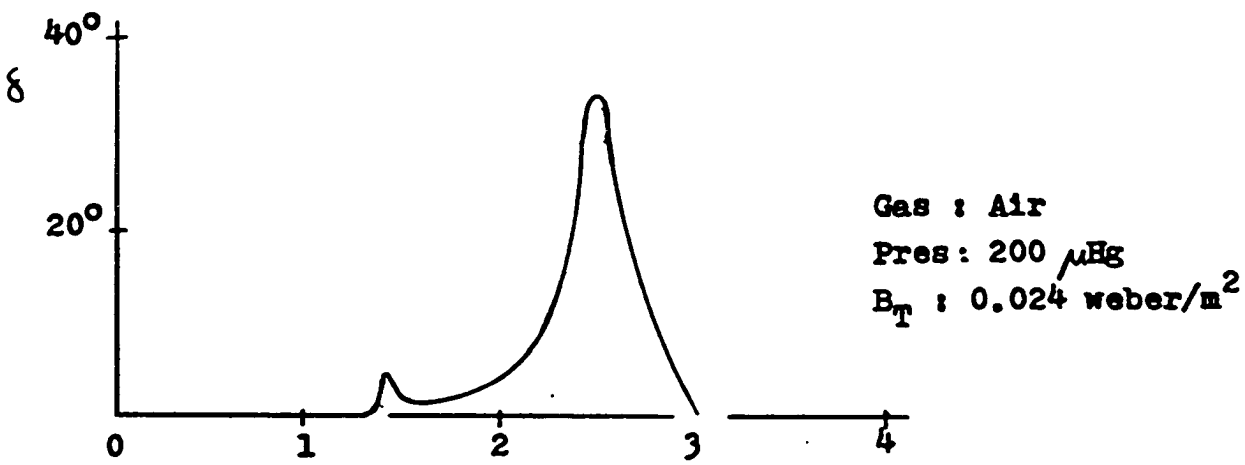

b.

Fig.III.23. The Angular Rotation 'δ'

Reproduced with permission of the copyright owner. Further reproduction prohibited without permission.

In summary, the significant effects of a bias magnetic field on the theta pinch are as follows;

Photography

1. A transverse bias magnetic field causes a rapid flip of the plasma ring in a theta pinch discharge.
2. The two current model of the theta pinch is confirmed.

Magnetic Probes

1. For a given air pressure, capacitor bank energy, and discharge coil, if $B_H \sin\phi$ is greater than a critical constant, flip occurs. B_H is the Helmholtz field and ϕ is the angle between the axes of the Helmholtz field and the theta coil.
2. For a given discharge coil and capacitor bank energy, $B_H \sin\phi_c$ varies as $p^{\frac{1}{2}}$ where 'p' is the air pressure. This relation is valid in the region of 16 μ Hg to 75 μ Hg air.
3. With theta coils of constant aspect ratio, $\frac{B_H \sin\phi_c}{p^{\frac{1}{2}}}$ varies as the radius of the discharge tube, provided the magnetic energy density in the coil is kept constant.

Reproduced with permission of the copyright owner. Further reproduction prohibited without permission.

Section C - Theory

In this section, a theoretical model is proposed to describe the radial and axial motions of the plasma. Experimentally it is found that if the plasma moves axially a distance greater than Z_c (Z_c is the axial displacement required to escape the containment of the coil), before it collapses to 0.8a (where 'a' is the initial radius), then the plasma oscillations are suppressed, i.e., criterion for flip. By using the experimental results given in the preceding section, the validity of the theoretical model can be checked in the following way.

First the axial and radial equations of motion are solved simultaneously by a power series approximation. Then from the solution of the radial equation, the time, t_c, for the plasma to collapse to $r \sim 0.8a$ is calculated. Substituting this value of t_c into the solution to the axial equation, the axial displacement, Z_o, at this time is found. If this value of Z_o is greater than Z_c (see above), then the plasma oscillations will be suppressed, that is, flip occurs. This value Z_o is a function of gas pressure, p, radius of the discharge tube, a, transverse magnetic field, B_T, etc. Thus, the dependence of the theoretical flip criterion on the experimental parameters (i.e. $Z_o(p, B_T, a) >$ constant) can be compared with that given in the experimental results. The radial equation is discussed first, followed by the discussion of the axial equation of motion.

Reproduced with permission of the copyright owner. Further reproduction prohibited without permission.

Section C.1 - Radial Equation Of Motion

The radial equation of motion is derived by equating the radial magnetic forces to the rate of change of radial momentum. (see Fig. III.3.). At the beginning of the radial contraction, we assume the plasma shell has a finite mass $m\pi a^2\epsilon$ because of the finite thickness of the induced current shell. If we assume that all the gas particles are swept up by the plasma and concentrated in a thin shell (Rosenbluth, 1954), then the momentum of the shell per unit length is,

$$(6) \qquad m\pi(a^2 - r^2)\frac{dr}{dt} + m\pi a^2\epsilon\frac{dr}{dt} \quad ,$$

where m = mass density of the gas,
a = internal radius of the discharge vessel,
r = radius of the plasma ring,
$m\pi a^2\epsilon$ = initial mass of the plasma ring per length.

The first term is the momentum resulting from the mass swept up by the collapsing shell. The second term represents the momentum arising from the initial mass of the shell.

The inertia force of the shell is:

$$(7) \qquad \frac{d}{dt}\left[m\pi(a^2 - r^2)\frac{dr}{dt}\right] + \frac{d}{dt}\left[m\pi a^2\epsilon\frac{dr}{dt}\right] .$$

Reproduced with permission of the copyright owner. Further reproduction prohibited without permission.

The radial magnetic forces are due to the differences in magnetic fields on the inside and on the outside of the plasma sheet. Two approximations are made in formulating the expression for these forces. The first is that the magnetic fields produced by the plasma currents and the theta coil currents can be represented by the field of an infinite solenoid, (for discussion see Page 81).

(8) i.e. $B = \mu_o I$,

where B = magnetic field,

I = current per unit length,

μ_o = permeability.

The second approximation is that the electrical conductivity of the plasma is infinite so that the magnetic flux enclosed by the plasma is conserved. Therefore the internal magnetic field, B_i, i.e. trapped field, can be represented by,

(9) $$B_i = \frac{B_o a^2}{r^2} ,$$

where B_o = initial magnetic field enclosed by the plasma,

a = initial radius of the plasma,

r = radius of the plasma.

Reproduced with permission of the copyright owner. Further reproduction prohibited without permission.

Thus, the radial magnetic force per unit length can be represented by the following expression:

$$(10) \qquad F_{radial} = 2\pi r \left[-\frac{B_c^2}{2\mu_o} + \frac{B_o^2 a^4}{2\mu_o r^4} \right] .$$

The theta coil field initially increases approximately linearly with time, therefore, let

$$(11) \qquad B_c \approx \dot{B}_c (t + \beta),$$

where $\dot{B}_c$ = rate of change of the theta coil field,

β = a constant to be determined by the initial conditions.

Substituting this value of B_c into the expression for the radial force, Eqn. (10), we have,

$$(12) \qquad F_{radial} = 2\pi r \left[-\frac{\dot{B}_c^2 (t+\beta)^2}{2\mu_o} + \frac{B_o^2 a^4}{2\mu_o r^4} \right]$$

From the initial boundary condition that at

$$(13) \qquad t = 0 ; \qquad F_{radial} = 0 , \quad r = a ,$$

then substituting these values into Eqn. (12), it is found that,

Reproduced with permission of the copyright owner. Further reproduction prohibited without permission.

(14) $$\beta = \frac{B_o}{B_c} \quad .$$

The radial equation of motion can now be written using Eqn. (7), (12) and (14):

(15) $$\frac{d}{dt}\left[m\pi(a^2-r^2)\frac{dr}{dt}\right] + \frac{d}{dt}\left[m\pi a^2\epsilon\frac{dr}{dt}\right] = 2\pi r\left[-\frac{\dot{B}^2(t+\beta)^2}{2\mu_o} + \frac{B_c^2 a^4}{2\mu_o r^4}\right]$$

To write Eqn. (15) in dimensionless form, the variables y, τ, and T are introduced where,

(16) $$y = \frac{r}{a} \quad ,$$

$$\tau = \frac{t}{T} \quad ,$$

$$T = \left[\frac{\mu_o m a^2}{\dot{B}_c^2}\right]^{\frac{1}{4}} \quad .$$

The dimensionless equation of motion is,

(17) $$\frac{d}{d\tau}\left[(1-y^2+\epsilon)\frac{dy}{d\tau}\right] = y\left[-(\tau+\beta)^2 + \frac{\beta^2}{T^2 y^4}\right]$$

Solving this equation by a power series solution and using the initial boundary condition,

(18) at $\tau = 0$; $y = 1$,

$$\frac{dy}{dt} = 0 \quad ,$$

it is found that

Reproduced with permission of the copyright owner. Further reproduction prohibited without permission.

(19) $$y = 1 - \frac{\beta}{3\epsilon T}\tau^3 - \frac{1}{12\epsilon}\tau^4 + \frac{\beta^3}{15\epsilon^2 T^3}\tau^5 + \cdots\cdots .$$

From the framing camera photographs it is found that at the critical conditions for suppression of oscillations, the plasma radius collapses to roughly 0.8 of its original value, i.e. $y \sim 0.8$, before it disappears. When $y \sim 0.8$, the following condition on τ is valid:

(20) $$\left(\frac{T}{\beta}\right)^3 \epsilon > \tau > \frac{4\beta}{T}$$

(see P.84 for numerical verification and P.90 for theoretical results if this approximation is not valid). Using this condition, Eqn. (20), it can be shown that 'y' can be represented by:

(21) $$y \approx 1 - \frac{\tau^4}{12\epsilon} \approx 0.8$$

The value of τ when $y \approx 0.8$ is denoted by the variable τ_c. It follows then that,

(22) $$\tau_c \approx (2.4\epsilon)^{\frac{1}{4}}$$

Note that this critical time, τ_c, is not dependent on β or T. The axial motion produced during the critical time, τ_c, is discussed below.

Reproduced with permission of the copyright owner. Further reproduction prohibited without permission.

Section C.2 - Axial Equation Of Motion

In this case, it is necessary to take into account the presence of the two current rings indicated by the framing camera photographs, (see Fig. III. 9.). At breakdown, the changing flux from the theta coil produces a current at the outer surface of the discharge gas which causes intensive ohmic heating. The heated layer expands across the magnetic field trapped within the plasma cylinder, thereby generating a current on the inner surface of the plasma cylinder. This current conserves the flux within the cylinder. It is apparent from Fig. III.25. that in the snowplough approximation the axial momentum of the elemental mass contained by the angle $\Delta\theta$ is,

$$(23) \qquad \frac{m}{2\pi}\Delta\theta(a^2-r^2)\frac{dz}{dt} + \frac{m}{2\pi}\Delta\theta a^2\epsilon\frac{dz}{dt}$$

per unit length,

where z = axial displacement,
$\Delta\theta$ = angle enclosing a small portion of the plasma, (Fig. III.25.).

Reproduced with permission of the copyright owner. Further reproduction prohibited without permission.

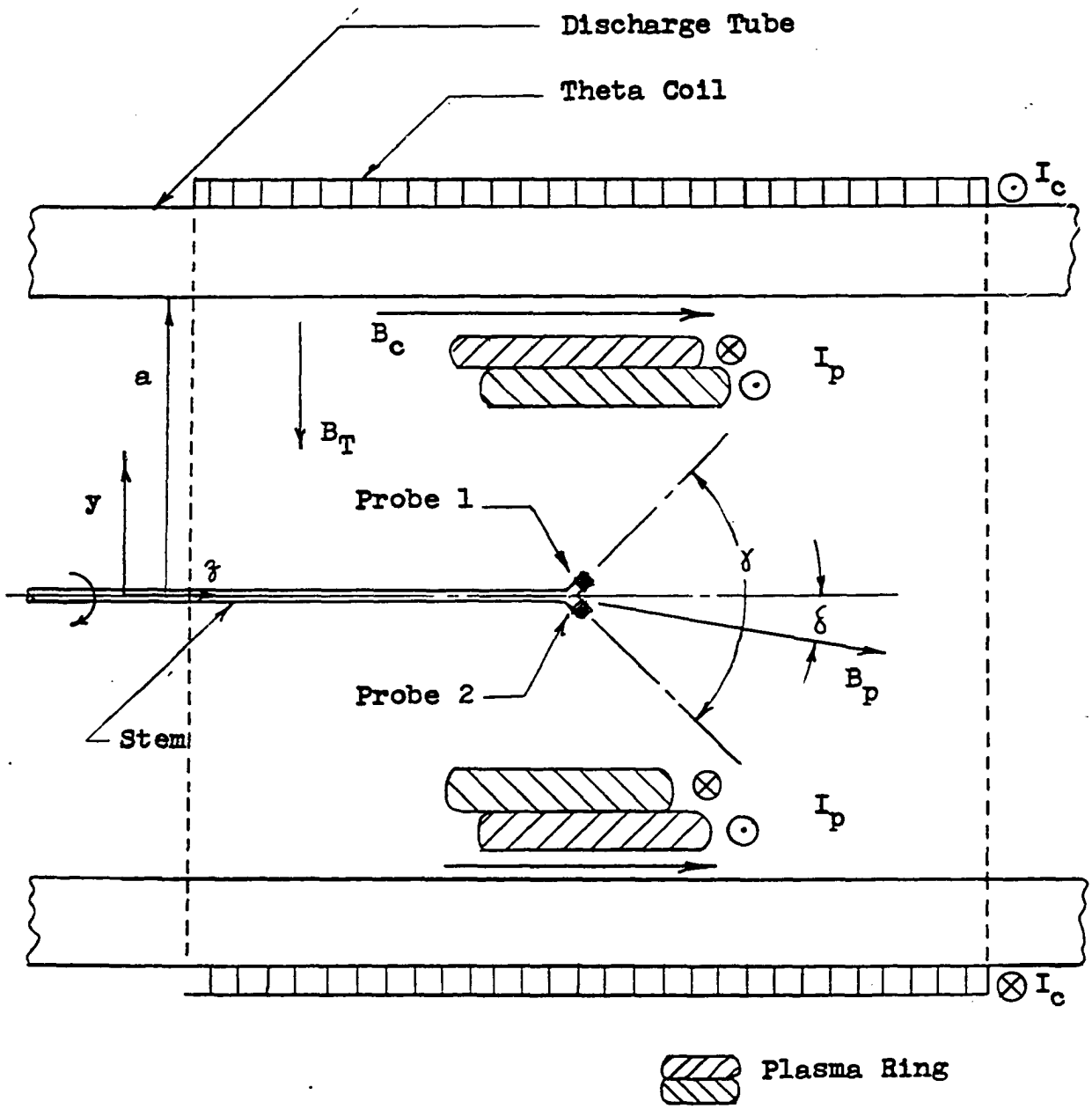

I_c = Theta Coil Current
I_p = Plasma Current
B_T = Transverse Magnetic Field
B_p = Plasma Magnetic Field
B_c = Theta Coil Magnetic Field

Fig. III.24. Axial Section Of The Theta Pinch Discharge

Reproduced with permission of the copyright owner. Further reproduction prohibited without permission.

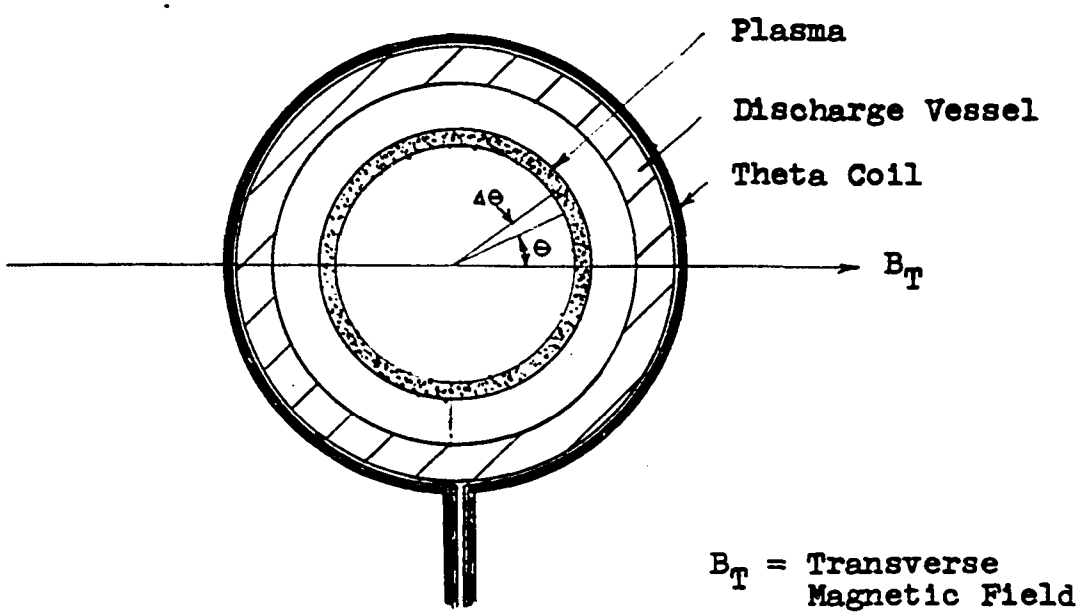

Fig. III.25. Specification Of The Angle 'θ'

The other variables have been previously specified (Page 69). The assumptions made in deriving the equation of radial motion (Page 69) are employed in this equation also.

In Eqn. (23), the first term is the momentum of the mass swept up by the collapsing shell and the second term is the momentum of the initial mass shell of the plasma. The total magnetic force acting on the plasma is,

(24) $$F_{axial} = r \Delta\theta \cos\theta B_H \sin\phi I_p - r \Delta\theta \cos\theta B_H \sin\phi I_c,$$

where I_p = the plasma current which conserves the initial trapped flux,

I_c = the plasma current induced by the theta coil,

Reproduced with permission of the copyright owner. Further reproduction prohibited without permission.

ϕ = angle enclosed by the theta field and Helmholtz field axis,

θ = azimuthal angle of the plasma, (Fig. III.25.).

The probe signal produced by the double probe technique corresponds to the net plasma field. However, it is assumed that when the inner current ring escapes confinement, the plasma conductivity drops and the radial hydromagnetic oscillations are suppressed. If viscosity is neglected, there is no coupling between the axial motions of the two current sheets and the motion of the inner current sheet can be considered separately. The motion of the inner current ring is discussed below.

The magnetic field produced by I_p, using the long solenoid approximation is then given by the equation below:

$$I_p \approx \frac{B_o}{\mu_o y^2} \tag{25}$$

where B_o is the magnetic field initially enclosed by I_p. If we let λK be the fractional mass initially occupied by the inner current layer, then the inertia force of the mass element is,

$$K\frac{d}{dt}\left[m\frac{\Delta\theta}{2\pi}\left(a^2 - r^2 + a^2\lambda\right)\frac{dz}{dt}\right] \quad , \tag{26}$$

where 'K' is the fraction of the mass through which the current shell passes that is retained in this shell ($K \approx 1$).

The equation of axial motion for this mass element becomes,

$$K\frac{d}{dt}\left[m\frac{\Delta\theta}{2\pi}\left(a^2 - r^2 + a^2\lambda\right)\frac{dz}{dt}\right] = r\Delta\theta\frac{B_o}{\mu_o y^2}\cos\theta\, B_r \sin\phi \quad . \tag{27}$$

Reproduced with permission of the copyright owner. Further reproduction prohibited without permission.

The maximum axial motion occurs at points where $\theta = 0^{\circ}$. If the variables y, τ, and T previously specified [Eqn. (16)] are used, then the dimensionless equation of motion at point of maximum axial motion becomes,

$$(28) \qquad y \frac{d}{d\tau}\left[(1-y^2+\lambda)\frac{dz}{d\tau}\right] = \frac{2\pi B_c B_H \sin\phi}{K B_c \mu_0^{\frac{1}{2}} a m^{\frac{1}{2}}}$$

$$(29) \qquad \text{where } Z = \frac{z}{a}$$

Substituting $y = 1 - \frac{\beta}{3\epsilon T}\tau^3 - \frac{1}{12\epsilon}\tau^4 + \frac{\beta^3}{15\epsilon^2 T^3}\tau^5$, Eqn. (19), and using a power series approximation, it can be shown that,

$$(30) \qquad Z = \frac{\pi B_c B_H \sin\phi}{K\lambda B_c \mu_0^{\frac{1}{2}} a m^{\frac{1}{2}}}\tau^2 + O(\tau^4)$$

Thus, the axial displacement in the time τ_c , will be,

$$(31) \qquad Z_0 = \frac{\pi B_c B_H \sin\phi}{K\lambda B_c \mu_0^{\frac{1}{2}} a m^{\frac{1}{2}}}\tau_c^2$$

However, $\tau_c^2 = (2.4\epsilon)^{\frac{1}{2}}$ from Eqn. (22), thus if $\frac{B_c \epsilon^{\frac{1}{2}}}{\lambda K B_c}$ is a constant, then the axial distance travelled by the elemental mass in the time τ_c is proportional to $\frac{B_H \sin\phi}{m^{\frac{1}{2}} a}$. If Z_0 is greater than some critical value, Z_c, then a flip occurs because the plasma confinement vanishes. This implies that $\frac{B_H \sin\phi}{m^{\frac{1}{2}} a}$ must exceed some critical value. However, $m^{\frac{1}{2}}$ is proportional to $p^{\frac{1}{2}}$, so that the experimental and computed criteria for flip are the same,

Reproduced with permission of the copyright owner. Further reproduction prohibited without permission.

(32) i.e. $\frac{\beta_n \sin\phi}{a p^{\frac{1}{2}}} > \text{constant}$

Section C.3 - Discussion Of The Assumptions

Section C.3a - The Trapped Field, B_o, Is Constant With Variation In Gas Pressure

From the integrated magnetic probe waveforms, the amplitude of the signals correspond to the strength of the magnetic field. Thus, by measuring the amplitude of the plasma signal when the oscillations are just suppressed, one can estimate the corresponding magnetic field. It is found that the plasma signal is identical (within accuracy of the measurements, $\sim 10\%$), for flip conditions at all pressures between 16 μ Hg to 75 μ Hg, thus implying that the trapped magnetic flux is approximately the same for all pressures, (see Fig. III.26.).

Reproduced with permission of the copyright owner. Further reproduction prohibited without permission.

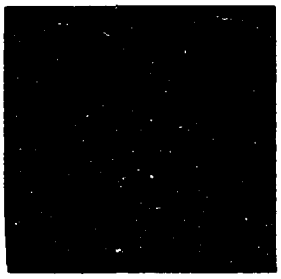

a. Pres: 15 μ Hg
Time = 1 μ sec/cm

b. Pres: 25 μ Hg

c. Pres 50 μ Hg

d. Pres 100 μ Hg

Top Of Double Beam Trace Corresponds To The Plasma Magnetic Field.

Fig. III.26. Probe Signals Showing B_o Is Constant For Different Pressures At Flip Condition

Reproduced with permission of the copyright owner. Further reproduction prohibited without permission.

Section C.3b - ϵ Is Constant With Respect To Variation In Gas Pressure

It is very difficult to verify quantitatively that the fractional portion of the mass, ϵ , in the initial collapsing plasma shell is approximately constant with varying gas pressure. However, it appears to be a reasonable assumption because the framing camera pictures show that the thickness of the plasma shell before it collapses under the flip conditions, is constant with varying pressures, (see Fig. III.27.). Thus, one would expect the fractional mass, ϵ , in the shell to be approximately constant with change in gas pressure.

Section C.3c - The Magnetic Field Can Be Approximated By The Magnetic Field Of An Infinite Solenoid

The infinite solenoidal approximation would be valid for a coil of high aspect ratio (i.e. $\frac{\text{length}}{\text{diameter}}$) but in this experiment, the aspect ratio is $\sim$ 1. However, in the region close to the walls of the discharge vessel, the solenoidal field representation becomes a reasonable approximation. Thus, in the radial equation of motion, when $y > 0.8$ (i.e., the region of interest in this experiment), a solenoidal field approximation is reasonable. From theoretical calculations, the field changes by $\sim$ 10% in this region, ($y = 1 \rightarrow y \approx 0.8$). The plasma field in the radial equation is a second order effect when $y > 0.8$ and thus the solenoidal approximation is not important.

Reproduced with permission of the copyright owner. Further reproduction prohibited without permission.

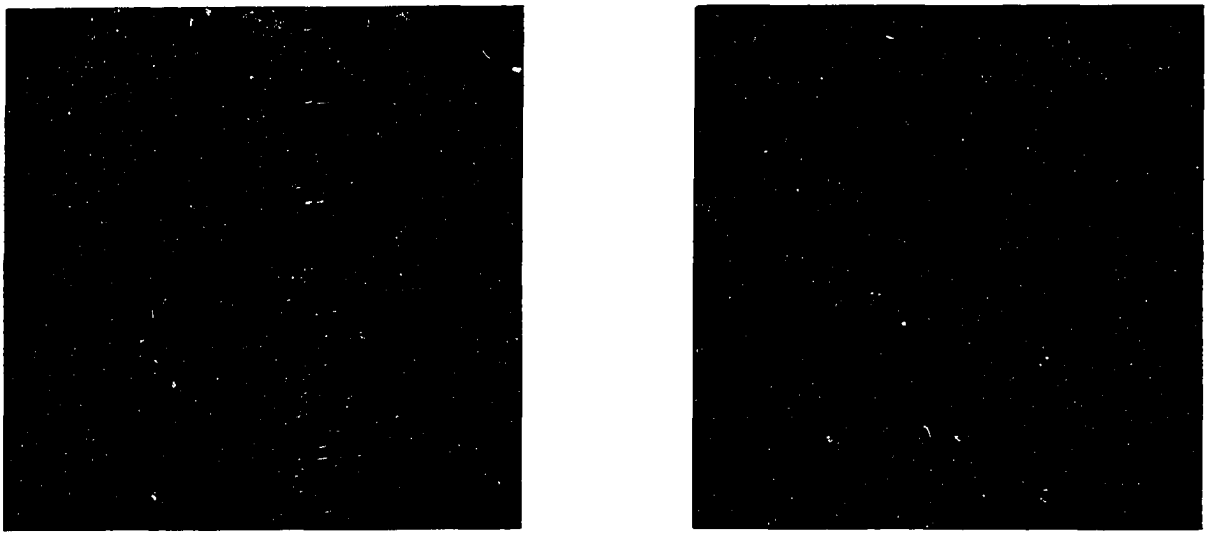

a. 50 μ Hg

b. 250 μ Hg

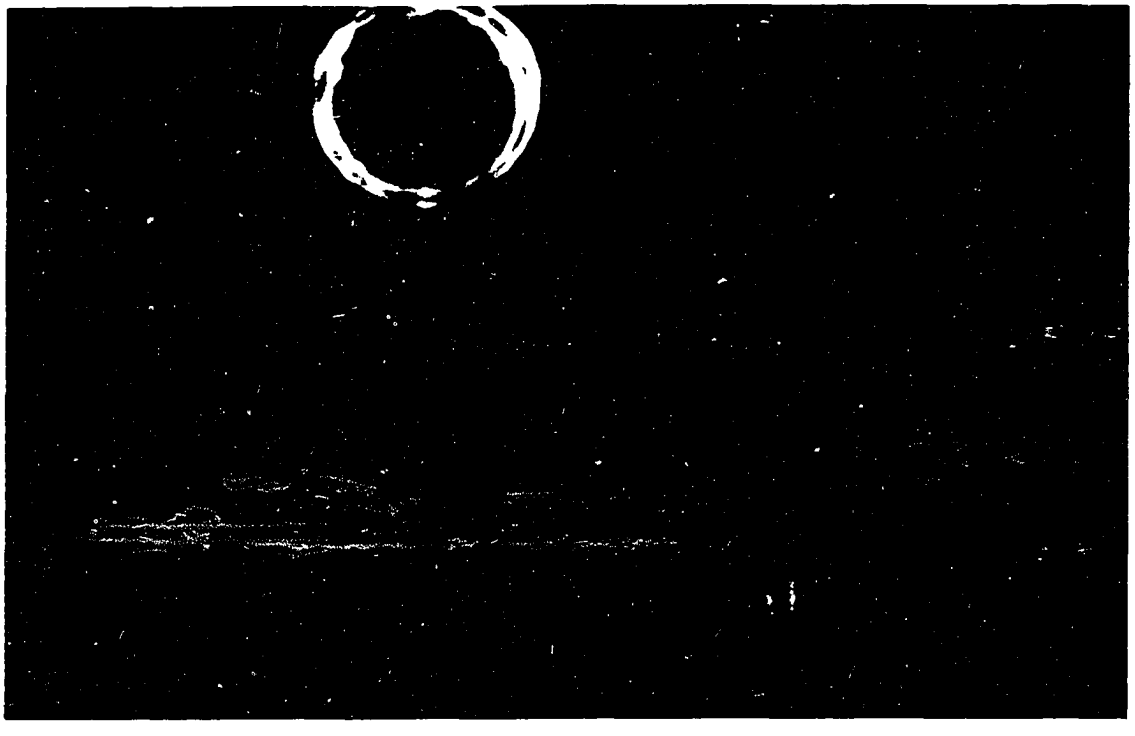

Gas: Air

c. 100 μ Hg

Fig. III.2 7. End On Photographs Of The Plasma At Flip Conditions

Reproduced with permission of the copyright owner. Further reproduction prohibited without permission.

In the case of the axial equation of motion, the plasma current interacting with the transverse magnetic field is the dominant force. However, this force, F_{axial}, is proportional to $I_p B_T$, and thus the geometry of the magnetic field produced by I_p is not important. The only necessary requirement is that the trapped field, B_o, be proportional to I_p, which is true for a plasma of any given geometry, i.e., $B_o = I_p F(r,z)$.

Reproduced with permission of the copyright owner. Further reproduction prohibited without permission.

Section C.3d - $\left(\frac{I}{\beta}\right)^3 \epsilon > \tau_c > \frac{4\beta}{I}$ Approximation

In this section, the approximation $\left(\frac{I}{\beta}\right)^3 \epsilon > \tau_c > \frac{4\beta}{I}$ is investigated by substituting typical experimental values for the variables. This approximation is used in deriving the expression $y = 1 - \frac{\tau^4}{12\epsilon}$. Now,

(16) $$T = \left[\frac{\mu_o m a^2}{\dot{B}_c^2}\right]^{\frac{1}{4}}$$

where μ_o = permeability = $4\pi \times 10^{-7}$ Henries/m

m = mass density $\approx 7.9 \times 10^{-5}$ kgm/m^3 for p = 50 μ Hg, air,

a = radius of the discharge vessel = 0.025 meters,

$\dot{B}_c$ = rate of change in the theta coil magnetic field $\approx 1.2 \times 10^6$ weber/m^2 sec

so that $T \approx 0.5\ \mu$ sec.

(14) $$\beta = \frac{B_o}{\dot{B}_c}$$

where B_o = initial trapped magnetic field $\approx \frac{1}{50} B_{max}$.

The value of B_o was derived from the fact that under flip conditions, the amplitude of the integrated probe signal due to the plasma magnetic field is $\approx \frac{1}{50}$ the amplitude of the signal corresponding to the theta coil field, (see Fig. III.28.).

Reproduced with permission of the copyright owner. Further reproduction prohibited without permission.

Upper Trace - Plasma Magnetic Field: 0.05 V/cm, Lower Trace - Theta Coil Magnetic Field: 1V/cm, Time : 1 μ sec /cm, Pressure : 25 μ Hg, air, Other conditions specified on Page 40.

Fig. III.28. Plasma Field Strength At Flip Conditions

$B_{max} = 2.8$ weber/m^2

$B_o = 0.056$ weber/m^2

$\dot{B}_c = 1.2 \times 10^6$ weber/m^2 sec

then $\beta = 0.046 \mu$sec.

Substituting into $\frac{4\beta}{T}$,

(33) $$\frac{4\beta}{T} = 0.37$$

Reproduced with permission of the copyright owner. Further reproduction prohibited without permission.

From Eqn. (22),

$$\tau_c = (2.4\epsilon)^{\frac{1}{4}} \tag{22}$$

From the end on photographs of the plasma, (Fig. III.27.), it is seen that the thickness of the plasma sheet before the collapse is $\approx \frac{1}{10}a$. Therefore it is reasonable to assume that $\epsilon \sim \frac{1}{10}$. Although the value of ϵ is difficult to determine accurately, it is seen from Eqn. (22) that τ_c is a weak function of ϵ. The particular value assumed for ϵ does not therefore critically affect the validity of the inequality, $(\frac{T}{\beta})^3\epsilon > \tau_c > \frac{4\beta}{T}$.
Using $\epsilon \approx \frac{1}{10}$

$$\tau_c \approx 0.7 \tag{34}$$

From the above values for T, β, and ϵ, it follows that

$$(\frac{T}{\beta})^3\epsilon \sim 100 \tag{35}$$

The inequality ($(\frac{T}{\beta})^3\epsilon > \tau_c > \frac{4\beta}{T}$, Page 84), then becomes

$$100 > 0.7 > 0.4 \tag{36}$$

Hence the expression employed for y in the axial equation (i.e. $y \approx 1 - \frac{\tau^4}{12\epsilon}$) is valid within the limits of experimental accuracy.

Reproduced with permission of the copyright owner. Further reproduction prohibited without permission.

Section C.4 - A Discussion Of The Interpretation Of The Suppression Of Oscillations As The Flip Instability

Two plausible ways in which the suppression of oscillations with increasing transverse magnetic field can be interpreted are the following: first, the plasma conductivity becomes too small to support the plasma current and thus the plasma dissipates, or secondly, the plasma has escaped from the ends of the coil because of axial motion.

In the conductivity model, the suppression of the oscillations is explained by assuming that as the transverse bias field is increased, the conductivity of the plasma is decreased thus causing the plasma to disappear. However, this model has a number of inherent difficulties.

1. One would expect preionization to enhance the hydromagnetic oscillations and thus effectively increase the stability constant. Yet, when preionization is applied, the stability constant is not affected (see Appendix, A).

Reproduced with permission of the copyright owner. Further reproduction prohibited without permission.

2. One would expect the stability constant to not increase if the length of the coil is increased and the peak induced electric field in the discharge tube is kept constant. Yet, on varying the length of the coil (see Appendix B) it is found that the stability constant increases as the length of the coil is increased.
3. One would not expect the transverse field to be important when the theta coil field becomes large. Yet in the magnetic probe waveforms, the oscillations are slowly damped when $\frac{B_T}{B_c} \approx \frac{1}{30}$ (2 - 3 μsec after the breakdown of the plasma).

On the other hand, if the suppression of the oscillations is due to axial motion of the plasma, then one would expect the stability to increase with the length of the coil because the plasma must travel a longer distance to escape the theta coil. Also, axial motion of the plasma will exist even when $\frac{B_T}{B_c} \approx \frac{1}{30}$, causing a gradual suppresion of oscillation because the axial force on the plasma is a direct function of B_T and not B_c.

At the time of suppression of oscillations, from the end on framing camera photographs (Fig. III.13.), there is no clear evidence that the plasma has a large axial motion because the plasma forms close to the edge of the coil and thus escapes after only a small displacement. However, from framing camera pictures where the axial velocity can be measured approximately, it is seen that for 100 μ Hg gas pressure, the axial velocity of the plasma is~1 cm / μ sec (see Fig. III.11). Thus, the

Reproduced with permission of the copyright owner. Further reproduction prohibited without permission.

axial motion can cause the disappearance of the plasma in $< 1\,\mu$ sec. As the plasma moves axially out of the coil it is probably forced into the walls because the magnetic field lines outside the discharge tube, intersect the walls of the tube. The contact with the walls rapidly cools the plasma and it dissipates, (see Fig. III.29.).

Because of the experimental evidence of the effect of preionization and the length of the discharge coil on the stability constant, and also the evidence from the framing camera pictures, the plasma's axial motion has been chosen to explain the suppression of the hydromagnetic oscillations.

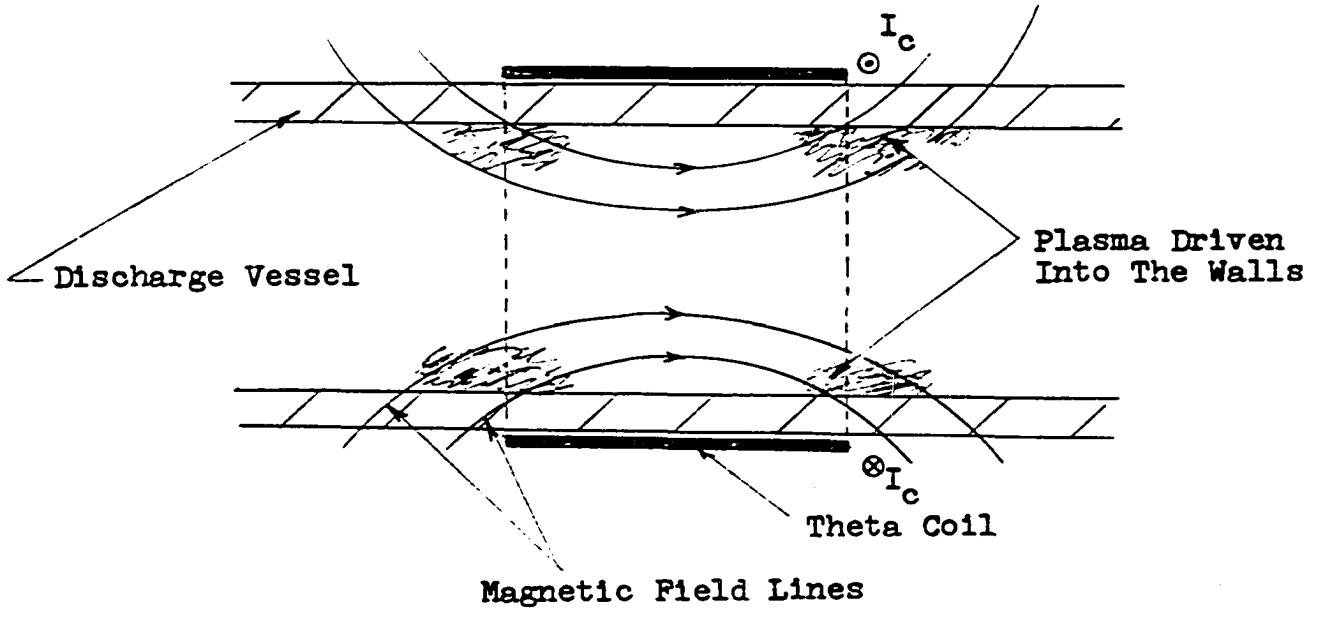

Fig. III.29. Magnetic Field Lines Of Theta Coil

Reproduced with permission of the copyright owner. Further reproduction prohibited without permission.

Section C.5 - Variations Of The Theoretical Model

In this section variations in the theoretical model are made that could describe the axial motion of the plasma. The corresponding criterion for the flip instability is then derived.

1. Suppose that the τ^3 term in the expression

(19) $$y = 1 - \frac{\beta}{3\epsilon T}\tau^3 - \frac{1}{12\epsilon}\tau^4 + \frac{\beta^3}{15\epsilon^2 T^3}\tau^5$$

is the dominant term, i.e. $\tau_c < \frac{4\beta}{T}$. Then the value of τ_c would be

(37) $$\tau_c \approx \left[\frac{0.6\epsilon T}{\beta}\right]^{\frac{1}{3}}$$

where $$T = \left[\frac{\mu_0 m a^2}{B_c^2}\right]^{\frac{1}{4}}$$

$$\beta = \frac{B_o}{B_c}$$

Substituting this value of τ_c into the solution of the axial equation of motion, Eqn. (31), then it follows that

(38) $$z_o = \frac{\pi B_o B_n \sin\phi}{K\lambda B_c \mu_o^{\frac{1}{2}} a m^{\frac{1}{2}}}\tau_c^2$$

So that the criterion for flip becomes,

(39) z_o varies as $\frac{B_n \sin\phi}{a^{\frac{1}{2}} m^{\frac{1}{2}}} >$ constant .

Reproduced with permission of the copyright owner. Further reproduction prohibited without permission.

Hence for this model, the stability constant would vary as $(am)^{-\frac{1}{3}}$. This is not borne out by the experimental results.

2. Suppose the axial motion of the outer current sheet is responsible for the disappearance of the oscillations. Then using the same assumptions as given in the text, Page 69, the power series approximation to the radial equation can be approximated by

$$y \approx 1 - \frac{1}{12\epsilon}\tau_c^4, \quad \text{at} \quad y \approx 0.8 \tag{21}$$

Thus

$$\tau_c \propto (2.4\epsilon)^{\frac{1}{4}} . \tag{22}$$

The axial equation of motion of the outer sheet is

$$(1-K)\frac{d}{dt}\left[m(1-y^2+\xi)\frac{dz}{dt}\right] = \frac{2\pi B_c B_m \sin\phi\cos\theta}{a^2\mu_0} , \tag{40}$$

where $(1-K)\xi a^2\pi$ = the initial mass of the outer current sheet.

Using the boundary conditions:

$$t = 0; \quad z = 0 , \tag{41}$$

$$\frac{dz}{dt} = 0 ,$$

Reproduced with permission of the copyright owner. Further reproduction prohibited without permission.

and using the usual assumptions described previously, (Page 69), the power series approximation to this equation is

$$(42) \qquad z_o = \frac{B_H \cos\theta \sin\phi}{(1-K)\xi a^{\frac{1}{2}} \dot{B}_c^{\frac{1}{2}}} \left(\frac{\pi}{\mu_o m}\right)^{\frac{1}{4}} \tau_c^3$$

where $\tau_c = (2.4\epsilon)^{\frac{1}{4}}$

so that

$$(43) \qquad z_o \propto \frac{B_H \sin\phi}{a^{\frac{1}{2}} m^{\frac{1}{4}}} > \text{constant} .$$

Hence for this model the stability constant would vary as $a^{-\frac{1}{2}} m^{-\frac{1}{4}}$, which again is not borne out by the experimental results.

3. Consider the case where the axial motion of the outer current sheet is responsible for the disappearance of the oscillations but the τ^3 term in the radial solution

$$(19) \qquad y = 1 - \frac{\beta}{3\epsilon T}\tau^3 - \frac{1}{12\epsilon}\tau^4 + \frac{\beta^3}{15\epsilon^2 T^3}\tau^5 + \cdots$$

is the dominant term, i.e.

$$(44) \qquad y \approx 1 - \frac{\beta}{3\epsilon T}\tau_c^3 \sim 0.8 ,$$

then

$$\tau_c \approx \left[\frac{0.6\epsilon T}{\beta}\right]^{\frac{1}{3}} ,$$

(37)

where $T = \left[\frac{\mu_o m a^2}{\dot{B}_c^2}\right]$,

$$\beta = \frac{B_o}{\dot{B}_c} .$$

Reproduced with permission of the copyright owner. Further reproduction prohibited without permission.

Substituting this value of r_c into the solution to the axial equation for the outer current sheet, Eqn. (42), the criterion for flip then becomes

(45) Z_o varies as $B_H \sin\phi_c >$ constant

Note that the flip condition in this case is independent of the mass density of the discharge gas and the radius of the discharge vessel - a prediction which is again not confirmed by the experimental data.

From the above discussion, it is seen that the model of the flip that is used in the text of the thesis is the model which best fits the experimental results and also the experimental conditions. In this model it is assumed that the plasma ceases to exist as soon as the inner current layer is driven a critical distance in the axial direction of the discharge.

Section D - Suggestions For Further Work

1. In the work reported above, the accuracy in the direct measurement of the rotation of the plasma has been limited by the time resolution of the framing camera. However, the results from the directional probes indicate that this method of measuring rotation, when perfected, is feasible to obtain quantitative results. To improve the spatial resolution of the probe waveforms, a discharge vessel of larger diameter could be employed; also the directional response of the probe could be improved by

Reproduced with permission of the copyright owner. Further reproduction prohibited without permission.

increasing the length of the search coil (see Fig. II.17.). To improve the time resolution of the probe waveforms, a heavier gas could be employed to slow down the dynamics of the plasma. A second improvement on the time resolution would be to increase the frequency response of the probe.

2. From the theory, it is seen that the object of this investigation is the inner plasma current which conserves the trapped magnetic field. To investigate the behaviour of the outer current sheet, it is necessary that the trapped flux in the plasma be negligible. Then using the double probe technique (see Page 26), the magnetic waveform would correspond to the magnetic field produced by the outer current sheet.

For this case, the theoretical flip criterion is,

$$(46) \qquad Z_0 \text{ varies as } \frac{B_4 \sin\phi}{a^{\frac{1}{2}} m^{\frac{1}{2}}} > \text{constant}$$

In this case, the stability constant varies as $a^{-\frac{1}{2}} m^{-\frac{1}{2}}$.

To attempt to obtain the experimental conditions when the trapped field is negligible, a heavy preionization of the discharge gas could be applied by a Z pinch discharge. If the conductivity of the plasma is sufficiently high at the beginning of the theta bank discharge, then there will be a negligible amount of magnetic flux that can diffuse into the plasma ring and become trapped. In this experiment the suppression of oscillation would be investigated at the beginning of the first half cycle of the theta current.

Reproduced with permission of the copyright owner. Further reproduction prohibited without permission.

CHAPTER IV

CONCLUSIONS

The results reported show that the flip instability can be produced in a theta pinch discharge and that the direction of rotation can be controlled by applying a magnetic field transverse to the theta pinch field. Using the suppression of hydromagnetic oscillations to detect the flip instability, it is found that if $\frac{B_H \sin\phi}{a\, p^{\frac{1}{2}}}$ is greater than a given constant, then the plasma ring flips.

The results also clearly demonstrate that if bias fields are used to improve the discharge characteristics, then these fields must be accurately aligned with the discharge axis. A misalignment of $\phi \sim 2^{\circ}$ with a 0.3 weber/m^2 bias field can produce catastrophic flip instabilities. Misalignment problems are best avoided by using the theta coil itself to produce any bias field required.

Another feature of the investigation is that the validity of the two current models of a theta pinch discharge is confirmed. This is difficult to do if only the radial dynamics of the plasma are observed. However, the transverse bias field clearly separates at least two current rings.

A theoretical model of the plasma flip is constructed to assist in the interpretation of the experimental results. In

Reproduced with permission of the copyright owner. Further reproduction prohibited without permission.

this model, the plasma consists of two main current rings. The outer current ring is the result of the change in the magnetic flux produced by the theta coil. The inner current ring is a result of the conservation of the magnetic flux trapped by the plasma. When the inner current ring escapes from the coil, the radial hydromagnetic oscillations are suppressed. The criterion for flip predicted by this model agrees with the experimental results given on Page 95 .

Reproduced with permission of the copyright owner. Further reproduction prohibited without permission.

APPENDIX A

EFFECT OF PREIONIZATION ON THE STABILITY CONSTANT

A tesla coil is used to preionize the discharge gas before the theta bank is discharged. The purpose of this experiment is to determine the effect of preionization on the flip instability. The experimental procedure for determining the critical value of the stability constant, $B_H \sin \phi_c$, as a function of pressure is identical to the experimental procedure as given for the investigation of air (Page 52), except that the gas is ionized by a tesla coil during the theta bank discharge. It is found that there is no appreciable difference in the experimental results. A plot of $B_H \sin \phi$ as a function of pressure is given for both with and without preionization in Fig. A.1.

Reproduced with permission of the copyright owner. Further reproduction prohibited without permission.

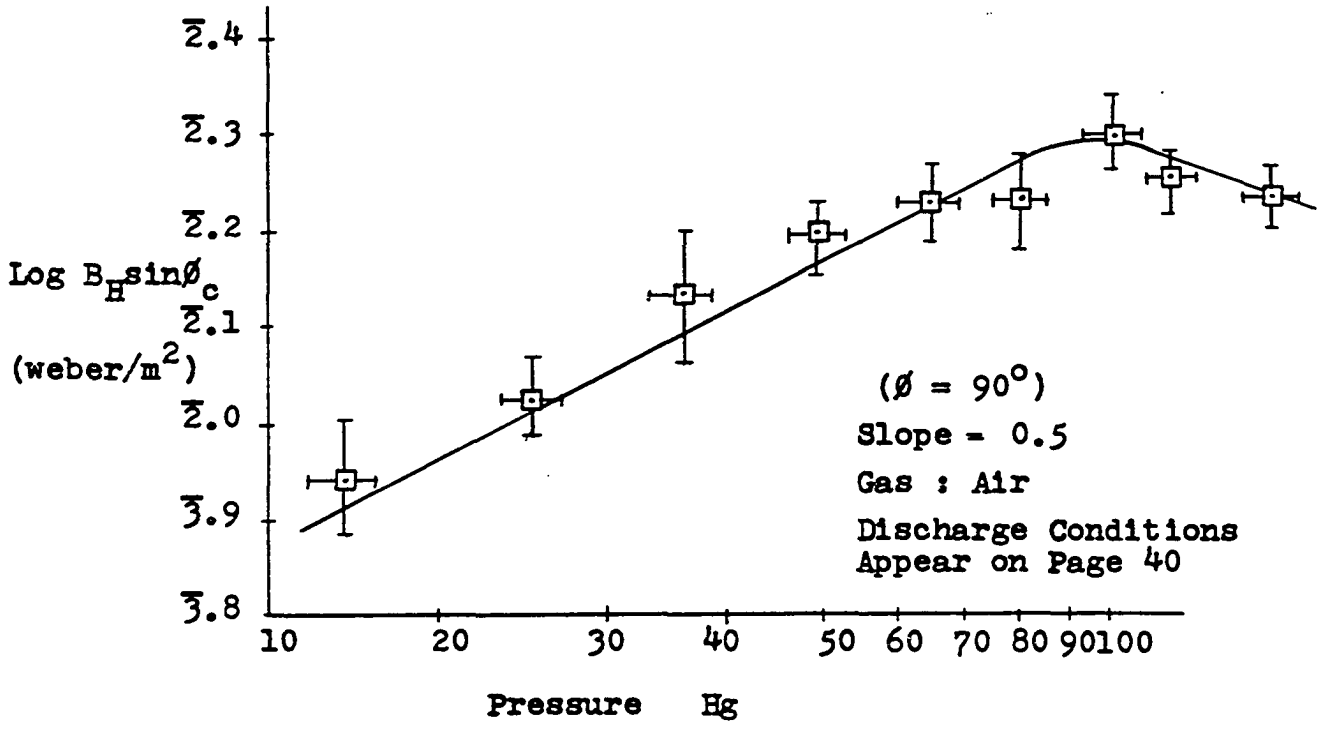

a. Without Preionization

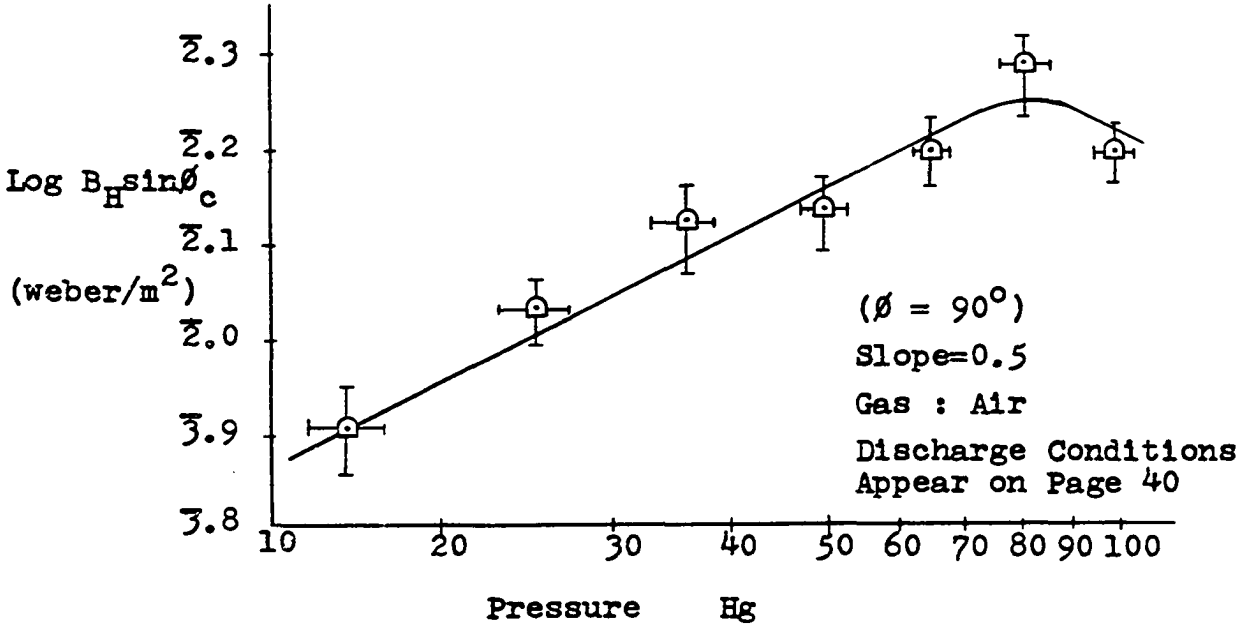

b. With Preionization

Fig. A.1. Plots Showing Effect Of Preionization On Stability

Reproduced with permission of the copyright owner. Further reproduction prohibited without permission.

APPENDIX B

CHANGE IN THE STABILITY CONSTANT WITH VARYING THETA COIL LENGTH

The purpose of this experiment is to determine how the constant, $\frac{B_H \sin\phi_c}{a\, p^{\frac{1}{2}}}$, varies with a variation in the length of the theta coil. In theory, a flip occurs if $Z_o > Z_c$, where Z_c is proportional to the length of the coil. This inequality can be expressed as

$$\frac{B_H \sin\phi}{p^{\frac{1}{2}}} > \text{constant which varies as the length of the coil.}$$

Thus, the theory predicts that the stability constant should be proportional to the length of the coil, i.e.,

$$\frac{B_H \sin\phi_c}{p^{\frac{1}{2}}} \text{ varies as the coil length}$$

In this experiment the value $B_H \sin \phi_c$ was found for a given gas pressure (100 μ Hg, air), for different coil lengths. Three coil lengths were used and the theta bank voltage was varied to keep $\frac{I^2_{coil}}{length}$ constant, see below.

Reproduced with permission of the copyright owner. Further reproduction prohibited without permission.

Experimental Conditions For Different Coil Lengths

Coil Length	3.4 cm	5.1 cm	6.8 cm
Theta Bank Voltage	9.4 kv	11.5 kv	13.5 kv
Induced Electric Field (Infinite solenoid approximation)	1.4 E_o	1.2 E_o	E_o

It is seen that the stability constant increases approximately linearly with increase in the theta coil length. (Fig. A.2.) However, the results are only qualitative because of the crude approximations that are made.

If the stability constant is a conductivity phenomenon. then one would expect the constant to decrease with decreasing induced electric field, but this is not supported by the experimental results.

The investigation was not carried on for longer coil lengths because of the limitations of the peak charging voltage of the theta bank.

Reproduced with permission of the copyright owner. Further reproduction prohibited without permission.

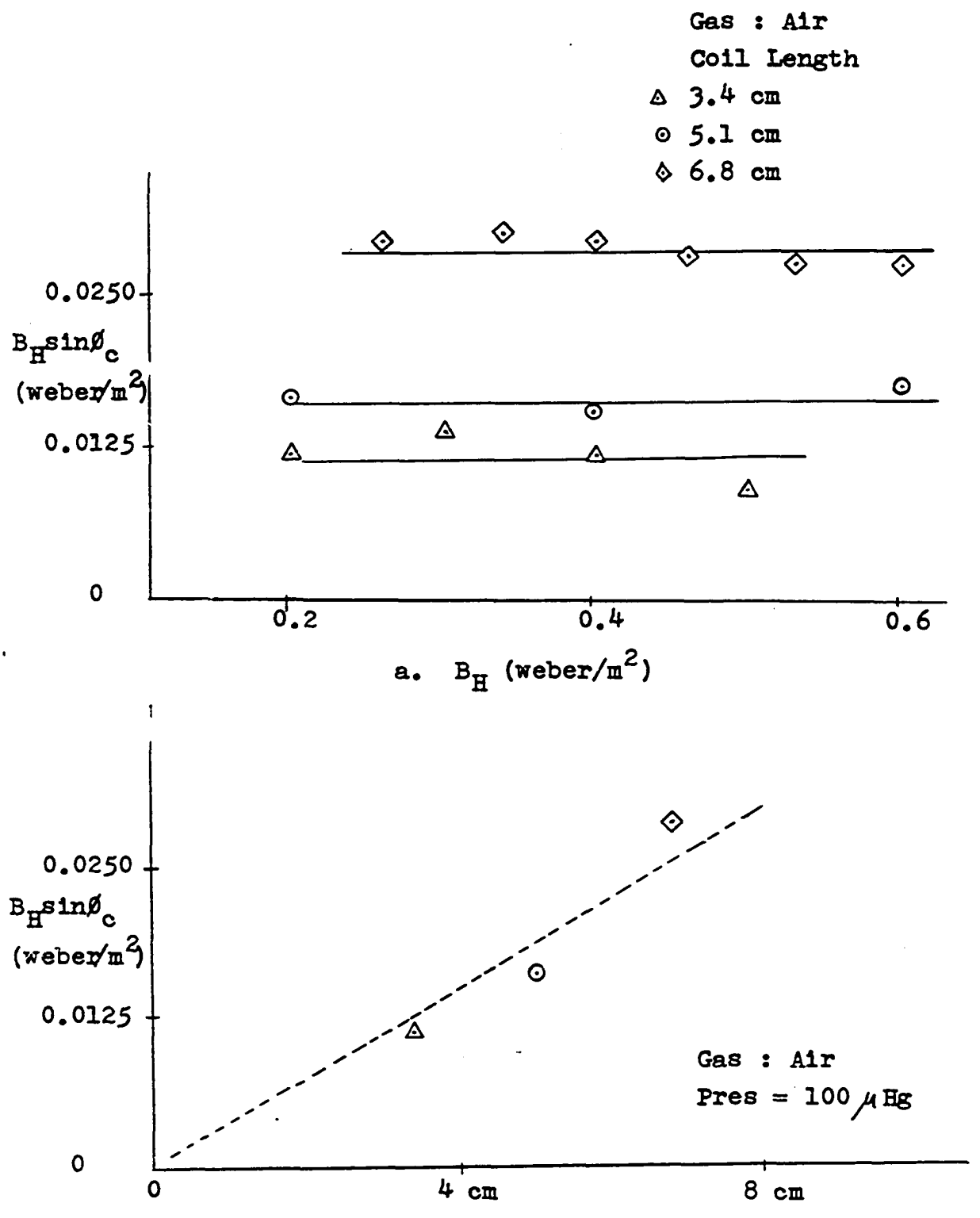

Fig. A.2. Stability Constant Variation With Coil Length

Reproduced with permission of the copyright owner. Further reproduction prohibited without permission.

APPENDIX C

SUMMARY ON THE ARGON EXPERIMENTS

An experiment to determine the variation of the critical value of the stability constant, $B_H \sin \phi_c$ (see Page 51), as a function of pressure is taken for argon. The experimental procedure is identical to the procedure given for the investigation of air (Page 51). The pressures investigated are 8 μ Hg, 17 μHg, 25 μ Hg, and 41 μ Hg.

Argon at a given pressure was found to be more stable to the flip instability than air, (see Fig. A.4.). The non-linear portion of the curve was not determined because the bias magnetic field was not sufficiently strong to suppress the oscillations at pressures greater than 50 μ Hg. Within experimental error, the constant $B_H \sin \phi_c$, varies as $(\text{pressure})^{\frac{1}{2}}$, (see Fig. A.4.).

Reproduced with permission of the copyright owner. Further reproduction prohibited without permission.

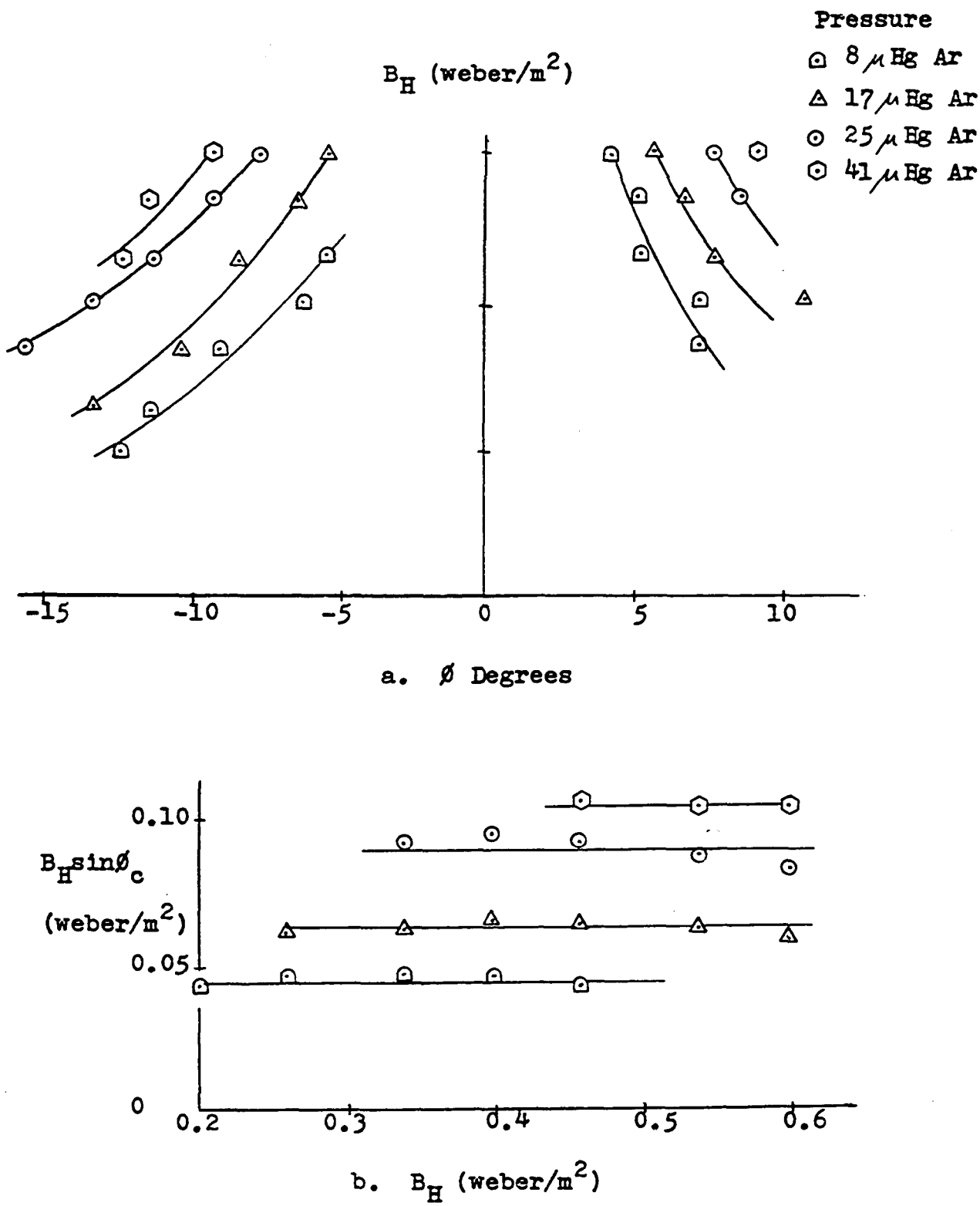

Fig. A.3. Value of $B_H \sin\phi_c$ For Different Gas Pressures (Argon)

Reproduced with permission of the copyright owner. Further reproduction prohibited without permission.

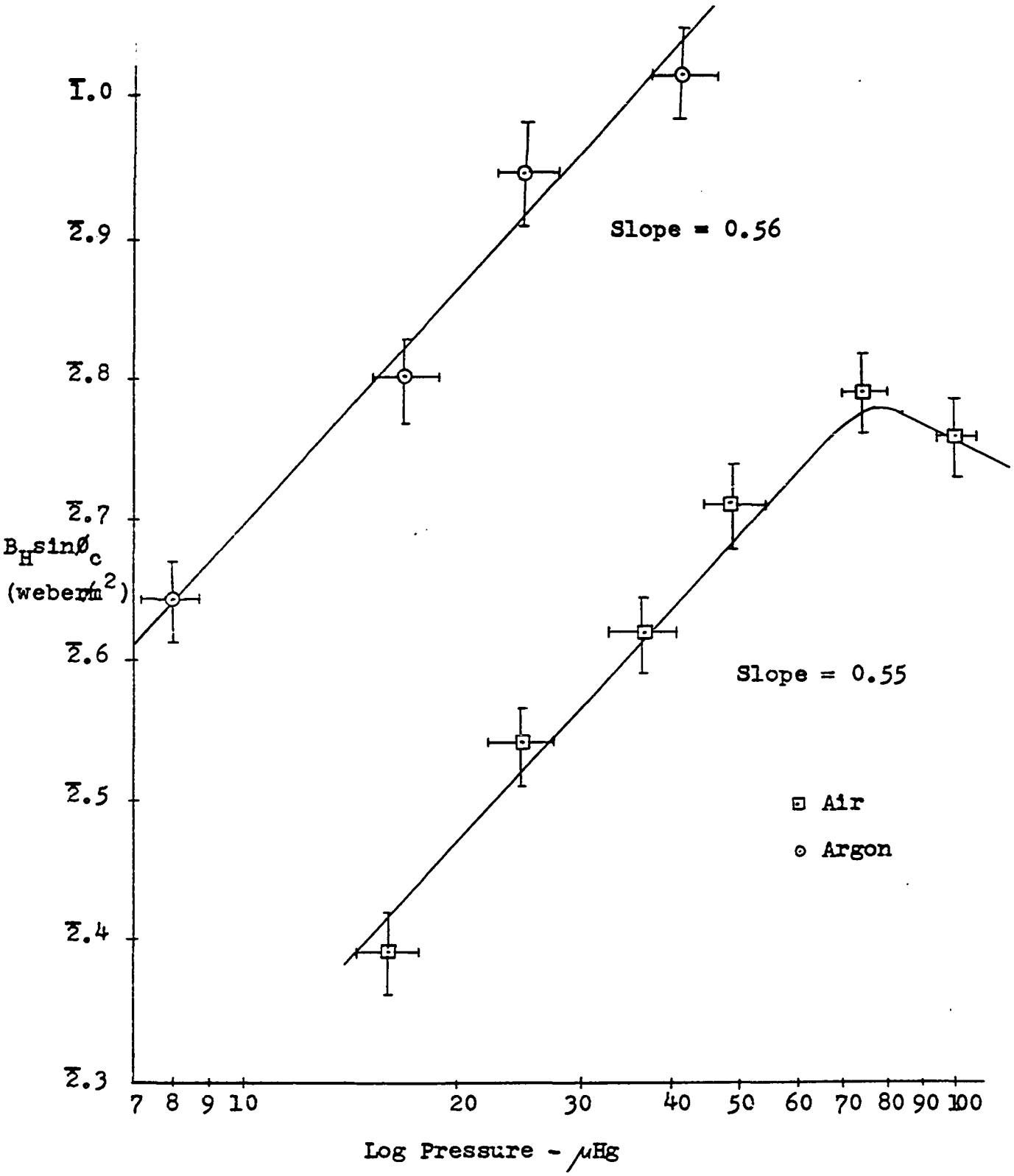

Fig. A.4. Comparison Of The Stability Constant Of Argon and Air

Reproduced with permission of the copyright owner. Further reproduction prohibited without permission.

APPENDIX D

PICTURES OF FLIP AT 100 μHg AND 250 μHg, AIR

Framing camera pictures of the plasma were taken for different gas pressures. As the mass of the plasma is increased, the dynamics of the plasma slows down and it is found that the actual rotation of the plasma about its diameter becomes more clear. At high pressures (i.e. 250 μHg, air, see Fig. A.5.) a new phenomenon also appears. As at lower pressures, two current rings are observed. However, the outer current ring is not the first to collapse radially. This indicates that the two current rings are not produced by axial tearing of the Niblett and Green model of the plasma. The tearing motion may be suppressed at high pressures because of the increased inertia of the discharge. We suggest that the outer current ring at high pressures is produced in material evaporated from the wall of the discharge vessel. At lower pressures ($\sim$ 50 μHg), the discharge spends less time near the wall so that the impurity rings do not develop so readily. The sluggish movement of the impurity current ring indicates that the current is probably fairly low, or that the ring is fairly massive.

Reproduced with permission of the copyright owner. Further reproduction prohibited without permission.

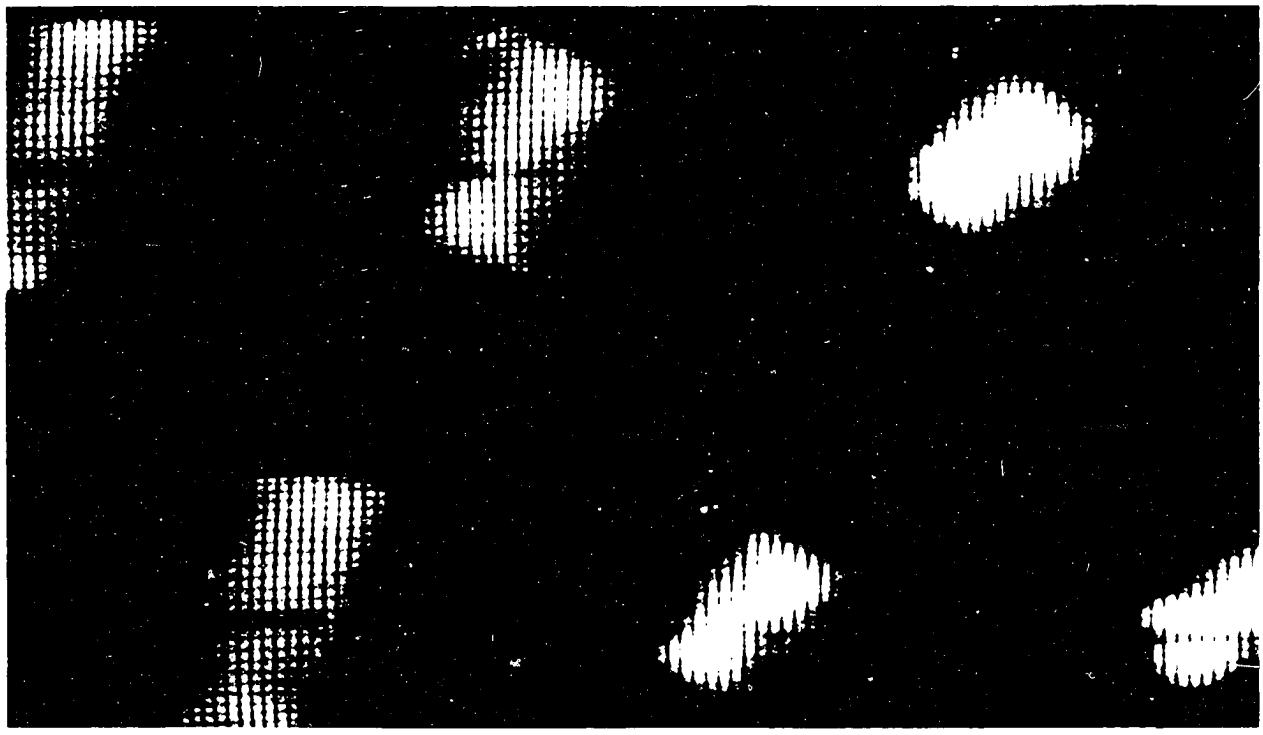

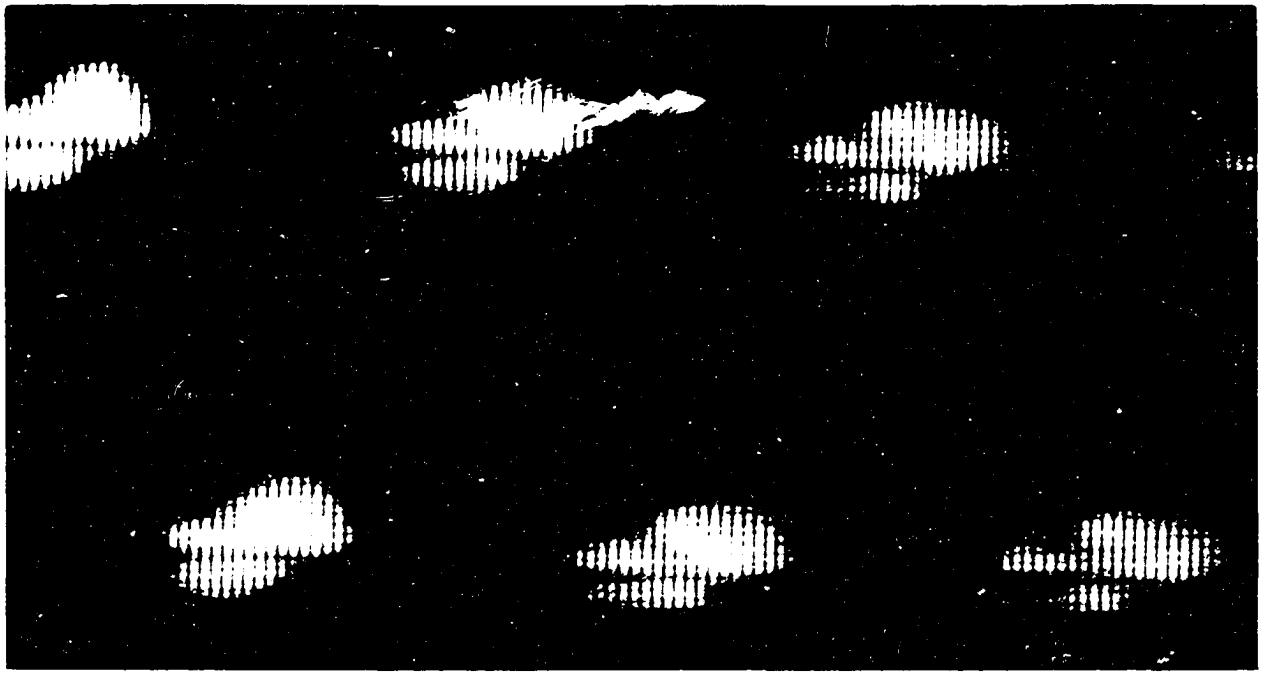

Fig. [illegible] Right, Frame Positions are Reversed, [illegible], Exposure Time = [illegible] .3 4 sec.

Fig. [illegible] Oscillograph Of Plasma [illegible]

Reproduced with permission of the copyright owner. Further reproduction prohibited without permission.

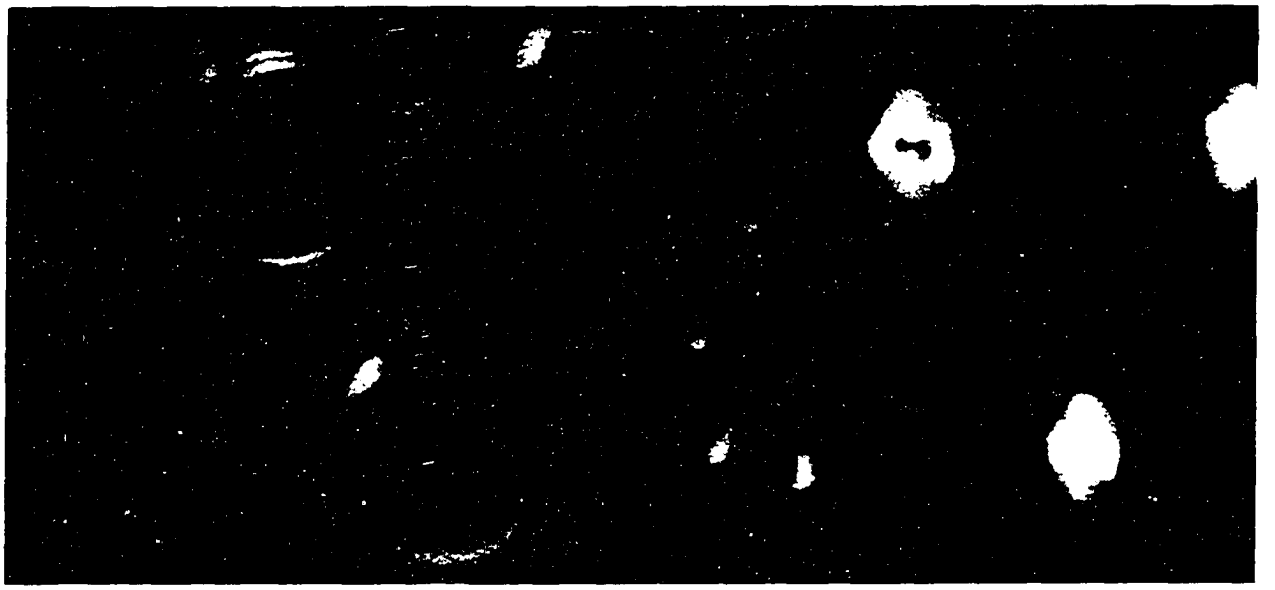

B_T = 0.024 weber/m^2, ($\phi = 90^\circ$).

Fig. A.6. End On Photograph At 200 μ Hg Pressure - Air

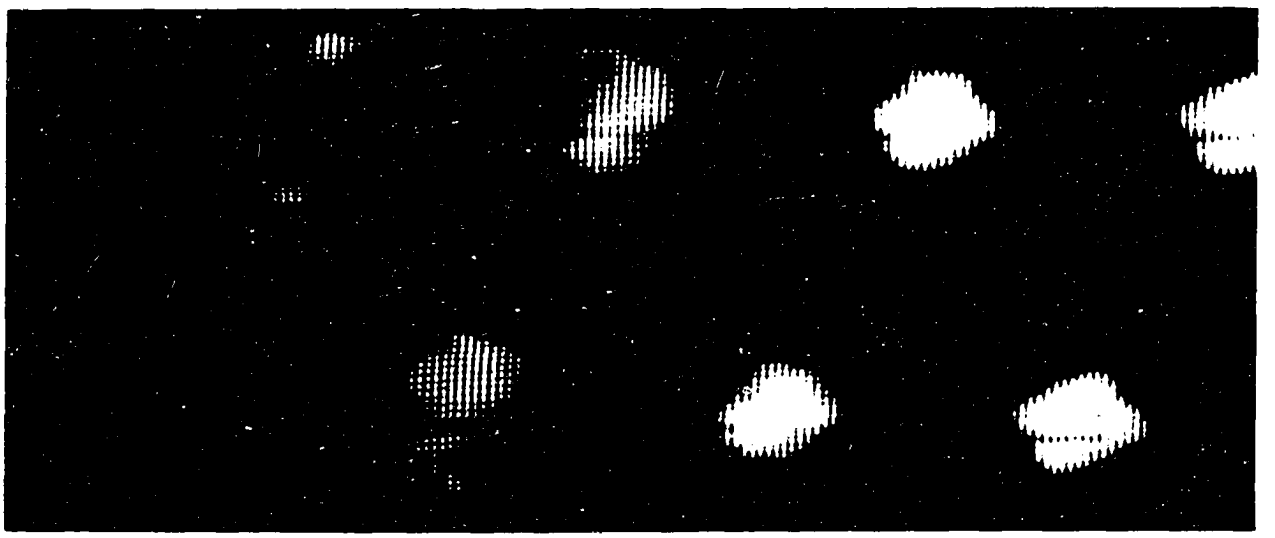

B_T = 0.042 weber/m^2, ($\phi \approx 0^\circ$)

Fig. A.7. Top On Photograph At 100 μ Hg Pressure - Air

Reproduced with permission of the copyright owner. Further reproduction prohibited without permission.

APPENDIX E

CHARACTERISTIC IMPEDANCE OF A MAGNETIC PROBE

One desirable characteristic of a magnetic probe when used to make measurements is that the frequency response be flat in the frequency range of interest (see Page 23). In a magnetic probe, there is a self inductance and stray capacitance which combine to form a resonant circuit. However, the resonance can be effectively damped (see Segre and Allen, 1960) by introducing an appropriate resistor, R, (see Fig. A. 6.).

The equivalent circuit for the magnetic probe can be written as shown below.

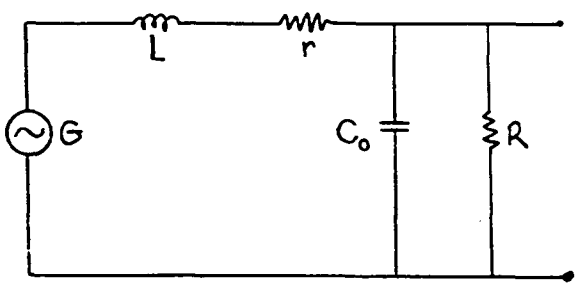

L = Self Inductance
C_o = Stray Capacitance
G = Generator
r = Resistance Of Probe
R = Arbitrary Resistor

Fig. A.8. Equivalent Circuit Of Magnetic Probe

Reproduced with permission of the copyright owner. Further reproduction prohibited without permission.

Solving the circuit equation, it can be shown that if $R > \sqrt{\frac{L}{C_o}}\left(2-\frac{r^2C_o}{L}\right)^{-\frac{1}{2}}$, then the attenuation curve has a resonance at

(1) $$\omega = \left| \frac{1-\frac{r^2C_o}{2L}-\frac{L}{2C_oR^2}}{LC_o} \right|$$

In practice $\frac{r^2C_o}{2L} < 5\%$,

(2) therefore $$\omega \approx \left[\frac{1-\frac{L}{2C_oR^2}}{LC_o} \right]^{\frac{1}{2}}$$

Thus if we let

(3) $$R = \sqrt{\frac{L}{2C}} = Z ,$$

then the resonance frequency decreases to zero.

To obtain the values of L and C_o, the following circuit is used.

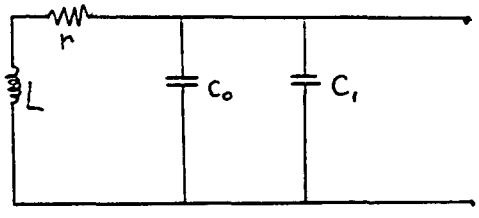

L = Self Inductance
r = Resistance Of Probe
C_o = Stray Capacitance
C_1 = Applied Capacitance

Fig. A.9. Circuit For Damped Probe Circuit

Reproduced with permission of the copyright owner. Further reproduction prohibited without permission.

The circuit is excited by a pulse and the resonance frequency ω_1 is measured,

(4) i.e. $$\omega_1 = \frac{1}{\sqrt{L(C_o + C_1)}} \quad ,$$

Then the capacitor C_1, is changed to C_2 and the corresponding resonance frequency ω_2 is found,

(5) $$\omega_2 = \frac{1}{\sqrt{L(C_o + C_1)}} \quad .$$

From equations (4) and (5), the values of C_o and L can be calculated. Using these values, the matching impedance is found for each probe and given below.

	C_o	L	$Z=\sqrt{\frac{L}{2C}}$
Magnetic Probe	540 pf	1.9 μH	43 Ω
Rogowski Coil	174 pf	25 μH	270 Ω

Reproduced with permission of the copyright owner. Further reproduction prohibited without permission.

REFERENCES

Bartoli, C. and Green T.S. 1963, Nuclear Fusion 3, 84.

Bodin, H.A.B., Green, T.S., Niblett, G.B.F., Peacock, N.J., Quinn, J.M.P., Reynolds, J.A., Taylor, J.B. 1962, Nuclear Fusion Supplement 2, 511.

Bogen, P., Hintz, E., Schlüter, J. 1964, Nuclear Fusion 4, 131.

Cillier, W.A., Driver, H.S., Irving, J., Lewis, I. 1963 Nuclear Fusion 3, 78.

Clarke, G.L. and Wuerker, R.F. 1962 Phys. of Fluids 5, 1503

Curzon, F.L. and Churchill, R.J. 1962 Can.J.Phys. 40, 1191

Curzon, F.L. and Smy, P.R. 1961 Rev.Sci.Inst. 32, 756

Eberhagen, A. and Glaser, H. 1964 Nuclear Fusion 4, 296.

Green, T.S. 1962. Nuclear Fusion 2, 92.

Niblett, G.B.F. and Green, T.S. 1959 Proc. Phys.Soc. (London) Ser. A, 74, 737.

Reproduced with permission of the copyright owner. Further reproduction prohibited without permission.

Rosenbluth, M.N. 1954 Los Alamos Report 1850.

Segre, S.E. and Allen, J.E. 1960 Jour. of Sci. Inst. 37, 369.

Theophanis, G.A. 1960 Rev. of Sci. Inst. 31, 427

Uchida, T., Masatomo, S., Hamada, S. 1962

Nuclear Fusion 2, 70.

Reproduced with permission of the copyright owner. Further reproduction prohibited without permission.